Louisiana Tech University
Louisiana Tech Digital Commons

Doctoral Dissertations | Graduate School

Summer 2005

DNA-templated assembly of metallic nanowires

Qun Gu
Louisiana Tech University

Follow this and additional works at: https://digitalcommons.latech.edu/dissertations

 Part of the Electrical and Computer Engineering Commons

Recommended Citation
Gu, Qun, "" (2005). *Dissertation*. 577.
https://digitalcommons.latech.edu/dissertations/577

This Dissertation is brought to you for free and open access by the Graduate School at Louisiana Tech Digital Commons. It has been accepted for inclusion in Doctoral Dissertations by an authorized administrator of Louisiana Tech Digital Commons. For more information, please contact digitalcommons@latech.edu.

DNA-templated assembly of metallic nanowires
Gu, Qun
ProQuest Dissertations and Theses; 2005; ProQuest

DNA-TEMPLATED ASSEMBLY OF METALLIC NANOWIRES

By

Qun Gu, B.S.

A Dissertation Presented in Partial Fulfillment
Of the Requirements for the Degree
Doctor of Philosophy

COLLEGE OF ENGINEERING AND SCIENCE
LOUISIANA TECH UNIVERSITY

August 2005

Reproduced with permission of the copyright owner. Further reproduction prohibited without permission.

UMI Number: 3184190

INFORMATION TO USERS

The quality of this reproduction is dependent upon the quality of the copy submitted. Broken or indistinct print, colored or poor quality illustrations and photographs, print bleed-through, substandard margins, and improper alignment can adversely affect reproduction.

In the unlikely event that the author did not send a complete manuscript and there are missing pages, these will be noted. Also, if unauthorized copyright material had to be removed, a note will indicate the deletion.

UMI®

UMI Microform 3184190

Copyright 2005 by ProQuest Information and Learning Company.

All rights reserved. This microform edition is protected against unauthorized copying under Title 17, United States Code.

ProQuest Information and Learning Company
300 North Zeeb Road
P.O. Box 1346
Ann Arbor, MI 48106-1346

Reproduced with permission of the copyright owner. Further reproduction prohibited without permission.

APPROVAL FOR SCHOLARLY DISSEMINATION

The author grants to the Prescott Memorial Library of Louisiana Tech University the right to reproduce, by appropriate methods, upon request, any or all portions of this Dissertation. It is understood that "proper request" consists of the agreement, on the part of the requesting party, that said reproduction is for his personal use and that subsequent reproduction will not occur without written approval of the author of this Dissertation. Further, any portions of the Dissertation used in books, papers, and other works must be appropriately referenced to this Dissertation.

Finally, the author of this Dissertation reserves the right to publish freely, in the literature, at any time, any or all portions of this Dissertation.

Author Qun Gu 

Date 08/08/2005

GS Form 14
(5/03)

Reproduced with permission of the copyright owner. Further reproduction prohibited without permission.

ABSTRACT

Nanowires are widely recognized as key elements in the development of futuristic nanoscale devices of nanoelectronics, optoelectronics and nano-electro-mechanic systems. Lithographic fabrication, however, faces increasing difficulties in the realization of continuously miniaturized features. The "Bottom-up" approach is a promising successor to lithography for fabrication of nanostructures. DNA is a natural template for nanowire assembly. The linear polynucleotide chain has a width of 2 nm and a length of 0.34 nm per nucleoside subunit.

One-dimensional magnetic Co and Ni nanoparticles have been assembled *in-situ* for the first time by use of single DNA molecules as templates. Target metallic nanowires that are 10-30 nm thick have been grown on DNA templates by catalysis of 2-3 nm Pd nuclei in a three-step electroless plating process. Au microelectrodes have been designed, fabricated, and used to assemble conductive Pd nanowires and DNA-templated Au nanowires. The wires have been characterized with various physical methods. Various methods have been utilized to orient DNA molecules on solid supports and between electrodes. In addition, a novel approach of pre-nucleated growth on designed and synthesized single-stranded DNA templates has been proposed to assemble highly uniform and conductive nanowires by metallic nanoparticle deposition. This research has resulted in the development of novel approaches to fabricate magnetic nanowires, study fundamental aspects of DNA molecule-based nanoassembly, and utilize standard tools of molecular biology in nanotechnology.

Reproduced with permission of the copyright owner. Further reproduction prohibited without permission.

LOUISIANA TECH UNIVERSITY

THE GRADUATE SCHOOL

July, 12, 2005
Date

We hereby recommend that the dissertation prepared under our supervision by Qun Gu

entitled DNA-Templated Assembly of Metallic Nanowires

be accepted in partial fulfillment of the requirements for the Degree of Ph.D. in Engineering

Donald J. Hayes
Supervisor of Dissertation Research

Ray Sterling
Head of Department

Engineering
Department

Recommendation concurred in:

Upali Siriwardane

Advisory Committee

Approved:
Director of Graduate Studies

Approved:
Dean of the Graduate School

Dean of the College

GS Form 13
(5/03)

Reproduced with permission of the copyright owner. Further reproduction prohibited without permission.

TABLE OF CONTENTS

Reproduced with permission of the copyright owner. Further reproduction prohibited without permission.

Reproduced with permission of the copyright owner. Further reproduction prohibited without permission.

Reproduced with permission of the copyright owner. Further reproduction prohibited without permission.

LIST OF TABLES

Reproduced with permission of the copyright owner. Further reproduction prohibited without permission.

LIST OF FIGURES

Reproduced with permission of the copyright owner. Further reproduction prohibited without permission.

Reproduced with permission of the copyright owner. Further reproduction prohibited without permission.

Reproduced with permission of the copyright owner. Further reproduction prohibited without permission.

ACKNOWLEDGEMENT

First of all, I would like to thank Dr. Donald T. Haynie, my primary advisor, for bringing me into his group, and for his instruction and suggestions on my study and research. I could not have fulfilled the Ph.D degree requirements without his support.

I highly appreciate the people in this group, C. Cheng and S. Suryanarayanan, and former members, K. Dai, S. Anabathula and R. Gonela for sharing knowledge and experience with me. Thanks to Dr. B. Li, Dr. S. Bharadwaj and Dr. Z. Zhi for many interesting discussions.

I acknowledge Dr. K. Xu for her help with SEM and AFM samples and electron beam fabrication. Thanks for Mr. J. Fang for much help with electrode fabrication. I also would like to thank Dr. N. Seetala (Grambling State University) for VSM and SEM sample measurement, Dr. C. Luo for wonderful discussions, and Dr. Y. Voziyanov for suggestions on DNA synthesis.

Thanks for Dr. B. Elmore, Dr. C. Luo, Dr. U. Siriwardane, and Mr. J. Fang for serving on my advisory committee.

Finally, I would like to thank my wife, W. Chen, for her endless support.

Reproduced with permission of the copyright owner. Further reproduction prohibited without permission.

CHAPTER I

INTRODUCTION

1.1 Lithography Challenges

Optical lithography has been the mainstream technology in the semiconductor industry since the late 1950s, when the first integrated circuit was invented. The sophisticated technology enables us to accurately transfer patterns from masks onto silicon wafers, where complex microprocessors and circuits are packaged. Almost all of the core components of today's electronic products, for example radio, TV, and computers, are fabricated by optical lithography.

Continuous downscaling of critical dimension and upscaling of packaging density on semiconductor chips have tremendously improved the device performance and reduced manufacturing cost. Dr. Gordon Moore predicted the tendency of chipmaking industry as early as 1965 when he noted "the doubling of transistors every couple of years." This is known as Moore's Law, the main goal in semiconductor industry since then. On the Intel 4004 microprocessor of 1971, for example, only 2,250 transistors were integrated on a single silicon chip (Figure 1.1). Exponentially increased numbers of transistors are crammed into a small area of chips on today's microprocessors. On the 2003 Intel Itanium® microprocessor, for example, ~410 M transistors are squeezed within 374 mm^2 areas (Figure 1.1). In the past 30 years, continuous improvement of lithography

Reproduced with permission of the copyright owner. Further reproduction prohibited without permission.

has been the major driving force to miniaturize printable patterns on chips. Feature sizes, for instance, were shrunk from 4 μm linewidth in the 1960s to 45 nm gate length in 2005.

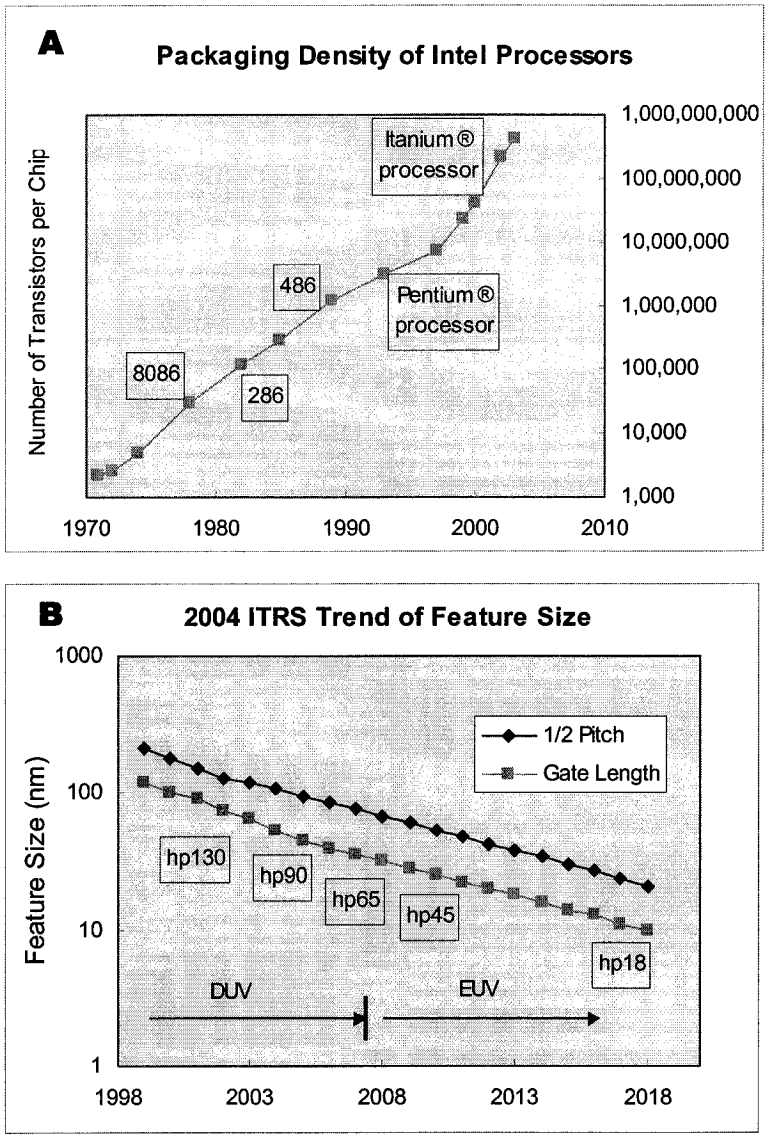

Figure 1.1. The trend of downscaling of semiconductor devices. (A) Packaging density of Intel microprocessors. Redrawn after Ref. [1]. Copyright 2002 Intel®. (B) 2004 ITRS roadmap of feature sizes. Redrawn after Ref. [2]. Copyright 2004 ITRS.

Capability of lithography to continuously downscale features is a must to maintain Moore's law. The latest International Technology Roadmaps for

Reproduced with permission of the copyright owner. Further reproduction prohibited without permission.

Semiconductors (ITRS) shows that lithography is in the era of Deep Ultra-Violet (DUV) (Figure 1.1). The 193 nm exposure systems with immersion are dominantly used at 90 nm and 65 nm technology nodes in the roadmap where the Intel Itanium® microprocessors were fabricated. Lithography, however, requires a new generation of exposure systems with even shorter wavelength at the beginning of the 45 nm node [2].

Extreme Ultra-Violet (EUV) of the 13.5 nm wavelength exposure system is widely referred to as the next generation lithography (NGL); however, it faces significant challenges prior to mass production. First, lack of high-reflectivity coating layers likely results in low throughput. Unlike conventional refractive optic system, all optic components in EUV system are reflective. Every additional surface between UV source and wafer absorbs incident light and thus lowers optical efficiency. Second, no pellicle to protect mask from particle contamination will lead to a higher possibility of defect printing. The thin transparent membrane used in almost all EUV testing systems has been demonstrated to absorb 50% light at 13.5 nm wavelength. Third, high source power needed to achieve high throughput of wafer patterning is not possible because current sources yield only 4 to 10 W. Approximately 100 W is required to achieve a throughput of more than 100 non-defective wafers per hour.

Is lithography forever? There is no known answer. The 193 nm wavelength exposure systems with immersion seem to be the solution for the next two nodes. The International Technology Roadmap for Semiconductors (ITRS), however, listed 157 nm exposure as a less likely option in the 2004 version. In a long term, ITRS predicted four technological challenges in <45 nm nodes beyond 2010 [2]: 1) Mask fabrication and process control, including defect-free NGL, timeliness and capability of mask-making

Reproduced with permission of the copyright owner. Further reproduction prohibited without permission.

tools in infrastructure, mask yield enhancement, pellicles for 157 nm immersion and protection of EUV masks from defects; 2) Metrology and defect inspection, including resolution and precision for critical dimension measurement down to 7 nm and for 2.2 nm 3 sigma linewidth roughness, metrology for overlay down to 7.2 nm, and defect inspection for patterned wafers for <30 nm defects; 3) Gate CD control improvements, process control and resist materials, including development of a process to control gate CDs <4 nm (3 sigma), development of new and improved alignment and overlay control methods, process control and design for low K1 lithography, resist with high index of refraction, high index fluids and high index optical materials, and limits of chemically amplified resist sensitivity for <50 nm linewidths due to acid diffusion length; 4) Tools and mass production, including optical and NGL exposure tools capable of meeting requirements of the ITRS, high output and cost-effective EUV source, and CaF_2 cost, yield, and quantity for 157 nm immersion.

The other big challenge of lithography is the manufacturing cost. Will each NGL be affordable? Today, approximately 30% cost of wafer printing comes from lithography. Lithography tools, masks, and numbers of wafer levels are three main components of the total cost [3]. It was only about 0.1 M USD for contact printers in the early 1970s. The cost of I-line steppers ranges from 1.6 M USD in 1992 to 4.4 M USD in 1998. In today's DUV exposure system, it rises to about 15 M USD. Future generations of leading-edge tools are predicted to cost exponentially more. The other two components of total cost are in similar situation. Photomasks for sub-wavelength lithography require more expensive writing tools, inspection tools, and repair tools in response to continuous downscaling of feature sizes. A mask set for an integrated circuit in 130 nm and 90 nm nodes typically

Reproduced with permission of the copyright owner. Further reproduction prohibited without permission.

costs about 2 M USD. The prohibitive price must be compensated by an increase of product volume. The more complex process, however, leads to lower yields and production volume. The expected EUV tool will cost above 40 M USD, which will make profit almost infeasible.

1.2 Nanotechnology

Nanotechnology is an emerging science and engineering. It concerns understanding, building and utilizing functional materials and systems in the nanoscale size range, typically 1-100 nm. They can be achieved by manipulating and assembling atoms or molecules to precise nanoscale "machines" that function as intended. Nanotechnology involves a wide range of disciplines: chemistry, physics, mechanical engineering, materials science, molecular biology, and computer science, etc.

Unlike bulk materials, many nanoscale materials behave with distinctive characteristics and phenomena. As their sizes are miniaturized to below 100 nm critical length, properties not only depend on chemical composition, but more importantly, depend on size. Carbon nanotube, for example, displays electrical conductivity of copper, thermal conductivity of diamond and 100-fold strength of carbon generated by only 1/6 weight.

One might have heard about the word "nanotechnology" from explosive stories of all kinds of media. But, how does it improve our life? It will not only improve, but also change our life in a number of different ways. Potential applications of nanotechnology cover polymers, electronics, cosmetics, automobile, computer, aerospace, environment treatment, agriculture, energy saving, water clean, catalysis, cloth making,

Reproduced with permission of the copyright owner. Further reproduction prohibited without permission.

pharmaceuticals and drugs, military uses and so on. The nanotechnology would execute sensational societal implications in the next decade. Dr. M.C. Roco, chair of the National Nanotechnology Initiative (NNI), predicated that the new world of nanotechnology products will cost 1 trillion USD per year in the period from 2010 to 2015, and about 2 million workers on nanotechnology would be needed worldwide.

A great deal of funding is required to support research and development of the nanotechnology. NNI has disclosed the rapid increase of federal investments on nanotechnology in the past years. According to the NNI budget request of FY 2004, the number was 270 M USD in 2000 and rose up about 849 M USD (requested) in 2004, averaging 33% increase per year over these 4 FYs. In 2003, the 21st Century Nanotechnology Research and Development Act was passed by the U.S. Congress. It promised about 3.7 billion USD for research over three years at the beginning of 2005. The whole world is excited about this future technology. Figure 1.2 shows the trend of the world government investment on nanotechnology [4]. West European and Japanese governments are the two major investors other than the US. The world-wide research funding sponsored by governments skyrockets to 30 billion USD in 2003, compared to less than 500 million USD in 1997. It would be about 45 billion USD in 2005.

"*There's plenty of room at the bottom.*" Richard P. Feynman, the Nobel Laureate for physics heralded advent of the era of small things in 1959: the principles of physics are not against the possibility to manipulate matters atom by atom. Nanotechnology, however, did not stride forward until the emergence of new metrology tools. The 1986 Nobel Prize of physics was shared by three microscopists, Ernst Ruska for the invention of the electron microscope (EM), and Heinrich Rohrer and Gerd Binnig for the invention

Reproduced with permission of the copyright owner. Further reproduction prohibited without permission.

of the scanning tunneling microscope (STM). It is the first time that a machine ever built can realize atomic resolution by measuring the tunneling current between a sharp probe and a sample surface. Five years later, the atomic force microscope (AFM) was invented by Binnig, Quate and Gerber. The feature of this machine is that conformation of insulating samples, such as DNA and protein, can be well characterized without destruction. Nowadays, more advanced EM, STM and AFM are widely used in the research and development of nanotechnology.

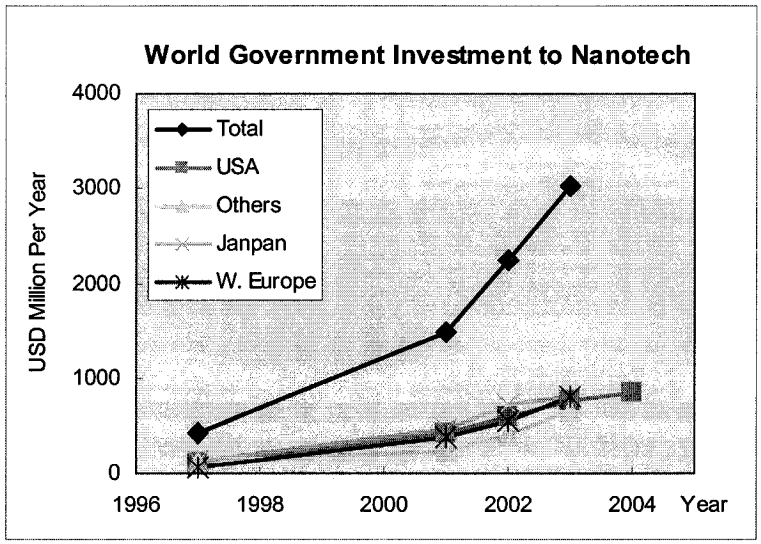

Figure 1.2. Investment on nanotechnology by government. Note: U.S. begins FY in October, six months ahead of Japan and EU; US does not have a commanding lead as it had in other fields, such as Bio, IT, space, nuclear; US accounts for ~ 35% of total in FY 2003. Redrawn after Ref. [4].

Rapid progress of nanotechnology has been made since Feynman's prophecy. The past 15 years, particularly, are the jump-start of a nano time. The bucky ball and carbon nanotube might be the two most representative achievements among a number of findings and discoveries in the nanoworld. The 0.7-1.5 nm bucky ball, also called fullerene, is the roundest and most symmetrical molecule ever known (Figure 1.3A). It is the only

Reproduced with permission of the copyright owner. Further reproduction prohibited without permission.

molecule composed of a single element to form a hollow spheroid. One molecule of fullerene is made of 60 carbon atoms arranged by interlocking hexagons and pentagons. The structure was discovered by Dr. Richard E. Smalley and Dr. Robert F. Curl Jr., who were awarded the 1996 Noble Laureates for chemistry. The development of drug delivery systems is one of the potential applications of fullerene.

Carbon nanotubes might be closer to commercialization than C60. Single wall carbon nanotube (SWNT) looks like a hollow graphite cylinder with well-organized structures (Figure 1.3B). Assembly of several coaxial SWNTs forms a multi-wall carbon nanotube. Tremendous effort has been made on the research of carbon nanotube since its discovery in 1991. The unique behaviors of nanoscale carbon nanotubes are characterized by remarkable tensile strength, high electrical and thermal conductivity, and large malleability. The first commercial product of carbon nanotube is probes for STM and AFM. Other proposed applications are components of nanoelectronics, energy storage and conversion devices, sensors, field emission displays, radiation sources, etc.

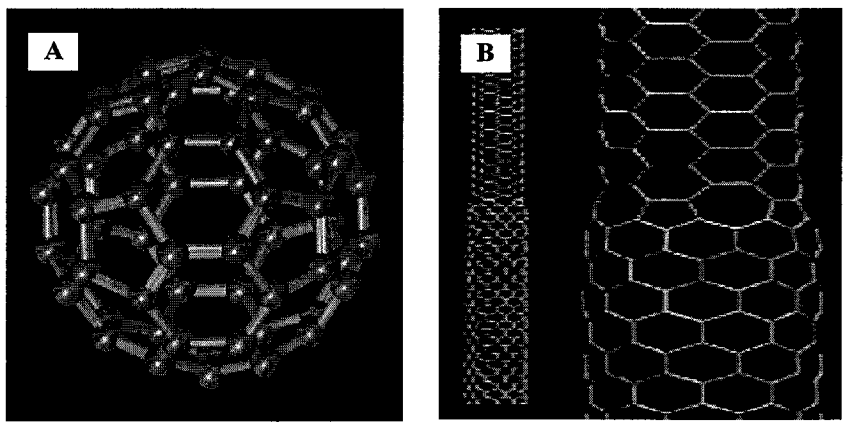

Figure 1.3. Simulated bucky ball and carbon nanotubes. (A) Bucky ball. Copyright Dr. Roger C. Wagner, University of Delaware; (B) Single-walled carbon nanotubes, Copyright Dr. Alain Rochefort, Center for Research on Computation and its Applications

Reproduced with permission of the copyright owner. Further reproduction prohibited without permission.

Nanobiotechnology is a special branch of nanotechnology. It studies biotechnology on the molecular level. Topics are wide, including life science, interactions between biomolecules, cell behavior, and integrated bionanosystems. Biomolecules meet nanotechnology not only because most biomolecules, for example, nucleic acid and protein, are typically nanosized, but also because they function with high specificity and fidelity. Antibody protein, for example, binds the unique sites of corresponding antigen and catalyzes certain biochemical reactions in immune systems of all organisms. Nanobiotechnology is a particularly promising field. Envisioned applications include novel biomaterials, tissue and cell engineering, drug discovery and delivery, point-of-care diagnostics, and bioprocess imaging, etc.

There are many challenges to the fast growing nanotechnology today; however, the cycle of R & D seems to be shorter than conventional industry. Carbon nanotube invented in 1991, for example, was commercialized to a high-brightness light source in 2000. Many nanoproducts are in or close to the stage of commercialization: for example, diagnostic biochips, nanostructured fuel cell, and nanocatalysts. Nanotechnology was involved in about 40 NASDAQ stocks by 2005.

There are always debates on the pathway to build and use nanomaterials and systems, but the potential of nanotechnology has never been debated. "The next big thing is really small" is perhaps best said about nanotechnology.

1.3 Nanowires

Interest in one-dimensional nanoscale materials and devices, often called nanowires, nanotubes or nanorods, has risen sharply in recent years. The material

Reproduced with permission of the copyright owner. Further reproduction prohibited without permission.

properties exhibited by such structures have considerable potential for the development of functional nanoscale electronic devices: for example, diode logic gates [5], bipolar transistor [6], and field effect transistors [7-9]. P-N junctions built on a single nanowire would be useful in optoelectronic devices, such as lasers [10-14], waveguides [14, 15], light emitting diodes [7, 16], photodetectors, and optical switches [17-19]. Nanowire-based sensors can be used to detect trace quantities of biomolecules and chemicals in nano-electro-mechanic systems (NEMS) [20-22]. Co, Ni and Fe nanowires with giant magneto-resistance have shown promise for high density storage memory [23-25].

It is well-known that conventional photolithography faces the physical limit of wavelength when features are downscaled to below 100 nm. Other lithographic methods, for example electron beam lithograph, X-ray lithograph, and EUV, are too expensive to be the general resolution for nanoscale fabrication. Academic science is eager to look for a novel strategy for mainstream submicron manufacturing. Nanometer or molecular-size components in electric circuits can be assembled from even smaller building blocks: atoms, molecules, and nanocrystals, by using self-assembly and molecular recognition processes. It thus would seem that innovative nanoscale properties and functions will be achieved through learning to control matter at an atomic or molecular level. This is known as a "bottom-up" approach.

Among the many "bottom-up" approaches to fabrication of 1D nanostructures, the most successful are vapor-liquid-solid (VLS) growth, Laser-assisted catalytic growth (LCG), and template-based methods (TBM). VLS was first used by Wagner and Ellis to grow single crystal Si whiskers in 1964 [26] and then developed by Givargizov in 1975 [27]. Recently, VLS has shown effectiveness in nanowire fabrication. Yang's group has

Reproduced with permission of the copyright owner. Further reproduction prohibited without permission.

disclosed the mechanism of VLS by the real-time observation of Ge nanowire growth [28]. The three-stage process was described for the Ge growth (Figure 1.4). In the first stage, Au nanocrystals and Ge vapor form an alloy that liquefies at high temperatures. With a temperature decrease, Au/Ge liquid alloy condenses and part of Ge crystal segregates. At the second stage, Ge nuclei precipitate at the liquid-solid interface. Vapor Ge source continues to be dissolved into the alloy, which facilitates further Ge segregation. In the third stage, condensed Ge grows into solid single crystal nanowires.

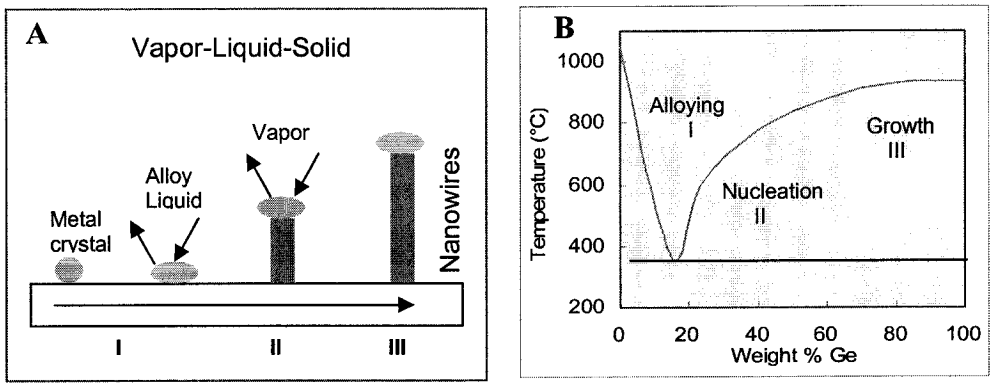

Figure 1.4. The mechanism of VLS. (A) The three-stage growth: Alloying, nucleation, and axial growth. (B) Temperature relates to composition. Redrawn after Ref. [28]. Copyright 2001 The American Chemical Society.

LCG, developed by Lieber's group, is an improved VLS for nanowire fabrication [29]. Si and Ge nanoclusters with diameter of 3-6 nm are generated by a pulsed laser. Photochemical energy condenses vapor species to solid nanoscale crystals. The rest of the process is similar to the growth by VLS. More recently, LCG has been used to fabricate semiconductor nanowires made of compounds from the III-V groups or II-VI groups, such as GaN [30], GaAS, GaP, InAs, InP, GaAs/P, InAs/P, ZnS, ZnSe, CdS, and CdSe [31]. Average diameters of these nanowires range from 11 to 30 nm, and orientation of crystal nanowires was mainly on <111>. Because laser can be used to generate nanoseeds

Reproduced with permission of the copyright owner. Further reproduction prohibited without permission.

made of virtually all materials, a wider range of nanowires may be prepared by this method.

Negative template method is one of the TBMs. Nanowires deposit into arrays of negative templates, long cylindrical pores. Width, length and distribution of nanowires are mainly determined by pore structure, orientation and distribution on template membrane. The track-etched membrane is the first method used. Discrete cylindrical pores are generated by ion bombardment and then membranes are chemically etched. Possin *et al.* have fabricated metal nanowires with the diameter of ~40 nm by filling track-etched pores on mica substrate [32]. Anodic alumina membrane is the other typical negative template. Well-ordered honeycomb-like nanopores can be achieved by anodization of aluminum in an acidic electrolyte. The size of pores and the distance between two adjacent pores are mainly determined by anodization conditions. Other negative templates, for example polymethylmethacrylate, polystyrene, glass and silica, have been used for nanowire fabrication.

Electrochemical deposition, introduced by Martin and coworkers [33], is the most widely used method for nanowire fabrication. One advantage is that nanowires made of metals [34-43], semiconductors [44, 45] and conducting polymers [46-49] can be prepared. The membrane is soaked in an electrodeposition solution. A metal film on the bottom of the standing membranes serves as electrodes of electrodeposition. Extraction of nanowire after deposition is achieved by chemical dissolution of membranes. An AC field is generally applied to alumina membranes that are naturally supported by a layer of Al film. The other advantage of electrochemical deposition is that fabricated nanowires can be highly conductive because electron transfer during electrodeposition is fast along

Reproduced with permission of the copyright owner. Further reproduction prohibited without permission.

the high conductive pathway. Other methods to nanowire fabrication using negative templates are chemical vapor deposition, electroless plating, and sol-gel chemistry.

Far beyond the conventional notion of "wiring", nanowire applications have extended to nanoelectronics, optoelectronics, and NEMS. Table 1.1 lists a variety of applications of metal and semiconductor nanowires. The sophisticated fabrication techniques enable single crystal growth of semiconductor nanowires with controllable length and diameter. They exhibit high electrical conductance through either n or p type doping. Elemental electronic devices, diode, logic gate, bipolar transistor and field effect transistor, which are conventionally integrated on a planar Si substrate, have been realized on one-dimensional nanowires now [5-9].

Table 1.1. Summary of main applications of nanowires.

Potential Applications		Nanowires	Fabrication	Width (nm)	Ref.
Nanoelectronics	Diode logic gates	Si/GaN	VLS/LCG	10-30	[5]
	Bipolar transistors	Si	LCG	20-50	[6]
	Field effect transistors	InP/Si/CdS	LCG/CVD	5-75	[7-9]
	Storage memory	Fe/Co/Ni	TBM	~ 200	[23-25]
	Interconnection	GaN/InP/Si	LCG	NA	[50]
Optoelectronics	Lasers	ZnO/GaN/CdS	VLS/LCG	10-200	[10-14]
	Waveguides	ZnO/SnO_2	VLS	40-350	[14,15]
	Photodetectors and Switches	ZnO/InP	VLS/LCG	20-60	[17-19]
	Light Emitting Diodes	InP/Si/GaN	LCG/VLS	45	[7,16]
NEMS	Sensors	Si/SnO_2	LCG/VLS	10-20	[20-22]

Reproduced with permission of the copyright owner. Further reproduction prohibited without permission.

Wide band-gap semiconductor materials, for example ZnO, GaN and InP, are natural laser cavities capable of emitting monochromic lights from UV to near infrared. Yang's group has demonstrated that ZnO nanowires emit monochromic light at the 385 nm wavelength after optical excitation [10]. GaN nanowire has been reported to function as UV-blue laser. Lieber's group has fabricated the first nanowire-based laser that is electrically driven [12]. Photodetectors, optical switches, and light emitting diodes have also been demonstrated on the basis of semiconductor nanowires [14-19].

Nanoscale biological and chemical sensors are the other new area of nanowire applications. Cui *et al.* have reported that conductance of modified Si nanowires was linearly related to pH of solution [20]. The relation may be used in the fabrication of pH sensors to detect trace amount of streptavidin. It was predicted that a variety of chemical and biological sensors can be built on single nanowires, useful in array-based screening and *in vivo* diagnostics. Hahm *et al.* have demonstrated than Si nanowire-based devices can be used to detect nucleic acid through high fidelity and sensitivity [22]. The application of nanowire-based NMES may extend to detect other protein, viruses, and pathogens.

One-dimensional nanowire is considered to be key building blocks in a variety of micro/nano systems. Besides semiconductor and metal nanowires, Bi and Bi_2Te_3 nanowires have been shown to exhibit unique thermoelectric property [51]. Resistivity decreases monotonically with temperature increase, which may be used in small cooling system. Overall, nanowire-based devices and systems are not far away from commercialization, although further research and development is required to better understand the unique properties of such one-dimensional structures.

Reproduced with permission of the copyright owner. Further reproduction prohibited without permission.

1.4 DNA-templated Nanowires

Biomolecules and nanotechnology meet at the same length scale. Naturally optimized biomolecules, such as proteins, nucleic acid, and supramolecular biocomplexes are revolutionarily used in the assembly of nanostructured materials and systems. The DNA molecule has recently been shown to be an excellent building block for fabrication of novel nanomaterials and functional nanosystems.

DNA templated-based approaches are attractive for the development of 1-D nanostructures. In early work in this area, Alivisatos *et al.* [52] and Mirkin *et al.* [53] exploited the molecular recognition properties of DNA and enabled the assembley of nanoparticles into organized structures with nanoscale precision. Later, Braun *et al.* [54] fabricated the first conductive nanowires from Ag nanoparticles and single DNA molecules. Since then, the development of DNA-templated nanowires has progressed rapidly. Nanowires of Pd, Pt, Au, Cu and CdS have been prepared by this approach.

The novel application of DNA molecules in nanoassembly may be explained by their unique structure and remarkable molecular property. The basic unit of DNA molecules, a nucleotide, consists of a 5'-carbon sugar (deoxyribose), a nitrogen-containing base and a phosphate group (Figure 1.5). The negative charged phosphate group and sugar form the covalent backbone of a linear DNA. DNA molecules have four different nitrogenous bases - adenine (A), thymine (T), guanine (G) and cytosine (C). The unique self-recognition of DNA comes for the nitrogenous base pairing. Within a normal double-stranded DNA, adenine (A) only pairs with thymine (T), forming two hydrogen bonds, and guanine (G) only pairs with cytosine (C), forming three hydrogen bonds. The distance between two adjacent bases is approximately 0.34 nm. DNA is a long and thin

Reproduced with permission of the copyright owner. Further reproduction prohibited without permission.

polymer. Two polynucleotide chains with complementary sequence in a molecule are twisted together to form a right-handed helical spiral, winding around a helix axis. The bases of the individual nucleotides are on the inside of the helix, stacked on top of each other like the steps of a spiral staircase (Figure 1.5A).

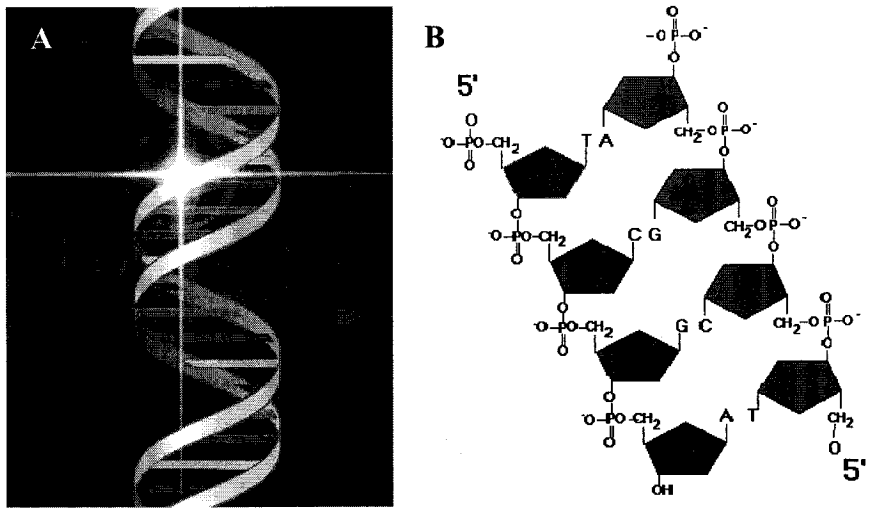

Figure 1.5. Schematic diagram of the structure of double-stranded DNA. (A) A simulated DNA double helix. Copyright Monkey Cosmos. (B) The chemical structure of a double-stranded DNA molecule. Each subunit consists of a phosphate group, a sugar and one of the four bases – adenine (A), thymine (T), guanine (G) or cytosine (C). Molecular recognition by Watson-Crick base pairing means that A pairs with T only, and G pairs with C only. Reprinted after Ref. [98].

DNA is a natural template for nanofabrication. The linear polynucleotide chain has a width of 2 nm and a length of 0.34 nm per nucleoside subunit (Figure 1.5). A wide range of molecular lengths, from nanometers to microns, can be realized with established technology in molecular biology: for example, DNA ligation, enzymatic digestion, and polymerase chain reaction. DNA-templated nanowires could be prepared with an almost unlimited range of aspect ratio. Binding sites on DNA stick to ions, nanoparticles, organic molecules, and other "building blocks" by electrostatic interaction or coordination coupling. The polyanionic backbone of the molecule can bind to metallic

Reproduced with permission of the copyright owner. Further reproduction prohibited without permission.

cations or positively charged nanoparticles. Various metal ions, for example, Pt(II) and Pd(II), are coordinated by the N7 atoms of DNA bases. DNA is uniquely suited to molecular recognition. Loweth *et al.* [55] have utilized Watson-Crick base pairing to assemble two or three individual Au nanocrystals on specific sites of an ssDNA molecule. As we discuss below, the specific molecular recognition capability could be developed to assemble highly uniform nanowires on an ssDNA template. A distinguishing feature of nanoassembly with ssDNA is that the precision of the spatial arrangement of assembled nanostructures can be on the order of a few nanometers.

One important role of nanowire in future nanoelectronics and NEMS will be interconnection of circuit elements with high conductivity and flexibility. Uncertainty regarding the conductivity of intrinsic DNA [56], might prevent its direct use in electronic circuits. A functional two-phase system, however, can be possibly assembled in such a way that a functional phase is built on the other structural phase. This is the principle of almost all template-based nanofabrications. Here, metallic nanoparticles - good electrical conductors will be directly assembled on linear DNA template. The resulted structure will be linear and conductive.

Cobalt and Nickel ferromagnetic nanowires are useful in the development of high density storage memory and field sensors. The quasi-one-dimensional wires exhibit unusual properties because wire diameters of 10-50 nm (Fe, Ni, Co) are close to or smaller than the width of domain walls. One approach that has been studied to fabrication of magnetic nanowires is electrochemical deposition using porous membranes. Little use has been made of the biotemplate approach to prepare magnetic nanowires. My work

Reproduced with permission of the copyright owner. Further reproduction prohibited without permission.

shows that nanoclusters of ferromagnetic Co and Ni can be "strung" into one-dimensional wires by DNA-templated self-assembly.

Metallization of DNA by Au, Co and Ni nanoparticles is the major work of my Ph.D study. Fabrication of Au electrodes by the standard optical and electron beam lithography will be described in Chapter II. One function of nanowires is to interconnect elements of circuits. Here it is simulated by conductive nanowires stretched and anchored between electrodes. At equilibrium, DNA molecules are often randomly-structured in aqueous solutions as a result of thermal fluctuation. They must be separated and stretched before metallization to serve as nanowire templates. A variety of methods to immobilize and orient DNA templates will be used and discussed in Chapter III. The three-step fabrication process and characterization of prepared Au, Co and Ni nanowires will be described in detail in Chapter IV. A novel approach to the assembly of highly uniform and conductive nanowires will be presented in Chapter V.

The basic objectives of my Ph.D work are: 1) to provide a novel approach to the assembly of magnetic cobalt and nickel nanowires by first using DNA molecules as templates, 2) to investigate the fundamental mechanism and process in assembling metallic nanoparticles by DNA templates and to study nucleation and growth of metal nanoclusters in the presence of DNA, 3) to utilize the methods to orient DNA molecules on a variety of solid supports and between Au electrodes, and 4) to utilize standard tools of molecular biology in nanofabrication. For example, PCR, gel electrophoresis, and enzyme digestion will be used for design and synthesis of ssDNA templates, by which Au nanoparticles can be placed on designed sites of the templates with the precision of a few nanometers.

Reproduced with permission of the copyright owner. Further reproduction prohibited without permission.

CHAPTER II

ELECTRODE FABRICATION

2.1 Introduction

Fabrication of Au electrodes is the first work of this research. Here, they are simulated as conducting elements in electric circuits. Inter-wiring function of nanowires is achieved by stretching DNA templates between two electrodes and then metallizing them. Sulfhydryl group modified DNA molecules bind tightly to the Au electrode surface by Au-thiol coupling. In addition, the electrode provides a simple way to characterize electrical behavior of fabricated Au nanowires. A λ bacteriophage DNA molecule (48,502 bp) is about 16 μm long, which is the basis in the design of electrode and fabrication masks. The micron-spaced electrodes are fabricated by standard lithography. To match the length of designed and synthesized ssDNA templates (Chapter V), Au electrodes with 200 nm to 500 nm spaces are fabricated by electron beam lithography.

The lithography work has been done using the Class 100 clean rooms at the Institute for Micromanufacturing at Louisiana Tech University. The optical microscope, white light interferometric roughness-step-tester (RST, NT1000, WYKO), stylus profilometer (Step 500, Tencor Alpha), scanning electron microscope (SEM, Amary 1830), and atomic force microscope (Q-350, Quesant Instrument) were used to inspect photoresist patterns and image fabricated electrodes.

Reproduced with permission of the copyright owner. Further reproduction prohibited without permission.

2.2 Optical Lithography

2.2.1. Mask Design

In optical lithography, photomask is a stencil from which designed patterns are transferred onto a resist-coated substrate. It is an ultra-flat glass or quartz plate with a film of metals, for example, chromium that is opaque to UV light. The resolution of features on a substrate after fabrication is partially dependent on the printing quality of mask. A film mask, made by prepress printing technology, is the simplest commercialized mask. Limited resolution, however, was not suitable for this work that requires at least 16 μm resolution. For example, the first mask of this project was made of a photographic film, whose minimum linewidth was only about 25 μm.

Chromium mask is usually a quartz plate coated with chrome film on one side. It is still a standard photomask in the industry because chrome easily adsorbs UV irradiation. Figure 2.1A shows the layout of electrode Design I. Twenty five electrodes spread on a 4 inch wafer. The four-pad electrodes (Figure 2.1B) have spaces varying from 5 to 20 μm to match lengths of stretched DNA in applied hydrodynamic flow (Chapter III). The comb-shape electrodes have spaces of 5-15 μm (Figure 2.1C). The vertical overlap of 5 μm between two adjacent electrodes was designed to limit numbers of possibly aligned DNA molecules. The patterns are designed using AutoCAD®.

The relatively newer Design II of electrodes was based on observation and experience in stretching experiments (Figure 2.2). Figure 2.2A shows the layout of electrode Design II. Vertical overlaps between two adjacent electrodes were changed to approximately 2,800 μm (Figure 2.2B). This has greatly improved the possibility of DNA molecules stretched between electrodes (Chapter III). In each of 25 electrodes, four

Reproduced with permission of the copyright owner. Further reproduction prohibited without permission.

parallel arrays of electrodes were designed at the corners of the comb-shape electrodes (Figure 2.2C). This could lead to more DNA molecules bound to Au electrodes by Au-thiol coupling. C. Cheng has used these electrodes of the Design II to assemble Pd nanowires in applied AC field.

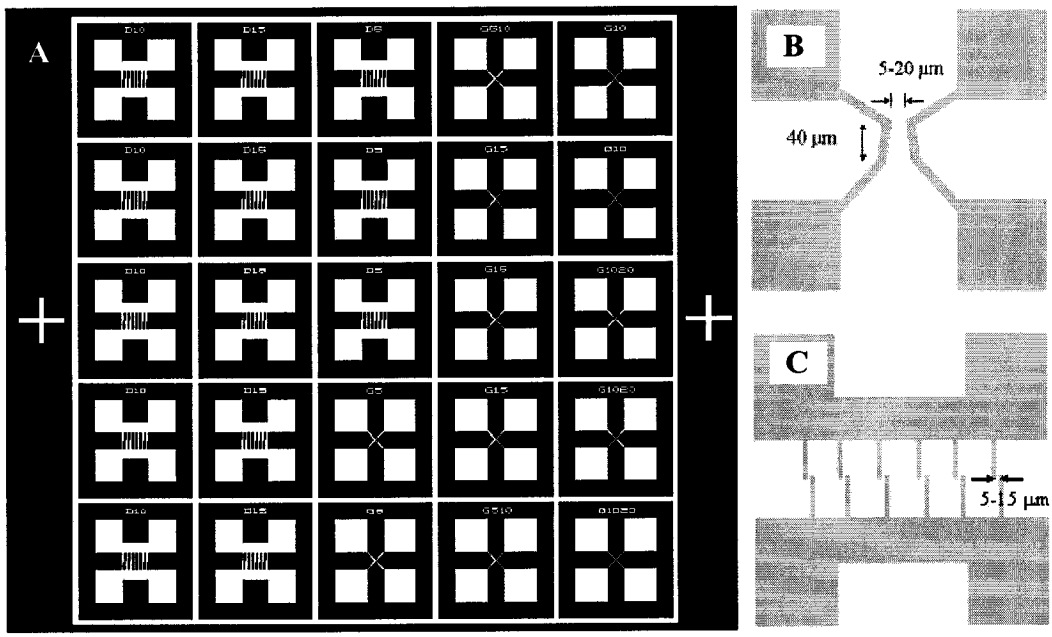

Figure 2.1. Schematic diagram of the electrode design I. (A) Layout of 25 Au electrodes on a 4 inch wafer. (B) Magnified view of the four-pad electrodes with 5-20 μm gaps. (C) Magnified view of the comb-shape electrodes with 5-15 μm gaps.

The chrome mask with the Design II was fabricated by the standard lithography. The DWL 66 Laser writer (Heidelberg Instruments) was used to expose the quartz plate that had been coated with a layer of chrome and photoresist. Line-by-line laser emission (244 nm) scanned the areas within polylines (Figure 2.2). Wet chemical etchant was applied to the mask after development. Stripping followed to remove unwanted resist on top of the chrome. The light field (within polylines) on mask will be the data field on the wafer after the lift-off process and Au deposition.

Reproduced with permission of the copyright owner. Further reproduction prohibited without permission.

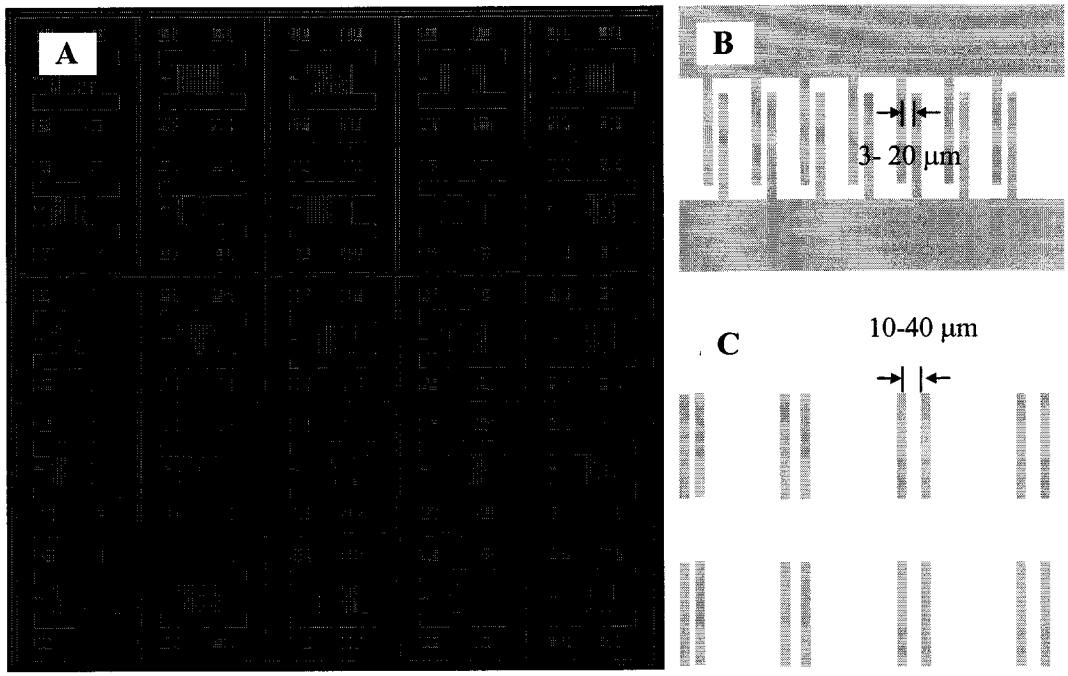

Figure 2.2. Schematic diagram of the electrode design II. (A) Layout of 25 Au electrodes on a 4 inch wafer. (B) Magnified view of the comb-shape electrodes with 3 -20 μm gaps. (C) Magnified view of the array of parallel electrodes with 10 - 40 μm gaps.

2.2.2.Chlorobenze Lift-off

Lift-off is an important process in IC and MEMS fabrication. It is widely used to pattern metals on a planar surface. Figure 2.3 shows a schematic diagram of the principle and process of lift-off. A photoresistor sensitive to exposure light is coated on a substrate. The photochemical reaction ruptures main and side chains of positive resist during UV exposure. Exposed resist will be much more dissolvable in the presence of developer than unexposed resist. Resist profile forms after development. Deposition of a layer of desired metal or other material is followed. Patterns are transferred onto substrate after stripping photoresist and deposited metal above resist.

Reproduced with permission of the copyright owner. Further reproduction prohibited without permission.

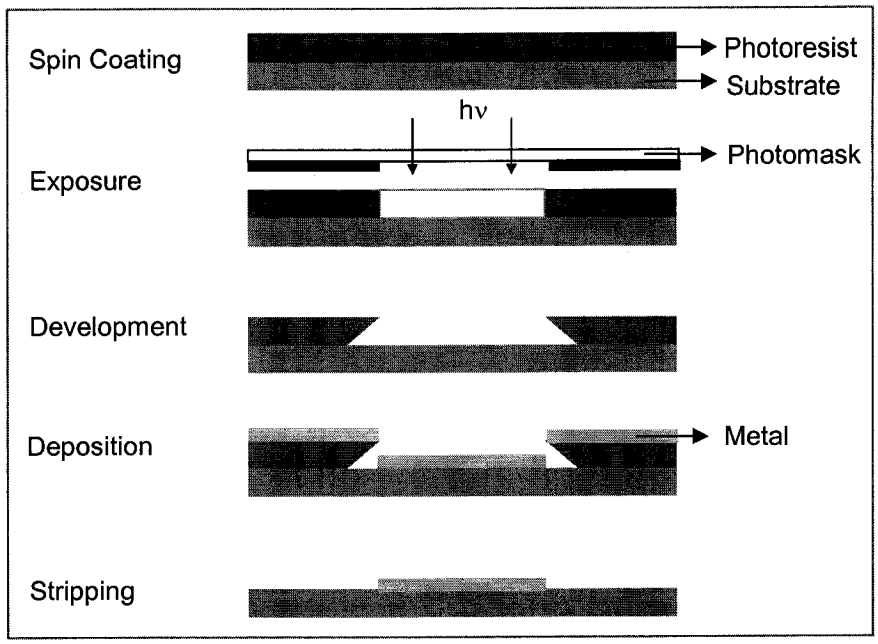

Figure 2.3. Schematic diagram of the lift-off process. From upper to bottom: spin coating, exposure, development, deposition and stripping. This is based on a positive resist.

The dual-side mask aligner (Electronic Vision) was used in all experiments of optical lithography. Equipped mercury lamp irradiates UV light at the 365 nm (i-line) wavelength. In fabrication of patterns of Design I, the chrome mask (LSI Inc.) was used with the mode of contact printing. Mask touches resist during exposure, thus minimizing diffraction of light and yielding best resolution. One micron thick positive photoresist (Shipley® S-1813) was spin-coated on a SiO_2 <100> wafer in all experiments. The ideal exposure was determined experimentally. With the fixed 1 min development, exposure time was changed from 5 to 8 sec. Figure 2.4A shows an RST micrograph of an over-exposed pattern. The 8 sec exposed resist in the middle of two electrodes collapsed. Seven seconds turned out to be optimal exposure time (Figure 2.4B and C).

Reproduced with permission of the copyright owner. Further reproduction prohibited without permission.

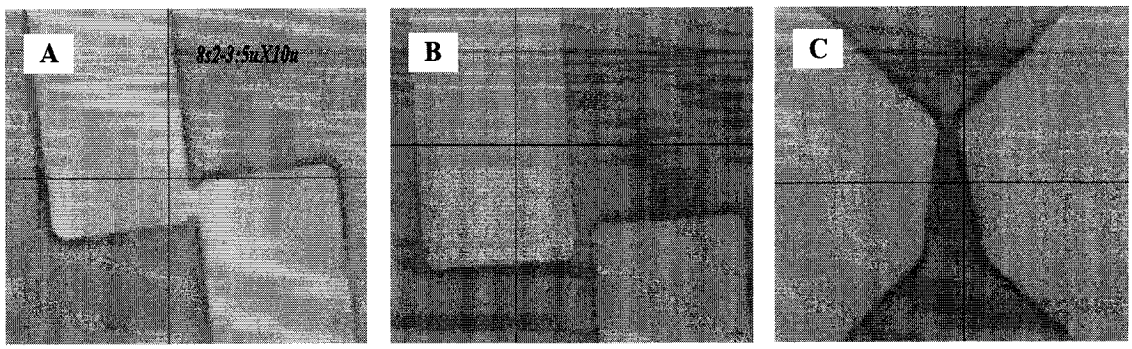

Figure 2.4. RST micrographs of resist profiles. (A) 8 sec exposure for 5 μm-spaced electrodes. The overexposed resist collapsed during development. (B) 7 sec exposure for 5 μm-spaced electrodes. (C) 7 sec exposure for electrodes with spaces of 5-20 μm.

The following procedure of optical lithography to fabricate electrodes with the 5 μm feature size has been tested to generate untouched resist profiles.

1) Clean a SiO_2 wafer with acetone, rinse with DI water and dry with a pressure nitrogen gun.
2) Pre-bake the wafer at 250 °C for 30 min to remove moisture on it.
3) Cool the wafer, apply S-1813 primer to improve adhesion, and spin the wafer at 1500 rpm for 40 sec.
4) Add resist S-1813 to cover 2/3 of the substrate, spin at 3000 rpm for 60 sec to yield a 1 μm thickness.
5) Soft bake the wafer at 115 °C for 60 sec to remove solvents and built-in stress and improve adhesion of the resist layer to the wafer.
6) Expose the wafer for 7 sec with the mask aligner.
7) Develop the resist profile with MF-319 developer (Shipley) for 60 sec with gentle shaking.
8) Rinse the wafer with deionized (DI) water and dry with a nitrogen gun.

Reproduced with permission of the copyright owner. Further reproduction prohibited without permission.

The specific side wall structures of resist profiles, however, have to be created prior to Au deposition. This is critical in the lift-off process. Structures of sidewalls are dependent on dose (emission power × exposure time) of UV source, backscattering of incident light, development time and others. Regular lift-off has three types of resist profiles: overcut, vertical, and undercut (Figure 2.5). Vertical sidewalls are not desired in lift-off because of the rounding effect of deposited features. In addition, vertical sidewalls can only be generated in perfect dose and development. Metal deposition on resists with an overcut profile typically leads to a continuous metal film that covers substrate, sidewall, and resist. It is difficult to strip unwanted metal that is likely sticking to sidewalls of resist. Therefore, overcut is generally not appropriate in lift-off. Undercut is the desired profile, because metal deposited on the top of resist can be easily stripped after the dissolution of resist (Figure 2.5).

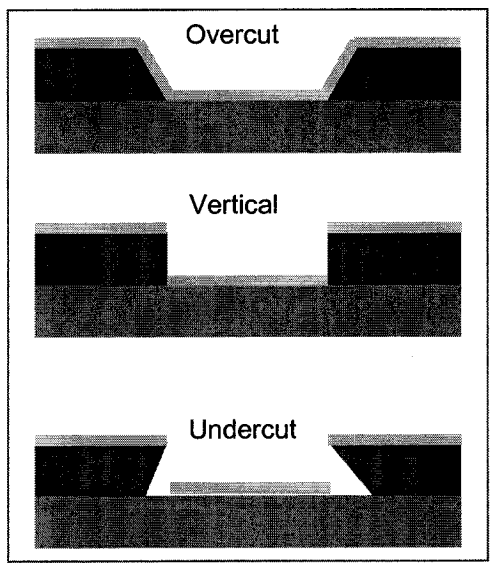

Figure 2.5. Three typical resist profiles in lithography.

SEM study has shown that no undercut of sidewalls has been generated by above 8-step procedures. Chlorobenzene soaking is a conventional and efficient mean to

Reproduced with permission of the copyright owner. Further reproduction prohibited without permission.

generate undercut during lift-off. Soaking can be done before or after exposure because the chemical is transparent to UV light. Chlorobenzene diffuses into resist, and thus hardens the top layer of coated resist. Therefore, the dissolution rate of the hardened resist to MF-319 developer is slower than the bottom layer of resist, which results in overhang structures of resist sidewalls.

The improved procedures of chlorobenzene lift-off are as follows:

1) Clean a wafer by rinsing with acetone 3 times and with DI water 3 times; dry with a nitrogen gun.
2) Pre-bake the wafer at 250 °C for 30 min to remove moisture from the substrate.
3) Cool the wafer, apply S-1813 primer to improve adhesion and spin the wafer at 1500 rpm for 40 sec.
4) Add enough S-1813 to cover 2/3 of the substrate, spin at 3000 rpm for 60 sec to yield 1 μm thickness.
5) Soft-bake the wafer at 115 °C for 60 sec to remove solvents and built-in stress and improve adhesion of the resist layer to the wafer.
6) Expose the wafer in the mask aligner for 7 sec.
7) Soak the wafer in 99% chlorobenzene for 5 min; dry with nitrogen gun.
8) Develop the wafer in MF-319 developer (Shipley) for 20 min with shaking.
9) Rinse the wafer using DI water with 3 times and nitrogen gun dry.

The overhang level can be controlled by time of development and chlorobenzene soaking. Figure 2.6 illustrates the scaling of undercut levels generated by 3 min and 5 min chlorobenzene soaking. In general, undercutting rate is faster in longer time

Reproduced with permission of the copyright owner. Further reproduction prohibited without permission.

chlorobenzene soaking and development. Five min soaking and 20 min development, for example, resulted in about 1.2 μm overhang, the maximum undercut in Figure 2.6.

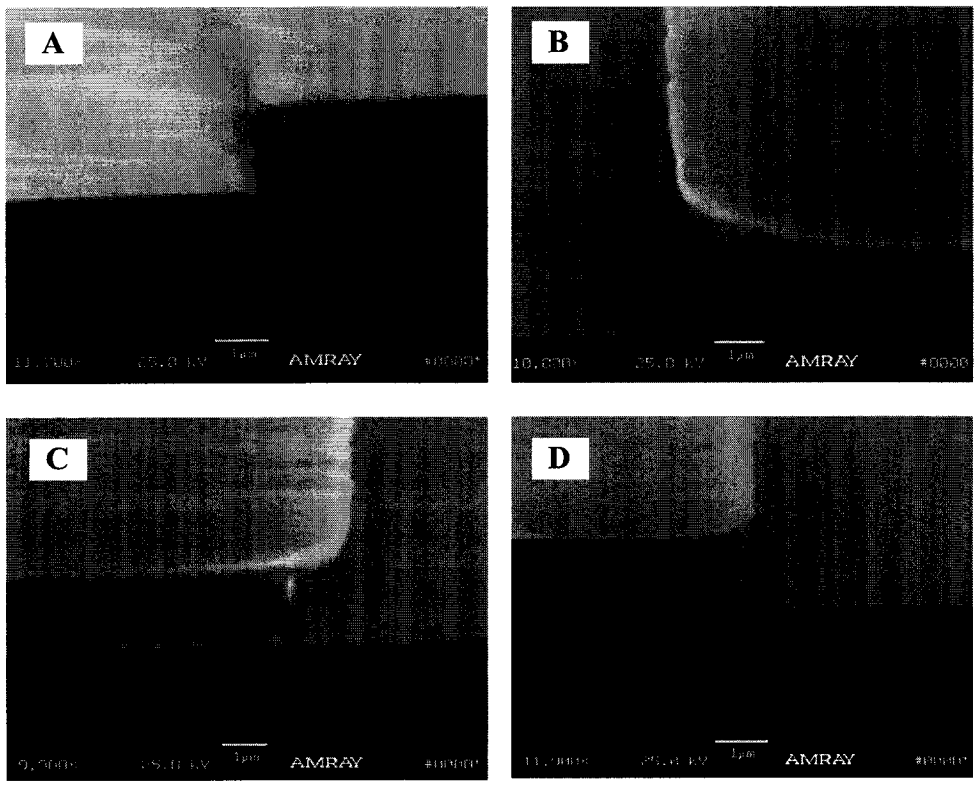

Figure 2.6. SEM micrographs of undercuts during the chlorobenzene lift-off. (A) ~0.5 μm undercut from 3 min soaking and 10 min development (B) ~0.75 μm undercut generated by 3 min soaking and 15 min development. (C) ~1 μm undercut from 5 min soaking and 15 min development. (D) ~1.2 μm undercut from 5 min soaking and 20 min development

Although the method of chlorobenzene soaking can create desired undercuts for successful lift-off, the organic reagent is harmful to both humans and the environment. In addition, the chemical is highly reactive to water, which could lead to failure of lift-off. It is not unusual that many white spots emerge on chlorobenzene-soaked wafers after development, because the chemical could have been contaminated during storage.

Reproduced with permission of the copyright owner. Further reproduction prohibited without permission.

2.2.3 LOR Lift-off

Bi-layer resist processing is the other widely used method in lift-off, in which the bottom layer of resist is more sensitive to exposure dose and thus has a higher dissolution rate in solution of developer than the top layer. LOR (MicroChem) is such a resist that can be combined with S-1813 to function as a bi-layer resist system. Based on polydimethylglutarimide platform, LOR resist is appropriate for a variety of critical lift-off processes, such as fabrication of GMR and MR heads, wireless devices, semiconductor lasers and detectors, MEMS, and many other microelectronic devices. Thickness of LOR resist and undercut rate can be easily controlled by adjustment of parameters in lift-off.

LOR resist must be coated as the bottom layer on the wafer in a LOR lift-off (Figure 2.7). Coating thickness depends on spin speed and time. Film with 600–700 nm thickness in LOR 7B resist, for example, can be generated on SiO_2 wafer with the spin rate of 3,000 rpm for 45 sec and the acceleration rate of 10,000 rpm/sec. Prebaking after coating is not only to remove remaining solvents in resist film, but also to determine the subsequent development time and undercutting rate. Prebaking temperature is a major factor to lateral etching rate. Prebaking at 190° C for 5 min generates the undercutting rate of 100 nm/sec.

The procedures of LOR lift-off are as follows.

1) Clean a SiO_2 wafer by rinsing with acetone 3 times and with DI water 3 times; dry with a nitrogen gun.
2) Pre-bake the wafer at 250° C for 30 min to remove moisture from the substrate.

Reproduced with permission of the copyright owner. Further reproduction prohibited without permission.

3) Cool the wafer, apply 3-4 mL LOR 7B and spin at 400 rpm for 5 sec, and then 3000 rpm for 45 sec with the acceleration of 10,000 rpm/s.

4) Prebake the wafer at 190° C for 5 min.

5) Add enough S-1813 to cover 2/3 of the substrate, spin at 3000 rpm for 60 sec to yield 1 μm thickness.

6) Soft-bake the wafer at 115° C for 60 sec to remove solvents and built-in stress and improve adhesion of the resist layer to the wafer.

7) Expose the wafer in the mask aligner for 18 sec.

8) Develop the wafer in the MF-319 developer (Shipley) for 15 sec with shaking.

9) Rinse the wafer with DI water 3 times and dry with a nitrogen gun.

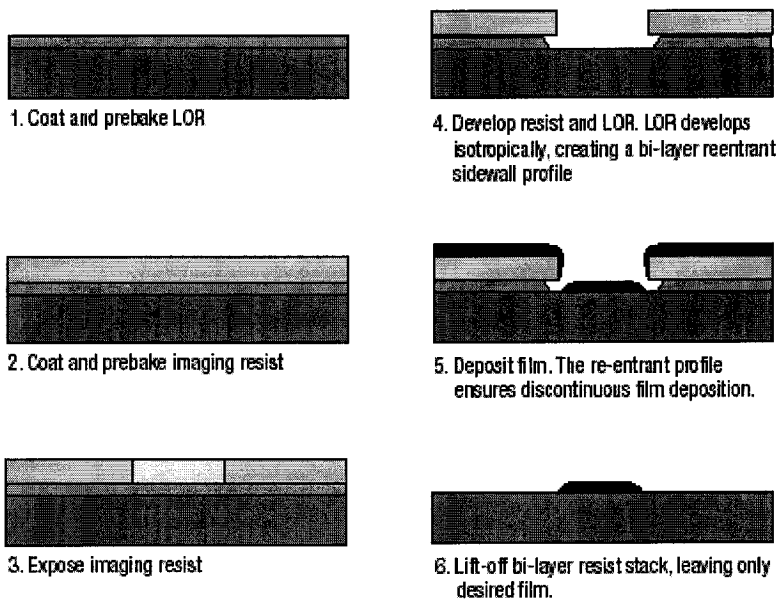

Figure 2.7. Schematic diagram of the LOR lift-off. It has two more steps, LOR coating and prebaking than the regular lithography. Reprinted after MicroChem catalogue. Copyright 2003 MicroChem Corp.

Figure 2.8 shows the ~1 μm undercut developed by MF-319 (Shipley) after following the procedures listed above.

Reproduced with permission of the copyright owner. Further reproduction prohibited without permission.

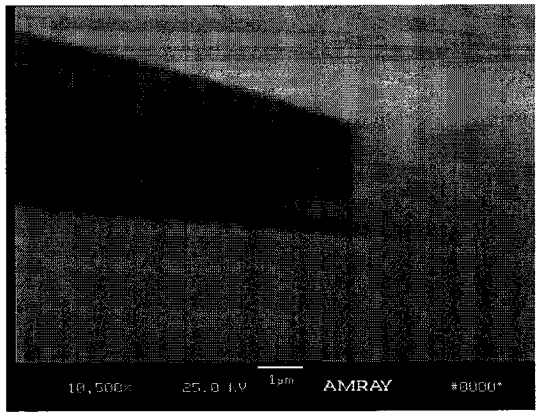

Figure 2.8. SEM micrograph of undercut in a resist profile. The ~1 μm undercut was generated by LOR and S-1813 bilayer resists.

2.2.4 Gold Deposition

Thermal evaporation and sputtering are two most popular methods to deposit thin metal film on patterned substrates. Both are physical vapor deposition, composed of three steps: 1) convert solid into vapor phase, 2) transport gas species from source to substrate, and 3) condense gas source on substrate and nucleate and grow into films. Sputtered metal normally have higher uniformity and density than thermal evaporated films. We chose sputtering in electrode fabrication. A layer of 3-5 nm chromium and 40-50 nm Au were sputtered on a patterned wafer. Stripping followed afterwards to remove Au on the top of S-1813 resist. Acetone was the stripper in the chlorobenzene lift-off and RPG stripper (MicroChem) was used in the LOR lift-off. In both cases, ultrasonic shaking enhances efficiency of stripping. Figure 2.9 shows Au electrodes with various spaces fabricated by the described chlorobenzene or LOR lift-off.

Reproduced with permission of the copyright owner. Further reproduction prohibited without permission.

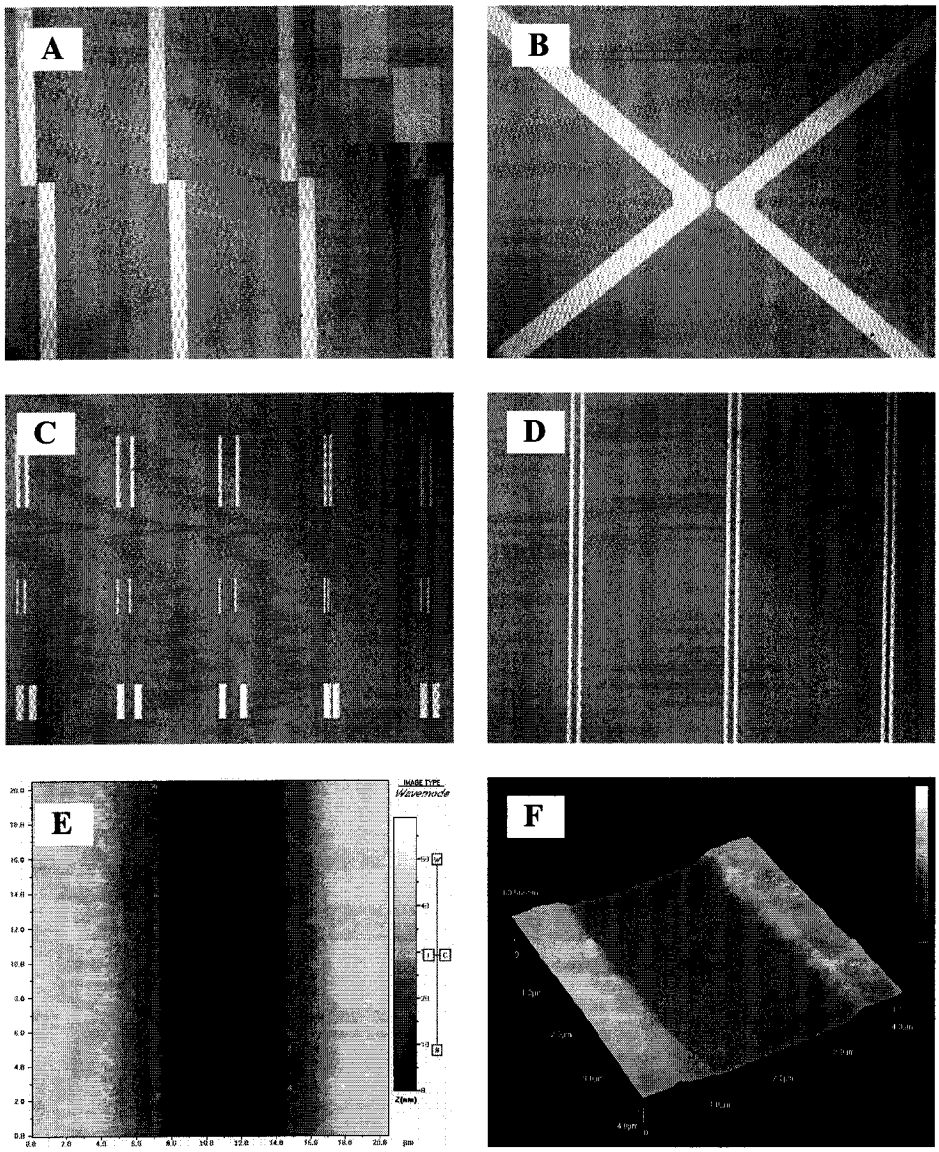

Figure 2.9. Fabricated Au electrodes with various shapes and spaces. (A) 5 μm; (B) 10 μm; (C) 5-30 μm; (D) 10 μm; (E) 7 μm; (F) 3 μm spaces. (A-D) are optical images. (E-F) AFM images with height scale of 60 nm.

2.3 Electron Beam Lithography

Because of the limit of standard optical lithography, electrodes that will be used in nanowire fabrication by designed single-stranded DNA templates must be fabricated by Electron beam lithography (EBL). EBL is a powerful tool to create patterns in the resolution of a few nanometers because of extremely short wavelengths of electron beams.

Reproduced with permission of the copyright owner. Further reproduction prohibited without permission.

The wavelength of electrons, for example, is about 0.008 nm in the 25 kV acceleration field, much smaller than UV wavelengths used in optical lithography. Because resolution is proportional to wavelength, EBL usually provides much better resolution than photolithography. It has been used to fabricate masks and key features in IC industry. The other advantage of EBL over photolithography is that EBL does need a mask. Electron beam scans designed areas on resist. High beam energy disrupts polymer molecules of a positive resist and results in an increase of dissolution rate during development. The contrast in solubility of exposed resist to unexposed resist determines resolution of patterns. Because beam spots are very small, it takes a long time to write certain scanning areas. Low throughput prevents EBL from application in mass production.

EBL electrodes will be used in nanowire fabrication by using designed and synthesized single-stranded DNA templates (Chapter V). The space of electrodes must match the length of DNA templates. The crystallographic length of designed 600 bp DNA is about 204 nm. Here, the minimum space of Au electrodes is designed as 200 nm, in consideration of capability of this EBL-100 exposure system. For longer DNA templates, larger spaces up to 1 μm are also designed. Figure 2.10A and B show the design of EBL electrodes.

Polymethylmethacrylate (PMMA), the E-beam resist, was diluted to 4.5% with 99% chlorobenzene and aged overnight to avoid bubbles. The EBL-100 exposure system was set to the accelerating voltage of 100 kV and the beam current of 200 pA in the dose of 700 mC/cm^2. The exposure was done by Dr. Xu. It took 10 h to write all six electrodes.

Reproduced with permission of the copyright owner. Further reproduction prohibited without permission.

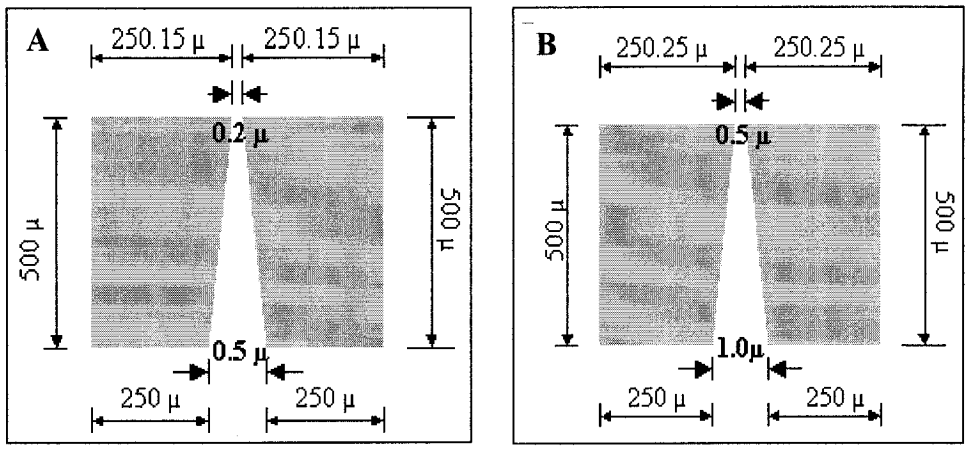

Figure 2.10. Design of EBL electrodes. (A) Electrodes with 200-500 nm gaps; (B) Electrodes with 500-1,000 nm gaps

The detailed procedures are as follows:

1) Clean a wafer with acetone and water; prebake at 190° C for 30 min.
2) Spin coating the 4.5% aged PMMA at 6,000 rpm/s (500 r/s ramping) for 60 sec to achieve film thickness about 350 nm.
3) Soft bake to remove remaining solvent in resist film. Maximum ramping to 180° C for 60 sec.
4) EBL-100 exposure (operated by Dr. K. Xu, IFM).
5) Develop the exposed wafer with isopropanol for 30 sec.
6) Pattern inspection by SEM and AFM.
7) Sputter 3 nm Ti and 22 nm Au.
8) Strip PMMA with acetone at 45° C.

Figure 2.11 shows fabricated Au electrodes with spaces from 200 nm to 3 μm. About 50% of the electrodes were good by the SEM inspection. They are suitable for assembly of nanowires based on ss-DNA templates. Convex spots appeared on developed resist in the first run of EBL writing. These result from bubbles developed in PMMA.

Reproduced with permission of the copyright owner. Further reproduction prohibited without permission.

Inductance coupling plasma (ICP) etcher removed the spots in the CF_4 and O_2 (20%) plasma with the flow rate of 50 sccm.

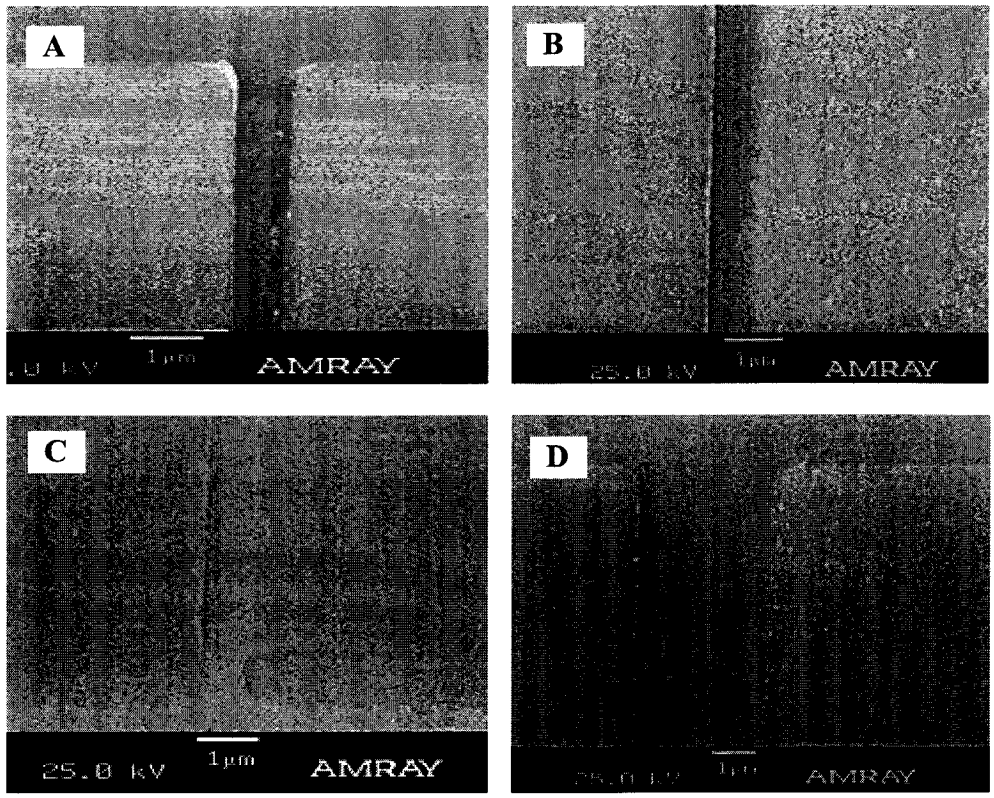

Figure 2.11. Au electrodes fabricated by Electron beam lithography. (A) Space from 200-500 nm. (B) Space from 200-500 nm. (C) Space from 500-1,000 nm (D) Space from 1-3 μm. Each of scale bar represents 1 μm.

Reproduced with permission of the copyright owner. Further reproduction prohibited without permission.

CHAPTER III

ALIGNMENT AND POSITIONING OF DNA

3.1 Introduction

Control of DNA-templated nanostructures requires the ability to manipulate DNA molecules on a surface prior to further processing. Individual DNA molecules must be separated and stretched to serve as templates for nanowire fabrication. The length of a DNA nanowire will be determined by the stretching process. Table 3.1 summarizes three common methods of DNA stretching. Appropriate "interfacing" of DNA and conductive elements by chemical modification or adjustment of conditions is indispensable to the interconnection of DNA-templated nanowires to devices in a nanoscale electronic circuit. This can be realized by a number of different approaches to the specific coupling of DNA to a conductive surface. Advanced manipulation of DNA can be important for the precise positioning of templates.

At equilibrium, a DNA molecule in aqueous solution will usually be randomly structured as a result of thermal fluctuations. Entropy will shorten the end-to-end distance, often to a much smaller size than the contour lengths. A DNA molecule therefore must be stretched to serve as a nanowire template. A common strategy is to tether one end to a surface and then to stretch the molecule by an external force, for example surface tension. Here, principles of various methods to immobilize and stretch

Reproduced with permission of the copyright owner. Further reproduction prohibited without permission.

DNA will be briefly reviewed. In the experiment parts, DNA was aligned by molecular combing, hydrodynamic stretching and spin stretching. Single DNA molecules were orientated and anchored between two 15 μm-space Au electrodes by Au-thiol coupling and hydrodynamic stretching. Cos-ends of λ DNA molecules were modified by the three biochemical reactions (see below). Enzymatic analysis was used to verify ligation of thiol-capped oligonucleotides to the sticky ends of DNA. A fluorescence microscope and AFM were the main tools to characterize alignment and positioning of DNA templates.

Table 3.1. Stretching and positioning of DNA molecules.

Methods	Surface	Chemical modification	Variables	Reference
Molecular combing	hydrophobic(a) hydrophilic(b)	not required	hydrophobicity, meniscus	[57-62]
Electrophoretic stretching	Au, Al, beads(c)	thiol, biotinylation	field strength, frequency	[63-68]
Hydrodynamic Stretching	Au, beads(c), mica	thiol, biotinylation	velocity, viscosity	[69-71, 74,75, 78,79]

(a) Hydrophobic surfaces include silane, polystyrene and polymethylmetacrylate (PMMA). (b) Hydrophilic surfaces include antiDIG, polylysine and dodecanol. (c) Polystyrene beads used in optical tweezers are coated with streptavidin that binds to biotinylated DNA through biotin-streptavidin interaction.

3.2 Review of DNA Stretching

3.2.1 Molecular Combing

Molecular combing was first described by Bensimon *et al.* [57]. Individual DNA molecules or bundles of molecules are stretched by a receding meniscus between the

Reproduced with permission of the copyright owner. Further reproduction prohibited without permission.

substrate and coverslip (Figure 3.1A). The structure of floating potential electrodes (FPEs) used in electrophoretic stretching is shown in Figure 3.1B. DNA solution is deposited on silanized glass and covered. A terminus reacts with surface vinyl groups, anchoring the molecules on the substrate. Surface tension, which acts perpendicular to the meniscus, extends DNA during movement, because this force is greater than the entropic force but smaller than the force needed to break covalent bonds. Combed DNA molecules can be well dispersed and strongly bound to the substrate. In later work, Bensimon *et al.* [58] found that the end-to-end distance of combed bacteriophage λ DNA molecules depended on the character of the substrate surface. On a silanized hydrophobic surface, the length was 21-24 μm, but on an antiDIG hydrophilic surface it was 16-18 μm. The estimated extension force was ~160 pN on silanized glass and ~54 pN on antiDIG-coated glass, in both cases greater than the entropic force. Polystyrene, polymethylmetacrylate (PMMA), and polylysine substrates have been shown suitable for molecular combing [59]. The effectiveness of combing on a hydrophobic surface is highest near pH 5.5.

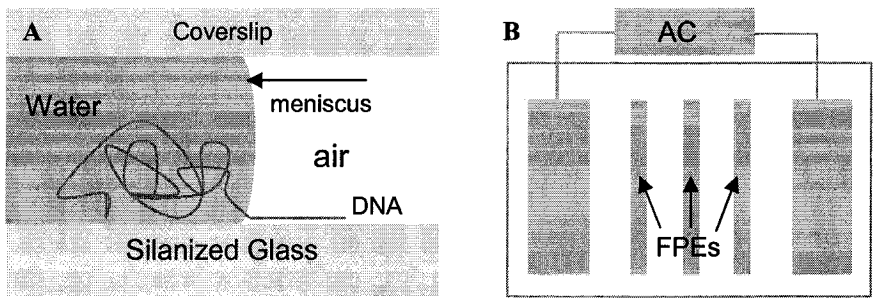

Figure 3.1. Schematic diagram of mechanisms of DNA stretching. (A) Molecular combing. Redrawn from Ref. [57]. Copyright 1994 The American Association for the Advancement of Science. (B) The structure of floating potential electrodes (FPEs) used in electrophoretic stretching. Redraw from Ref. [68]. Copyright 2000 IEEE.

Molecular combing can also be achieved by dipping a silanized coverslip into DNA solution [60]. Termini of DNA molecules bind spontaneously to the substrate. After

Reproduced with permission of the copyright owner. Further reproduction prohibited without permission.

5 minutes of incubation, the coverslip is removed from the solution at a constant speed of 300 μm/s. The meniscus exerts a constant force on the DNA molecules and aligns them. The long molecules become oriented in a single direction over the entire coverslip. For preparation of templates for nanowire fabrication, the length distribution can be narrowed by moving the meniscus at a steady speed to generate a constant extension force on the molecules.

Molecular combing has been improved by mechanical control of meniscus movement after deposition of DNA solution on a silanized substrate [61]. A coverslip is attached to a motor-driven droplet-spreading apparatus that drags the coverslip across the substrate at a certain rate, for example 3 cm/min. Surface tension coupled to controlled movement of the meniscus stretches DNA molecules with high uniformity. Deposition of non-target blocking DNA on the substrate prior to combing compensates for variation in affinity between the target DNA molecules and the surface. Addition of a small amount of $MgCl_2$ to the solution increases the number of stretched molecules on the substrate; Mg^{2+} binds to the sugar-phosphate backbone of DNA. Otobe *et al.* [62] have stretched DNA by moving the substrate instead of the coverslip, with the substrate mounted on a computer-controlled microscope stage. DNA droplets are dispensed on silanized glass through the capillary tip of a microinjector. Relative displacement between capillary tip and substrate controls movement of the meniscus. The shear force generated at a displacement rate of 15 cm/min was found to stretch bacteriophage λ DNA to ~21 μm. An advantage of this method is that DNA molecules can be precisely localized on the substrate and visualized after combing.

Reproduced with permission of the copyright owner. Further reproduction prohibited without permission.

3.2.2 Electrophoretic Stretching

Both direct current (DC) and AC electric fields can be used to stretch DNA. An advantage of the electrophoretic approach is that nanowire templates can be stretched and positioned directly between electrodes. After metallization, electrical properties of nanowires between two electrodes are readily characterized. No further modification of DNA is required.

3.2.2.1 DC Electrophoretic Stretching. Gel electrophoresis is widely used in molecular biology to separate DNA fragments by length. Application of a uniform electric field causes polyanionic chains to migrate toward the anode. The same principle is used to stretch DNA in a DC field. DNA molecules tethered at one end in solution are stretched by an applied electrophoretic force. Tethering is accomplished in a variety of ways. For example, a terminus of a DNA molecule can be bound to a bead trapped by optical tweezers or immobilized to a solid support by chemical coupling.

Smith *et al.* [63, 64] have studied the relationship of DNA extension to external electric field strength by assuming that DNA molecules are uniform polyionic chains. Plasmid DNA (66 kb) and bacteriophage λ DNA (48.5 kb) were immobilized in agarose gel. Both molecules behaved like entropic springs and became fully extended in a low electric field. In the absence of an electric field, λ DNA molecules are random coils and the average end-to-end distance is only ~1.47 μm. Stretching DNA by "free electrophoresis" (without a gel) has been reported by Zimmermann *et al.* [65]. A gold surface was coated with a layer of biotin thiol. Lambda DNA biotinylated at one end was bound to the substrate by way of streptavidin-labeled beads. DNA thus tethered was stretched in a 5 V/cm DC field. The non-covalent bonds of the Au-biotin-streptavidin-

Reproduced with permission of the copyright owner. Further reproduction prohibited without permission.

biotin-DNA construct held fast and allowed chromosomal DNA molecules to be stretched to its full length.

3.2.2.2 Dielectrophoretic Stretching. Dielectrophoresis (DEP) is a non-uniform field effect. It aligns dipolar objects parallel to the direction of the electric field. A DNA molecule is polarizable because its polyanionic backbone is surrounded by a cloud of counterions at equilibrium. When the frequency and field strength are high, the applied electric field stretches polarized DNA molecules to their full length and orients them parallel to the field. The molecules then migrate toward one electrode or the other by dielectrophoresis. If the electrode is made of electrochemically active metal such as aluminum, the DNA end in contact with the electrode can become permanently anchored.

The effect of DEP on DNA has been studied by Washizu *et al.* [66-68]. In a 1 MHz and $>1\times10^6$ V/m field, bacteriophage λ DNA was stretched and positioned between two electrodes. Termini of the DNA molecules became tightly bound to the electrodes. In some cases, however, one end only of DNA becomes bound to an electrode, and an applied field generates thermal hydrodynamic flow and fluctuation of liquid near the electrodes, decreasing reproducibility. Floating-potential electrodes (FPEs) have been designed to reduce thermal fluctuations. The potential is not applied to the floating electrodes, reducing thermal flow near them. The two outer electrodes generate a dielectrophoretic force that influences DNA structures (Figure 3.1B). This approach was found to increase the number of stretched and positioned DNA molecules.

Reproduced with permission of the copyright owner. Further reproduction prohibited without permission.

3.2.3 Hydrodynamic Stretching

Another widely used method is to stretch DNA by hydrodynamic flow. DNA tethered at one end is stretched by the shear force generated by the momentum gradient between the applied flow and the DNA chain. Aligned molecules are oriented in the direction of the flow. The end-to-end distance of extended DNA depends mainly on the velocity of flow and viscosity.

Perkins *et al.* [69, 70] have investigated extension and relaxation of DNA in applied steady flow. Figure 3.2A shows a schematic diagram of the apparatus. One end of a DNA molecule is attached to a 1 μm bead trapped by optical tweezers. A drag force is provided by constant hydrodynamic flow. DNA molecules are stretched by a flow of 2 μm/s or greater (Figure 3.2B). The fractional extension is related to the viscosity, velocity, and contour length by a power law, consistent with the worm-like chain model for DNA extension under an applied force. The same authors have also studied relaxation of fully extended DNA. Immediately after cession of flow, free ends of DNA recoil rapidly and visual length decreases by 30% within a few seconds. Relaxation is slower thereafter. For example, a 39.1 μm-long DNA molecule recoiled to ~6 μm during the initial 50 seconds of relaxation. At the end of relaxation, some molecules appeared as ~1 μm diameter compact balls. Smith *et al.* [71] have studied the mechanics of single DNA molecules. Force-measuring laser tweezers were used to stretch λ DNA to its contour length by a ~10 pN force. A ~65 pN force extended DNA to ~170% of its contour length. The structure of B-DNA is altered by overstretching.

Reproduced with permission of the copyright owner. Further reproduction prohibited without permission.

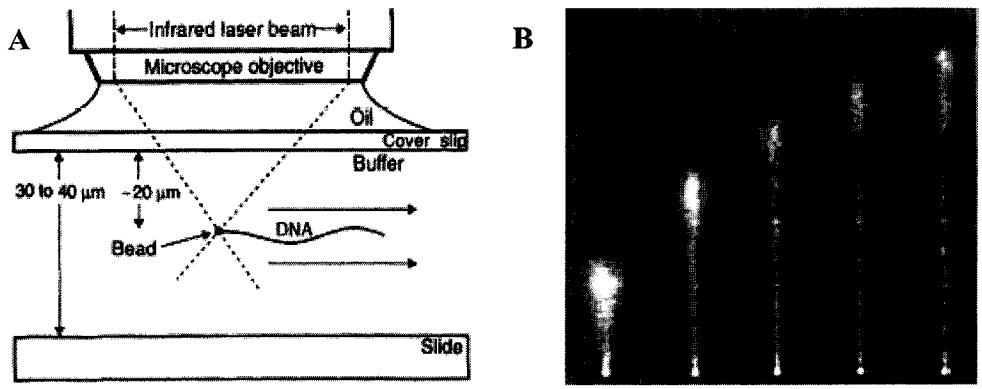

Figure 3.2. Stretching DNA by hydrodynamic flow. (A) Schematic diagram of apparatus. Reprinted from Ref. [69]. Copyright 1994 The American Association for the Advancement of Science. (B) Time-averaged fluorescence micrograph of a DNA molecule (67.2 μm) stretched in a 0.95 cP fluid flow with a velocity of 2, 4, 6, 8 or 10 μm/s. The ratio of extended length to the contour length was 19, 33, 44, 50 and 55% (left to right). Reprinted from Ref. [70]. Copyright 1995 The American Association for the Advancement of Science.

Spin stretching is a simple and effective method of aligning DNA. No chemical modification is needed [72, 73]. Viscous force generated by rotational flow extends the polymer. DNA molecules on silanized glass spun at 3000-5000 rpm become aligned and stretched. At the periphery of the DNA solution, molecules are more extended than those near the center. The higher linear speed at the periphery leads to a higher viscous force on the DNA molecules and a greater end-to-end distance after stretching.

Molecular combing is an effective approach to stretching and dispersing individual DNA molecules. The end-to-end distance of aligned DNA is determined by surface hydrophobicity and control of meniscus movement. As with spin stretching, molecules are randomly distributed on the surface. By contrast, DNA tethered at one end can be stretched by an electrophoretic force or shear force and localized more precisely on a substrate, for example between two electrodes. Au-thiol or biotin-streptavidin coupling is often used to immobilize a DNA terminus on a substrate. In hydrodynamic

Reproduced with permission of the copyright owner. Further reproduction prohibited without permission.

stretching, DNA molecules are oriented by the direction of applied flow. The velocity and viscosity of flow determine the end-to-end length of aligned molecules. Polarized DNA can be stretched and positioned in a AC field with high strength and frequency.

3.3 DNA Alignment

Dehydrated DNA molecules on a surface may assume quite distinctive conformations – balls, networks, worm-like chains, bending loops and knots, etc. because of aggregation of molecules. Morphology of dehydrated DNA molecules depends on DNA concentration, buffer conditions, surface characteristics, and various interactions between the molecules and the surface. The molecular mechanics and physics are complex and beyond this topic. Here, I mainly focus on practical aspects in separation and alignment of DNA molecules that will serve as nanowire templates.

Lambda DNA bacteriophage (New England Biolabs), isolated from the bacterium *E. coli*, was used for all experiments. The molecule has ~48,500 base pairs and the crystallographic length of ~16 μm. It has been widely used in DNA-templated fabrication of nanowires and other DNA-based nanoassembly. YOYO®-1 iodide (Molecular Probes, USA), a dimeric cyanine dye for nucleic acids, was used to stain DNA in all samples for fluorescence microscopy. The dye molecule binds to DNA by intercalating itself between base pairs. DNA-YOYO complex is excited by light at the 491 nm wavelength and emits green light at the 509 nm wavelength. High quantum yield enhances the visibility of DNA-YOYO complexes in a microscope. All images were taken by the fluorescence microscopic system (TS100F inverted microscope, Coolpix 4700 digital camera, Nikon, Japan) attached with an oil immersion 100 × objective lens at Dr. Haynie's lab. The size

Reproduced with permission of the copyright owner. Further reproduction prohibited without permission.

scale of fluorescence images was calibrated by a Richardson test slide (Gen III, Electron Microscopy Sciences, USA). The tapping mode of AFM was used to characterize samples in air. Equipped silicon nitride cantilever tips have resonance frequency about 175 KHz. All micrographics were taken at 1-2 Hz scanning rate. Sample substrates were microscopic glass coverslip or silanized glass (Electron Microscopy Sciences, USA).

3.3.1 Evaporation

Evaporation is a simple way to characterize molecular macroscopic conformations as a reference of stretched and combed DNA molecules. DNA-YOYO complex solution with various DNA concentrations was pipetted to glass substrates. After evaporation in chemical hood for 10-20 min, samples were rinsed with water and imaged by the fluorescence microscope and AFM. The detailed procedures of preparation of fluorescence samples are as follows:

1) Dilute YOYO-1 10,000 fold with 1× TBE buffer (10.8 g/L Tris, 5.5 boric acid, 0.93 g/L EDTA, pH 8).
2) Pipette 1 μL stock DNA (500 ng/μL) into appropriate amount of diluted YOYO solution to reach the ratio of 5:1, DNA base pairs to dye molecules.
3) Incubate the mixture at room temperature for 1 h to allow binding.
4) Pipette 10-20 μL DNA-YOYO complex on glass.
5) Evaporate at the ventilation chemical hood for 20-30 min.
6) Rinse off unwanted salts.
7) Fluorescence microscopy.

Reproduced with permission of the copyright owner. Further reproduction prohibited without permission.

Figure 3.3 shows the four typical conformations of dehydrated DNA molecules on a surface. At high concentrations, one or a few DNA molecules aggregated into a 2-5 μm ball (Figure 3.3A) which connected duplexes into a large scale network. The ball structures possibly result from coiled DNA in the solution. DNA molecules also form into tree-like macroscopic structures with stems and branches (Figure 3.3B). The stems and branches are likely bundles of molecules that aggregated together. They are usually much longer and thicker than individual molecules. The thinnest DNA appears on the top of the DNA trees. Another typical conformation is the open loop of DNA, composed by single or multiple molecules after evaporation (Figure 3.3C). Most of them were not closed. After evaporation DNA tends to aggregate on the edge of droplets (Figure 3.3D). This happens to almost all evaporation samples. The reason is possibly the surface tension that drags DNA from liquid to the air-water interfaces to achieve minimum surface energy.

It is widely reported that AFM can be used to characterize topography of individual DNA molecules. Fluorescence microscope samples suggested that low concentration favors to separate individual polymer chains from compact bundles. In a typical experiment, stock DNA was diluted to 0.5-0.1 ng/μL with 1× TE buffer (10 mM Tris, 1 mM EDTA, pH 8). 10-20 μL solution was pipetted onto coverslip or silane slide. After evaporation in air samples, were rinsed with DI water.

Reproduced with permission of the copyright owner. Further reproduction prohibited without permission.

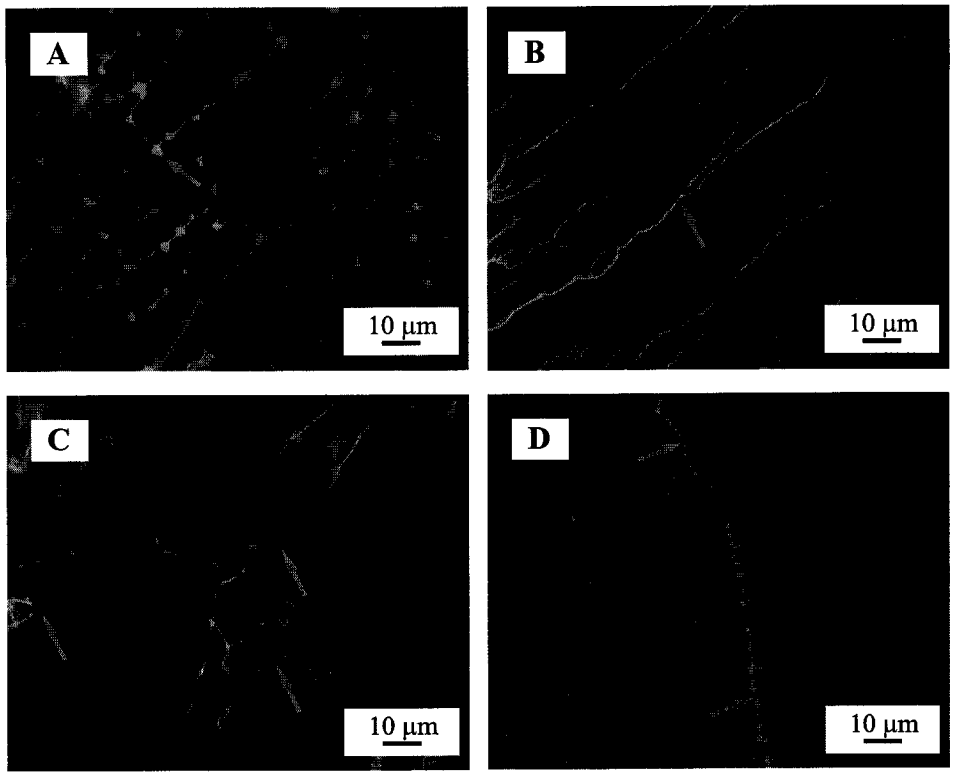

Figure 3.3. Fluorescence images of evaporated DNA molecules on glass. (A) Networks connected by ball-like junctions after evaporation of 25 ng/μL DNA. (B) The tree-like structures after evaporation of 10 ng/μL DNA. (C) Loops and knots after evaporation of 1 ng/μL DNA. (D) The Droplet edge after evaporation of 0.5 ng/μL DNA.

AFM provided much smaller scanning areas and better resolution than optical imaging systems. Individual molecules were found in the 2.5 × 2.5 μm field (Figure 3.4A). Most of them, however, aggregated into multi-stranded chains or bundles after evaporation at the concentration of 0.5 ng/μL. Network and loop structures were also obvious. The apparent height of single molecules averages 0.8-1 nm, much smaller than the 2 nm crystallographic diameter. In addition, the apparent width was much larger than 2 nm. This indicates the well-known convolution effect of AFM tips in AFM images for soft materials. Reduction of sample concentrations helped separate DNA bundles and remove inter-stand networks. Figure 3.4B shows a closed DNA loop composed of a

Reproduced with permission of the copyright owner. Further reproduction prohibited without permission.

single molecule after evaporation of DNA at the concentration of 0.1 ng/μL. Since DNA is a polymer with contour length much larger than its persistence length, it is often thought of as worm-like chains. The structure of DNA in liquid is most likely kept after evaporation. Long entropic elastic rods are easy to recoil or bend. As a result, complex intra-strand loops form after dehydration.

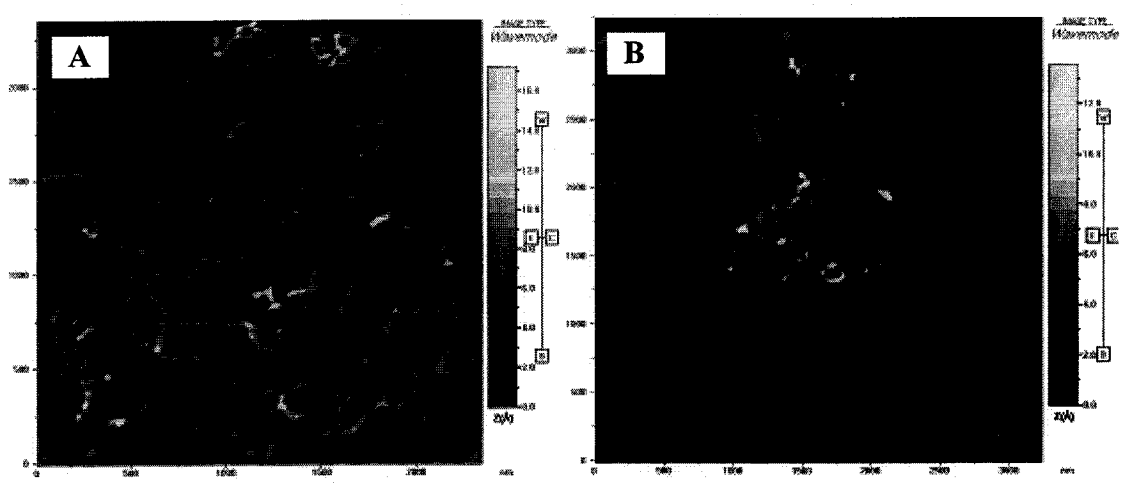

Figure 3.4. AFM micrographs of evaporated DNA molecules on glass. (A) Network structures after evaporation of 0.5 ng/μL DNA; image size 2.5 × 2.5 μm, height scale 1.7 nm. (B) Randomly coiled loops composed by a single molecule after evaporation of 0.1 ng/μL; image size 3 × 3 μm, height scale 1.3 nm.

3.3.2 Molecular Combing

Although DNA may be extended and orientated through evaporation on occasion, most dried molecules are randomly distributed on the surface with various uncontrollable conformations. More reliable methods must be performed to separate and align individual molecules. Molecular combing is simple but efficient for this purpose. The key of molecular combing is that extension force is greater than entropic force but smaller than the force to break covalent backbones of DNA. The force is strongly determined by surface property. Octadecylchlorosilane was used to form a monolayer covalently bound

Reproduced with permission of the copyright owner. Further reproduction prohibited without permission.

on glass substrate. Silane treated surfaces are hydrophobic because of exposed alkyl groups [74]. Therefore, hydrophobic aromatic bases of sticky ends of λ DNA will attach to silane substrate through hydrophobic interaction. Hydrophobicity was verified by measurement of contact angle of surfaces. One-end-tethered DNA was aligned by meniscus in air-water interface.

The detailed procedures of molecular combing are as follows:

1) Clean glass coverslips with acetone, ethanol and DI water. (Only clean glass surface have free OH groups that are necessary for silane coating.)
2) Immerse cleaned coverslips into silane solution (1% silane in 99% toluene) for 1 h; rinse with toluene and dry with nitrogen gas three times.
3) Pipette 10-20 μL YOYO-stained DNA solution (0.5-0.1 ng/μL, 1× TE, pH 8.0) onto silanized surface.
4) Incubate for 0.5 h to allow hydrophobic interaction.
5) Cover the droplet with a unmodified clean coverslip.
6) Incubate overnight; rinse with DI water and dry with nitrogen gas.
7) Fluorescence microscopy.

Figure 3.5 shows combed DNA at different concentrations. Distribution of end-to-end length of extended DNA resulted from non-uniform local meniscus and interaction between DNA molecules at higher concentrations (Figure 3.5A-B). Since surface tension is in the range of tens to hundreds of pN, even small variations of surface treatment may have an effect on DNA stretching. Samples at low concentrations were extended with uniform length distribution. The average end-to-end distance was estimated to be ~21 μm, 131% of its crystallographic length (Figure 3.5C-D). Combed individual DNA

Reproduced with permission of the copyright owner. Further reproduction prohibited without permission.

molecules were well dispersed and strongly bound to the silanized surface. They were stable up to a few weeks at 4° C.

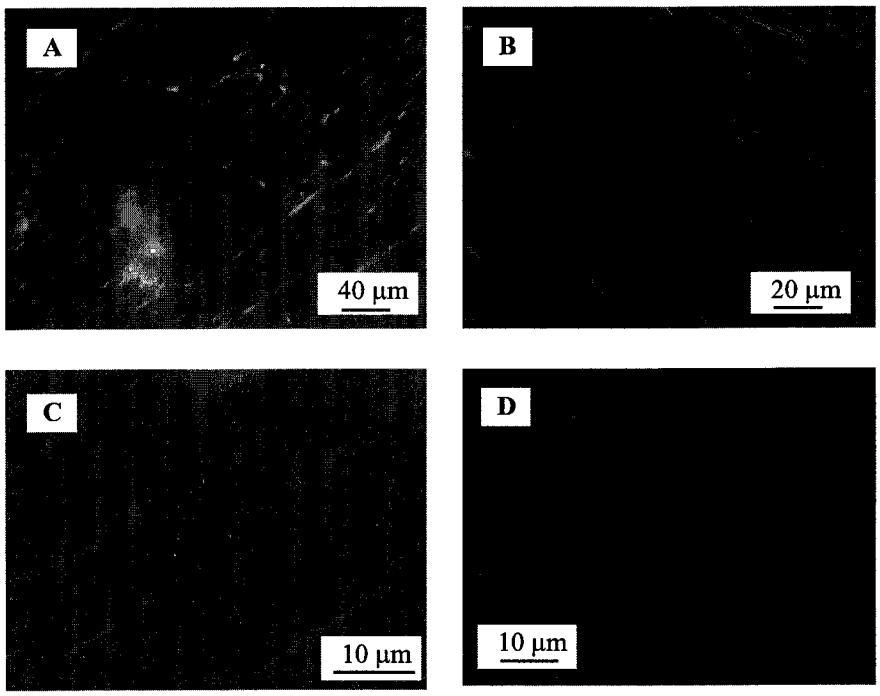

Figure 3.5. Fluorescence images of combed DNA on silanized glass. DNA concentration is 0.5 ng/μL in A and B, and 0.1 ng/μL in C and D.

As a molecule is stretched beyond the entropic limit, where extension is larger than its B-form contour length, DNA molecules can be considered as a stretchable solid. The extended length is approximately proportional to the extending force [57, 58]. The average surface tension on silanized surface acting on DNA is estimated by the equation to describe a linear elastic spring:

$$F = E \times A \times (x / L - 1)$$

where F is the extension force, E is the Young's modulus, A is the cross area, x is the extension, and L is the natural contour length. By taking E as ~ 1 $\times 10^{9}$ N/m^2 [75], A as 3.14 $\times 10^{-18}$ m^2 and x/L as 1.3, the calculated extension force perpendicular to combed

Reproduced with permission of the copyright owner. Further reproduction prohibited without permission.

molecules is ~ 97 pN. The extending force and experimental extension (21 μm), however, do not match with the curve of force versus extension reported by Smith et al. [71]. This discrepancy probably results from the factor that as dsDNA is stretched to 130% of its contour length, the polymer is in the range of overstretching transition. The linear elastic model is not suitable any more. The surface tension, however, is much less than 500 pN that is the breaking force for covalent bound molecules [58].

3.3.3 Hydrodynamic Stretching

Spin stretching was performed on a silanized glass; the procedures are as follows:

1) Rinse silanized glass coverslip (for the preparation method see 3.3.2) with DI water; fix it on the spinner.
2) Pipette 10 μL 1 ng/μL YOYO-dyed DNA on coverslip for 20 min to allow adsorption.
3) Spin at 5,000 rpm for 1 min; rinse with water.
4) Fluorescence microscopy.

Figure 3.6 shows stretched λ DNA on silanized glass with the spinning rate of 5,000 rpm. Nearly all DNA was stretched straightly and distributed radially on surface. Molecules at the peripheral area of the droplet center (Figure 3.6A) extended more straightly than those near the droplet center (Figure 3.6B). Higher linear speed at peripheral areas led to higher viscous force that stretched DNA to longer end-to-end distances. The shear force can be estimated by the simplified Stokes model, assuming rotating flow laminar. The stress on the droplet disk was estimated by the equation:

$$\tau = 0.8 \times \mu \times r\sqrt{\omega^3 / \nu}$$

Reproduced with permission of the copyright owner. Further reproduction prohibited without permission.

where the viscosity μ equals to 0.01 poise (water), the angular spinning rate ω equals to 523 rad/s, and the kinetic viscosity ν equals to 0.01 stokes for water. Estimated shear force acting on DNA molecules at $r = \sim 1$ cm is about 10 pN which extends a dsDNA molecule to about its B-form contour length. The estimated force and experimental extension match with the Smith's curve [71].

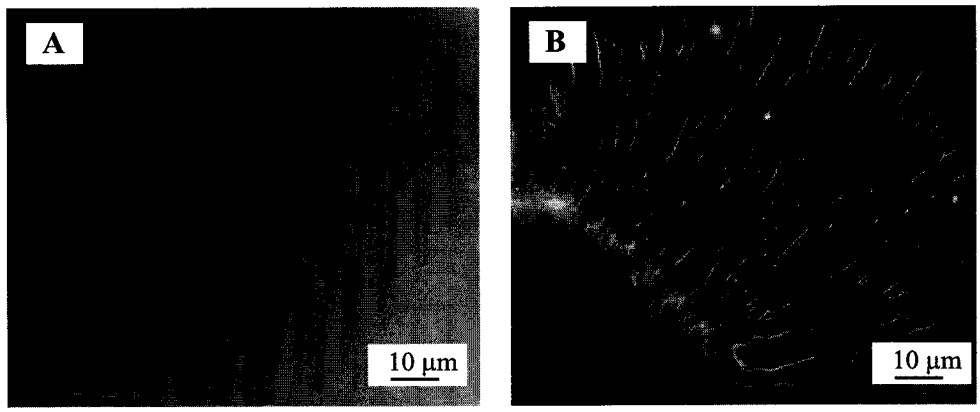

Figure 3.6. Fluorescence images of spin-stretched DNA. Spin at the speed of 5,000 rpm. (A) DNA at peripheral area of droplet (r = ~ 1 cm) (B) DNA near the spinning center.

The other simple way to align DNA is found in experiments for metallization of DNA (Chapter V). DNA adsorption on a freshly cleaved muscovite mica (Grade-1, SPI Supplies, USA) was often imaged by AFM to monitor changes of sample topography as a result of metallization. Many molecules, if not all, were aligned in the direction of flow of nitrogen gas that is used to dry samples after 15-20 min adsorption. Figure 3.7 shows two such samples. The possible mechanism was that the viscous force, similar to the one used in hydrodynamic stretching, extends DNA chains. The extension force was generated by velocity gradient between the moving buffer (10 mM HEPES, 5 mM $MgCl_2$) and immobilized DNA.

Reproduced with permission of the copyright owner. Further reproduction prohibited without permission.

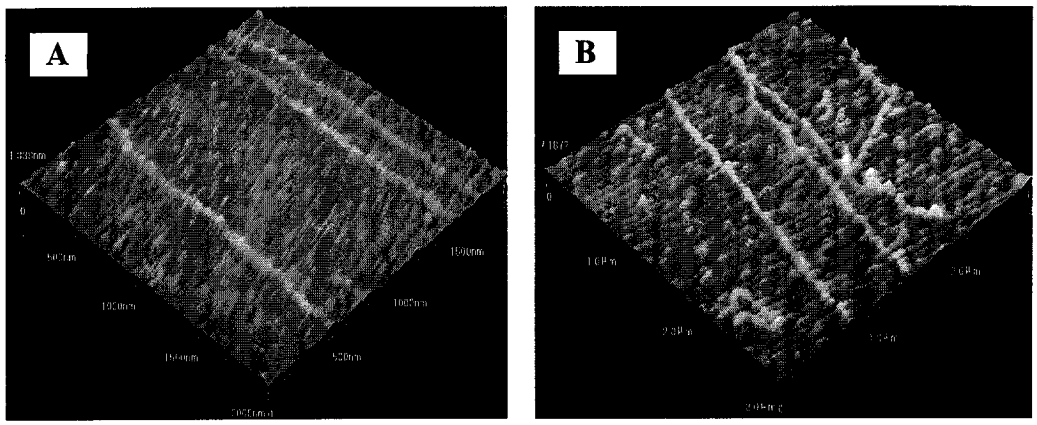

Figure 3.7. AFM micrographs of DNA stretched by hydrodynamic flow. (A) 2 × 2 μm with the height scale of 1.3 nm; (B) 3 × 3 μm with the height scale of 0.8 nm. 1-2 ng/μL λ DNA was pipetted on mica for 20 min and then rinsed with water and dried with nitrogen gas.

3.4 Positioning of DNA Between Electrodes

Reliable interface between nanowire and specific surface is a key to realize its function of "wiring" in electronic devices. Nanowires may interconnect conducting elements in nanocircuits by DNA-surface coupling. I will discuss principles and experiments to connect two adjacent Au electrodes by single DNA molecules through Au-thiol coupling and hydrodynamic stretching. The basic strategy and procedures are illustrated in Figure 3.8. Each of cos sticky ends (12 bases) of λ DNA is capped with a sulfhydryl (thiol) group by hybridization and ligation. One end of DNA is attached to one Au electrode through Au-thiol coupling. DNA was stretched by micropump-controlled dipping flow. The other end of DNA is anchored to the other electrode through Au-thiol coupling.

Reproduced with permission of the copyright owner. Further reproduction prohibited without permission.

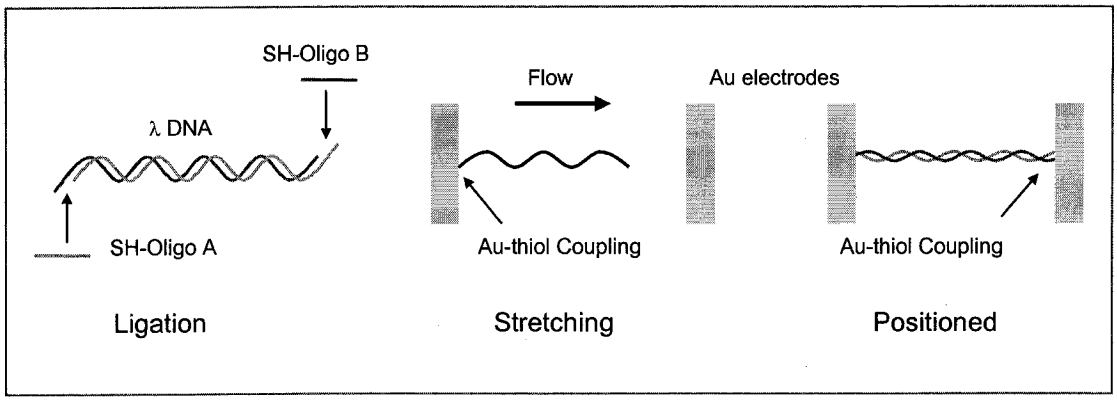

Figure 3.8. Schematic diagram of stretching and positioning of single DNA molecules between Au electrodes.

3.4.1 Hybridization and Ligation

Hybridization and ligation play irreplaceable roles in molecular biology. Hybridization is a thermal process where two single strands of DNA with complementary bases form relatively stable double helix. Two strands are held by hydrogen bonds. Unique molecular recognition of nucleic acids ensures that base A only pairs with base T, and base G only pairs with base C (Chapter I). Ligation is a biochemical reaction where 3'-hydroxyl group of one strand of DNA attacks 5'-phosphate group of another adjacent stand. As a result, a covalent phosphodiester bond forms and two pieces of DNA joint together. Ligation reaction must be catalyzed by a specific ligation enzyme, for example, T4 DNA ligase.

The thiol (SH) modified oligonucleotides (Oligo) A and B were from Alpha DNA, Inc. The sequence of Oligo A (12 bases) was 5'-GGGCGGCGACCT-3'-SH, complementary to one sticky end of λ DNA. The sequence of Oligo B (12 bases) was 5'-AGGTCGCCGCCC-3'-SH, complementary to the other sticky end of λ DNA. Prior to ligation of oligos to DNA, two oligos were phosphorylated by using T4 polynucleotide kinase (M0201S, New England Biolabs, USA) that catalyzes the transfer of phosphate

Reproduced with permission of the copyright owner. Further reproduction prohibited without permission.

groups from γ position of ATP to the 5' terminus of Oligo A and B. The presence of phosphate groups at the 5' ends of oligos is a must for ligation.

Two levels of undesired self-ligation of λ DNA may be not avoidable without dephosphorylation. The first level is intra-strand ligation: two complementary sticky ends of one DNA molecule might ligate together and form a DNA circle. The second level is inter-stand ligation: the sticky end of one molecule might ligate to the sticky end of another molecule and form λ DNA concatemers. To avoid these two ligations, dephosphorylation of λ DNA was performed in the presence of alkaline phosphatase from calf intestinal (CIP, New England Biolabs) to remove 5' phosphates from λ duplex. Hybridization of phosphorylated oligos to dephosphorylated λ DNA was carried out in the thermocycler (TC-512, Techne). T 4 DNA ligase (M0208S, New England Biolabs, USA) are used in all ligation experiments. Detailed procedures for these three reactions are as follows:

Reaction 1: Phosphorylation of Oligo A and B:

1) Mix 1.2 μL oligo (200 μM) with 42.8 μL water (Millipore, 18.2 MΩ) and 5 μL 10 × ligase buffer (containing 10 mM ATP).
2) Add 1 μL kinase (10 Units).
3) Incubate at 37° C for 40 min.
4) Heat inactivation at 65° C for 20 min.

Reaction 2: Dephosphorylation of λ DNA:

1) Mix 10 μL stock DNA (16 nM) with 89 μL 1× NEBuffer 3.
2) Add 1 μL diluted CIP (0.1 Unit).
3) Incubate at 37 °C for 60 min.

Reproduced with permission of the copyright owner. Further reproduction prohibited without permission.

Reaction 3: Hybridization and ligation:

1) Purify dephosphorylated DNA with QIAEX II (Qiagen).
2) Add 40 μL phosphorylated oligo to ~ 10 μL DNA from the step 1; keep at least 2000:1 molar ratio of oligo to DNA; concentration was determined by absorbance at 260 nm.
3) Anneal the mixture from step 2 in the thermocycler; step down temperature uniformly from 75 to 4° C for 4 h.
4) Mix 45 μL solution from the step 3 with 5 μL 10× ligase buffer and 1 μL T4 DNA ligase; spin down and gently mix with pipette.
5) Incubate at RT for 1 h; heat inactivation at 70° C for 20 min.
6) Purify with QIAEXII.
7) (Option) Ligate the other oligo to products from the step 6; repeat step 2-6.

3.4.2 Enzymatic Analysis

Subtle changes of λ DNA molecules, for example, dephosphorylation and ligation with small oligos, were not ready to confirm. Restriction endonuclease analysis and gel electrophoresis, however, can be combined to verify each of those changes. The principle of restriction enzymes and gel electrophoresis will be discussed in Chapter V. Here, I'll describe the analytic approach and experiment to confirm that the thiol-modified oligos have been ligated to cos ends of λ DNA after these three reactions. Restriction enzymes, *Hind III* and *Nru I* were from New England Biolabs.

The basic strategy is that only dsDNA fragments having a phosphate group on at least one of two 5' ends is ligatable. Unmodified λ DNA can self-ligate into a circle or

Reproduced with permission of the copyright owner. Further reproduction prohibited without permission.

concatemer. In contrast, dephosphorylated λ DNA (simplified as De-P λ) and λ DNA that has been ligated to oligos (simplified as Oligo A-λ, Oligo B-λ and Oligo A-λ-Oligo B) can not self-ligate. After λ DNA, De-P λ, and Oligo-λ were subjected to conditions of self-ligation by using T4 DNA ligase, products will have different patterns in gel electrophoresis after restriction digest.

Hind III digests λ DNA into 6 fragments, 2 kb, 2.3 kb, 4.3 kb (end), 6.6 kb, 9.4 kb, and 23 kb (end). The digested pattern is in the lane 4-7 (Figure 3.9A). In gel electrophoresis, self-ligated and then *Hind III* digested λ DNA should have an additional band of 27.3 kb (4.3 kb + 23 kb) that results from circularization or concatemerization of λ DNA during self-ligation, even if efficiency of self-ligation would not be high. Furthermore, the 4.3 kb band should lose part of intensity, because part of the fragments was incorporated in the extra 27.3 kb. The lane 3 in Figure 3.9A, for example, was the product of λ DNA after self-ligation and *Hind III* digestion. The 4.3 kb band was nearly invisible by comparison with the 2 kb and 2.3 kb bands. This indicates part of 4.3 kb contributed to λ DNA circles or concatemers during self-ligation. The other indicator, the additional 27.3 kb band that should be present, however, can not be separated from the 23 kb band in a 0.7% agarose gel.

Use of *Nru I* digestion was able to overcome this problem. It cuts λ DNA into 6 fragments, 0.7 kb, 3.7 kb, 4.6 kb (end), 6.7 kb (end), 9.4 kb and 23.5 kb. The extra band, 11.3 kb (4.6 kb + 6.7 kb) fragment, resulting from self-ligation and then *Nru I* digestion, would be resolvable from the nearest 9.4 kb. The lane 3-6 in Figure 3.9B was from *Nru I* digested fragments of λ DNA (the 0.7 kb moved fastest and was out of the gel image).

Reproduced with permission of the copyright owner. Further reproduction prohibited without permission.

The extra band of 11.3 kb, however, was present without self-ligation. This fake ligation must result from the self-annealing of cos-ends of λ DNA (Tm, ~55° C) before loading.

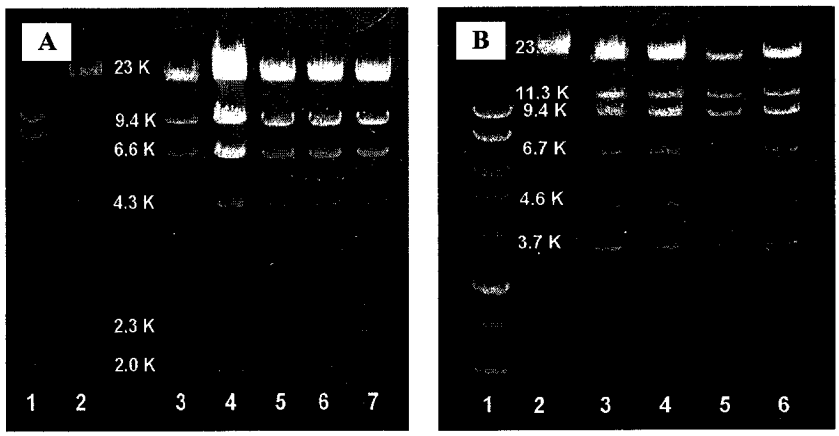

Figure 3.9. Gel electrophoresis of restriction digested λ DNA fragments. (A) *Hind III* digestion. Lane 1: 1 kb ladder (Promega); Lane 2: λ DNA; Lane 3: λ DNA after self-ligation and digestion; Lane 4-7: λ DNA after digestion. (B) *Nru I* digestion. Lane 1: 1 kb ladder; Lane 2: λ DNA; Lane 3-6: λ DNA after digestion. (0.7% agarose gel in 60 V).

Figure 3.10 shows gel electrophoresis images for *Nru I* digestion analysis to approve dephosphorylation (reaction 2) and ligation of oligos to λ DNA (reaction 3). No special design for approval of phosphorylation of oligos (reaction 1) is needed because reaction 3 bases reaction 1. De-P λ was subjected to self-ligation and then followed by *Nru I* digestion before gel analysis (Figure 3.10A, lane 5-6). False ligation was ruled out by heating and rapid cooling samples prior to loading. No 11.3 kb band was present, indicating that De-P λ was not self-ligated into either circles or concatemers because phosphate groups were removed from the 5' end of De-P λ. In contrast, the 11.3 kb band was present in lane 4, indicating that λ DNA was self-ligated into a circle or concatemers. In addition, the intensity of bands of 4.6 kb and 6.7 kb was less than 3.7 kb, unlike the

Reproduced with permission of the copyright owner. Further reproduction prohibited without permission.

intensity in lane 5-6, where relative intensity of all 5 bands presented a sense of gradient by ratios of molecular weights of the fragments.

Fake ligation was ruled out by heating samples at 65° C for 10 min and rapid cooling in ice immediately before loading into gel. In lane 2 (Figure 3.10B), for example, no 11.3 kb band appeared after the heat treatment. The other advantage of *Nru I* digested maps is that the digestion is a blunt-end cutting. In normal ligation conditions, the only re-ligatable digested fragments are 4.6 kb and 6.7 kb that have the cos sticky ends. Success of ligation of Oligo A or Oligo B to λ DNA was approved in lane 4-5 in Figure 3.10B, respectively. These two modified λ DNA was not self-ligated during self-ligation because of the lack of sticky ends. Lane 3 was the control sample and resulted from self-ligation and digestion of λ-DNA. Similar to lane 4 (Figure 3.10A), there was the extra band 11.3 kb, indicating that λ-DNA was self-ligated to circles or concatemers during the same self-ligation condition as lane 4-5.

Reaction 3 was further approved by re-ligation of digested fragments (Figure 3.9C). The end fragments 4.6 kb and 6.7 kb from stock λ DNA digestion (Figure 3.10B, lane 2) were extracted and re-ligated. The 11.3 kb band was present (Figure 3.10C, lane 2). In contrast, no 11.3 kb band was present in lane 3, which was the re-ligation product of extracted 4.6 kb and 6.7 kb from lane 4-5 in Figure 3.9B. Digested fragments of Oligo A-λ and Oligo B-λ were not re-ligatable: one end of these modified λ DNA was covered by oligo and the other end was blunt because of *Nru I* digestion.

Oligo A-λ and Oligo A-λ-Oligo B synthesized and verified as above were stored at -20 °C for all following stretching experiments. One mM dithiothreitol (DTT) was

Reproduced with permission of the copyright owner. Further reproduction prohibited without permission.

added to avoid oxidation of thiol groups. QIAEXII purification must be performed to remove excessive oligos and DTT immediately before use.

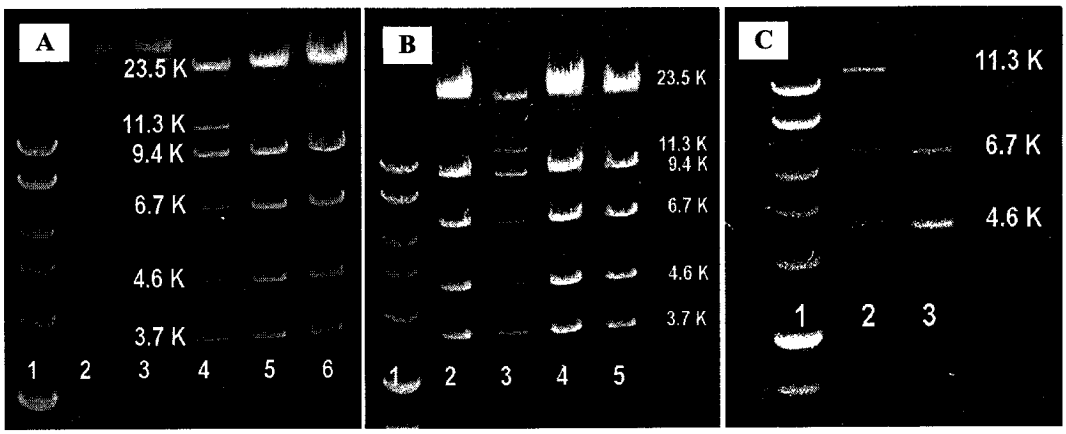

Figure 3.10. Gel electrophoresis for *Nru I* digestion analysis. (A) Approval of dephosphorylation. Lane 1: 1 kb ladder; Lane 2-3 λ DNA; Lane 4: λ DNA after self-ligation and digestion; Lane 5-6: De-P λ after self-ligation and digestion; (B) Approval of OligoA-λ and OligoB-λ. Lane 2: λ DNA after digestion; Lane 3: λ DNA after self-ligation and digestion; Lane 4: OligoA-λ after self-ligation and digestion; Lane 5: OligoA-λ-OligoB after self-ligation and digestion; (C) Religation analysis. Lane 2: ligation of fragments 4.6 k and 6.7 k from Lane 2 (B); Lane 3: ligation of fragments 4.6 kb and 6.7 kb from Lane 4-5 (B). (0.7 % agarose gel in 60 V)

3.4.3 Alignment and Positioning

One end of modified DNA templates must be tethered onto Au surface through Au-thiol coupling prior to stretching. Substantial literatures have reported thermodynamics and kinetics of formation of various self-assembled monolayers based on Au-thiol coupling [76-77]. It is stated unanimously that thiol groups quasi-covalently binds to Au with high efficiency and reliability, although many factors remain unclear. Here, the most common conditions reported in Au-thiol coupling were followed for a general qualitative analysis. Contact angle measurement system (OCA15, Future Digital Scientific, USA) was utilized to monitor hydrophilicity changes of Au electrode surface after soaked into oligo-SH solution.

Reproduced with permission of the copyright owner. Further reproduction prohibited without permission.

Cleanliness of Au surface is critical to immobilize thiolated oligos. Electrodes were treated with the piranha solution (1 v. of 30% H_2O_2, 3 v. of 98% H_2SO_4) for 20 min, and followed by rinsing with acetone and DI water. Alternatively, Nanostrip solution (Cyantek Corp., CA) was substituted to the piranha for safety reason. Cleaned electrodes were stored in 100% ethanol for further use. Figure 3.11 shows that contact angles of water droplets on Au surface changed from 60° C before electrode soaking to 42° C after. The measurement was taken after immersion of cleaned electrodes in 1 μM oligo-SH solution for 0.5 h and rinsing with DI water. The decrease of contact angles qualitatively demonstrated that oligo-SH molecules were coated on fabricated Au electrodes during incubation. The modified surface was more hydrophilic because of exposed phosphate groups of immobilized nucleic acids.

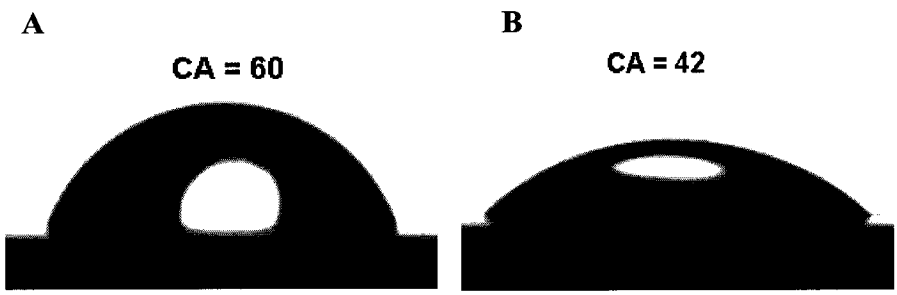

Figure 3.11. Contact angles of Au electrode surface. (A) Before oligo-SH immobilization. (B) After immersion of electrodes in 1 μM oligo-SH solution for 1 h.

Construction of individual DNA molecules across two electrodes is a real trial-and-error experiment. Many unpredictable factors sometime may overshadow those plausible hypotheses about the mechanics of a single polymer chain [69-71]. Two scenarios involved in construction of DNA bridges across two electrodes are possible. The first is to directly apply flow and stretch droplets of Oligo A-λ-Oligo B that has been covered on two Au electrodes. It was not possible to cover one droplet only on one of two

Reproduced with permission of the copyright owner. Further reproduction prohibited without permission.

16 μm-spaced electrodes without a more sophisticated micromanipulator. The problem of this scenario is the possibility of both ends of Oligo A-λ-Oligo B to attach on one electrode. Half of the molecules, however, may have one free end. The key is to heat the droplets to provide thermal energy and thus unwind random coils during incubation. The other end of flow-linearized DNA will attach to the other electrode very fast.

The second scenario starts with Oligo A-λ. One end of Oligo A-λ was immobilized without any problem. The molecules would not cover the whole effective areas of two adjacent electrodes because of low concentration (~3 pM) of added Oligo-λ. Then Oligo B and ligase were added. Oligo B was involved in two ways. One is that part of Oligo B was annealed and ligated to Oligo A-λ. The other is that part of Oligo B was immobilized on the uncovered Au surface. After hydrodynamic stretching, the free end of Oligo A-λ-Oligo B would attach to an electrode through Au-thiol coupling. Alternatively, the sticky end of non-ligated Oligo A-λ would be annealed to adsorbed Oligo B. Both scenarios were tried. The second was found better. The detailed procedures are as follows:

1) Purify Oligo A-λ by QIAEXII to remove DTT and non-ligated Oligo A.
2) Pipette 10-20 μL 0.1-0.05 ng/μL Oligo A-λ (YOYO-1 stained) on electrodes for 0.5 h; (binding of OligoA-λ not cover full surface); rinse with water.
3) Pipette 1 μL 1 μM Oligo B, 8 μL 1× ligase buffer, and 1 μL ligase into the same area of electrodes; incubate for 30 min; rinse with water.
4) Pull up the electrode chip from a beaker full of water at the constant rate of 50-100 μm/s by the direct of perpendicular to electrodes. Speed controlled by the micropump (KDS 200, KD Science, USA).
5) Second ligation (optional) by adding ligase and buffer.

Reproduced with permission of the copyright owner. Further reproduction prohibited without permission.

Modified λ-DNA was aligned between 15 μm (C, D) and 16 μm (A, B) spaced electrodes (Figure 3.12). Marko and Siggia have proposed an approximation to describe the relation of drag force of hydrodynamic flow to the extension of WLC chains [78]. The equation is:

$$\frac{FP}{K_B T} = \frac{1}{4(1-x/L)^2} + \frac{x}{L} - \frac{1}{4}$$

where F is extension force, P is the persistence length of DNA, K_B is the Boltzmann constant; T is temperature, x is extension and L is the contour length of DNA. By taking P as 53 nm [71], x as 16 μm and L as 16.5 μm, the estimated drag force is ~22 pN acting on DNA. The calculated force, however, does not match with the Smith's force and extension curve [71], by which the extending force would be ~10 pN. This result is similar to molecular combing. This shows that the mechanics of aligned molecules in Figure 3.12 deviates from the WLC model even in the transition of entropic elasticity regime and linear elasticity regime. The other reason for this difference could be the buffer condition. Experiments here used pure water, while Smith used 100 mM NaCl as hydrodynamic flow.

The thickness of DNA bridges looks much bigger than its natural diameter due to the fluorescence blooming effect (Figure 3.12). Steady flow stretches DNA molecules very fast. A 16 μm-long molecule, for example, can be fully extended to its contour length within 10 sec [79]. However, stretched molecules recoil rapidly after the cessation of flow [69]. Vertically moving electrodes must be kept in water long enough to keep the free end of DNA on the target electrode, thus allowing Au-thiol interaction or annealing between Oligo B on target electrodes and the free end. When electrodes are pulled out of water, flow stops and stretched molecules may recoil immediately. 6 cm height of water

Reproduced with permission of the copyright owner. Further reproduction prohibited without permission.

was added in beaker to keep electrodes, moving at the rate of 100 μm/s, in dynamic flow for 10 min. Oligo-capped DNA is preferentially adsorbed at the edges of electrodes (Figure 3.12) because electrode corners also physically adsorb molecules. Once trapped there, molecules have a harder time dissociating than when trapped on SiO_2 surface. Local accumulation of molecules might facilitate Au-thiol coupling and ligation

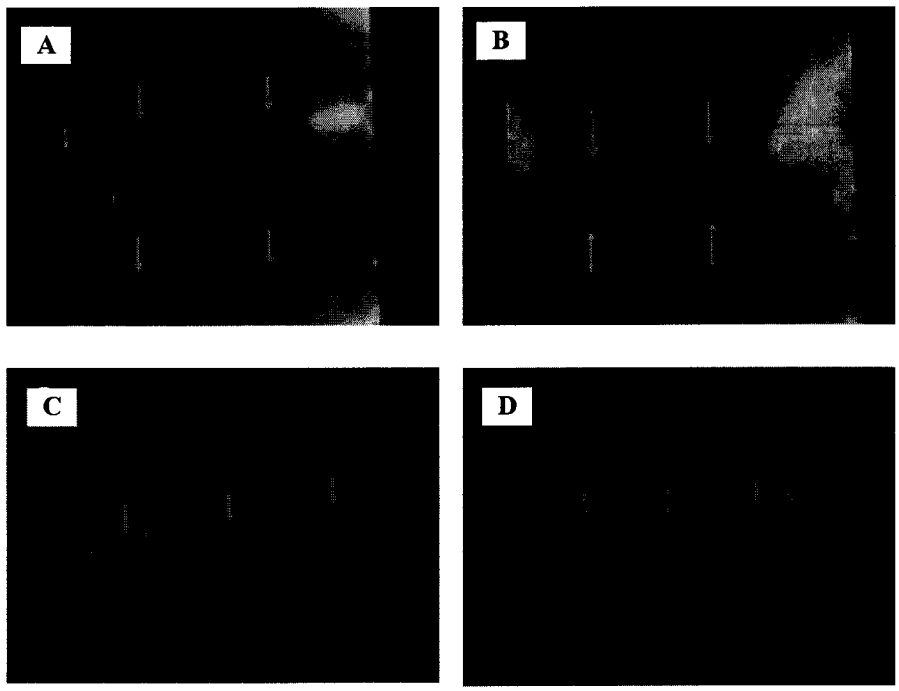

Figure 3.12. Stretching and positioning of DNA molecules between two Au electrodes. The spaces are 15 or 16 μm.

Reproduced with permission of the copyright owner. Further reproduction prohibited without permission.

CHAPTER IV

METALLIZATION OF DNA

4.1 Literature Review

Unmodified DNA has a low conductivity, limiting its usefulness for electronics. DNA, however, can be metallized by virtue of its electrostatic properties. Braun *et al.* [54] used silver nanoparticles for this purpose. Conductivity was enhanced. Ag ions bind to DNA by Ag-Na ion exchange. Hydroquinone can reduce DNA-bound Ag ions to Ag(0) metallic clusters, which then autocatalyze further reduction of Ag ions from a solution. DNA stretching and positioning were achieved by hydrodynamic flow and Au-thiol coupling. Figure 4.1 shows a prepared Ag nanowire between two Au electrodes. The diameter is ~100 nm (Figure 4.1A). The resistivity, 3.4×10^{-3} Ω-m (Figure 4.1B), is higher than that of bulk silver. Nevertheless, the method has become the prototype for metallization of single DNA molecules.

DNA-templated assembly has led to great progress in nanowire fabrication in the past few years. A variety of metallic nanowires made in this way have been reported: Pd [80-82], Pt [83-85], Au [86-91], and Cu [92, 93]. Fabrication is based on principles of electroless plating, a mature technology widely used in industry to make metallic films. During the step known as DNA "activation", metallic cations bind to bases or phosphate groups of the DNA molecule. Pd(II) and Pt(II), for example, bind to nitrogenous bases of

Reproduced with permission of the copyright owner. Further reproduction prohibited without permission.

B-DNA, mainly on the N7 sites of purines; Cu(II) binds to polyanionic backbones of DNA by the electrostatic interaction. Activated metal-DNA complexes are then reduced by a chemical agent, resulting in one-dimensional metallic clusters on DNA, normally 1-7 nm in diameter. The clusters act as nucleation centers to catalyze metallic growth of continuous nanowires.

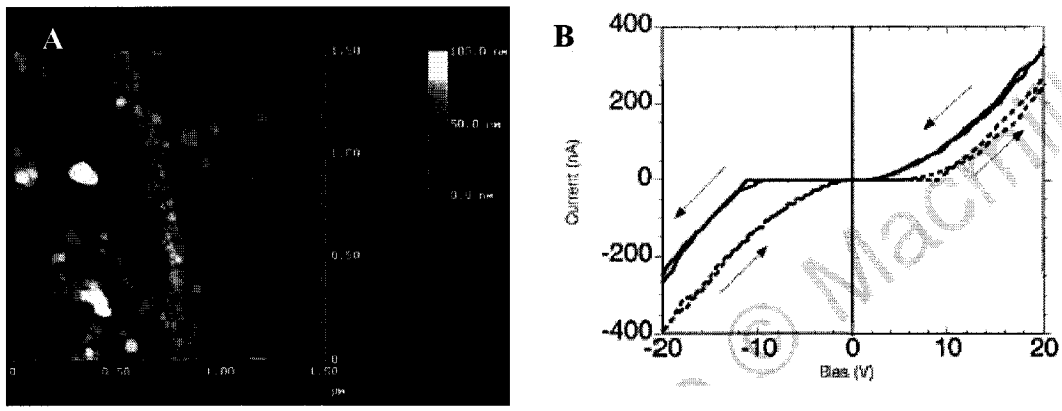

Figure 4.1. Characterization of metallized DNA. (A) Atomic force microscope (AFM) micrograph of a 100 nm wide Ag nanowire using DNA-templated assembly. (B) I-V characteristics of the nanowire. Reprinted from Ref. [54]. Copyright 1998 Macmillan Publishers Ltd.

Richter *et al.* [80, 81] have used bacteriophage λ DNA as a template to fabricate conductive nanowires of Pd. The wires had an average diameter of 50 nm and an estimated conductivity of 2×10^4 S cm^{-1}, only 10-fold smaller than bulk Pd. During activation, Pd(II) ions became bound to bases of DNA. Dimethylamine borane, a common reducing agent, reduced DNA-bound Pd(II) to clusters with a diameter of 2–4 nm. A second treatment with Pd plating bath led to continuous nanowires, catalyzed by pre-formed Pd nuclei. In recent work [82], the same authors measured the temperature-dependent resistance of ~60 nm diameter Pd nanowires that were pinned between two electrodes with a space of 5 μm. Interesting electrical properties were found. At

Reproduced with permission of the copyright owner. Further reproduction prohibited without permission.

temperatures above 30 K, the Pd nanowires displayed ohmic behavior and resistance decreased linearly with decreasing temperature. Below 30 K, resistance increased with decreasing temperature. Such behavior differs from that of most bulk metals. The authors ascribed the phenomenon to quantum effects. Increased resistance at low temperature may result from weak localization and electron-electron interaction in the nanoscale materials. Annealing of Pd nanowires was found to improve conductivity by reducing structural disorder. A 9-10 fold decrease in resistance was found after 200° C annealing.

Catalytic metal nanoclusters can not only initiate deposition of the same type of metal, but also catalyze growth of a second type of metal. This is so-called heterogeneous nucleation and growth. Ford *et al.* [83] have used this approach to metallize DNA with Au. Pt(II)-activated DNA was reduced by sodium borohydride, and ~1 nm Pt nanoclusters were found on the template. Electroless plating with Au resulted in 4-6 nm Au nanoparticles being deposited on the DNA template.

Activation of DNA is a critical step in DNA nanowire assembly. How metal ions bind to DNA will determine the coverage of metal deposits on templates and heterogeneity of the resulting nanowires. Seidel *et al.* [85] have investigated the effects of the activation process on the heterogeneity of prepared nanowires. They found that DNA was not metallized by Pt(0) without prior activation by Pt(II). By contrast, DNA activated with Pt(II) at 37 °C for 16 h was uniformly metallized by 3-5 nm Pt(0). Mertig *et al.* [84] have used first-principles molecular dynamics to simulate effects of activation on clustering of Pt(0) on a DNA substrate. Pt(II)-DNA adducts prepared in the activation process could control the structure and heterogeneity of Pt(0) clusters on DNA after chemical reduction. A long activation time was required to deposit Pt(0) nanoparticles

Reproduced with permission of the copyright owner. Further reproduction prohibited without permission.

that are able to initiate growth of nanowires with high coverage and heterogeneity. This was confirmed by Seidel *et al.* [85] in an extensive study on the synthesis of Pt nanocluster chains on DNA templates. The authors have suggested that Pt metallization of DNA obeys the so-called "DNA-controlled" mechanism. Electronic affinity of Pt(II)-DNA complexes are greater than Pt(II) ions in solution due to the heterocyclic bases of DNA, favoring nucleation on DNA templates. Pt(II)-DNA is reduced to Pt(I)-DNA or Pt(0)-DNA in an early stage of the reaction. Then Pt(II) ions in solution diffuse to Pt(I)-DNA and form Pt(I)-Pt(II) dimers, limiting reduction of Pt(II) ions in solution. This explains the favorable growth of metallic nanoclusters on the templates.

Complete confinement of the growth of metallic particles on templates, however, is difficult when fabricating nanowires in aqueous solution. Inevitably, metallic ions are reduced in solution and become randomly deposited on the substrate. This leads to low nanowire heterogeneity, despite favorable growth on the templates by the "DNA-controlled" mechanism. Typical low heterogeneity nanowires show irregular branching and necklace structures. Keren *et al.* [86] have developed a new scheme of metallization to help overcome this difficulty. Aldehyde bound to DNA by a Michael-type addition functions as a reducing agent for Ag(I). Reduced Ag(0) clusters deposit predominantly on the template where the reducing agent is localized prior to metallization. Ag nuclei on DNA were prepared by this approach.

Highly compact nanocircuits will require the precise patterning and interconnection of wires at the molecular level. A single nanowire can be patterned by molecular recognition of DNA by protein – a type of "molecular lithography". In recombination reaction, RecA nucleoprotein filaments bind to the segments of aldehyde-

Reproduced with permission of the copyright owner. Further reproduction prohibited without permission.

derivatized DNA at specific nucleotide sequences. RecA (2027 bases, ~678 nm) then prevents the Ag(0) deposition that occurs elsewhere on aldehyde-derivatized DNA. As a result, a 678 nm-long insulating gap is formed on a single nanowire after Au metallization. Molecular lithography has been improved by standard tools of molecular biology: restriction digestion and DNA ligation [87]. Restriction enzymes and ligase act on aldehyde-derivatized DNA as effectively as unmodified DNA. A 2054 bp (~700 nm) fragment of DNA treated with aldehyde and a 1106 bp (~350 nm) fragment not treated with aldehyde were digested by *Hga I* and then ligated. This yielded DNA fragments with alternating aldehyde-derivatized and non-aldehyde-derivatized parts. The fragments were then metallized with Ag. Prepared Ag structures were isolated by 350 nm gaps, because the non-aldehyde-derivatized parts did not become metallized.

Localization of a reducing agent on templates may enhance heterogeneity of metallized DNA. Bererril *et al.* [93] have reported a method to reduce background called "ionic surface masking". K^+ or Cs^+ ions bind to SiO_2. The resulting cationic surface provides a physical and electrostatic barrier to adsorption of Ag(I) and Cu(II) during activation. Ag and Cu nanowires can then be assembled on the surface. A 51% decrease in non-specifically deposited Ag nanoparticles was found by this approach, and a 74% decrease in non-specifically deposited Cu nanoparticles.

Nucleation and growth of metal clusters on DNA is the main approach to DNA nanowire assembly. DNA-directed assembly of nanoparticles, however, has also received a good deal of attention. Kumar *et al.* [88] and Sastry *et al.*[89], for example, have reported that linear arrays of lysine-capped colloidal Au (~4 nm) can be assembled on DNA by electrostatic interaction between the polyanionic DNA backbone and positively

Reproduced with permission of the copyright owner. Further reproduction prohibited without permission.

charged Au nanoparticles. Patolsky *et al.* [90] have developed an approach to nanowire assembly in which nanoparticles bind directly to DNA bases. 1.4 nm Au particles labeled with amino psoralen are intercalated into a poly-A and poly-T DNA duplex by a photochemical reaction. UV irradiation catalyzes covalent binding of amino psoralen to bases of DNA. About 4 nm high Au nanowires can be assembled by this approach. Harnack *et al.* [91] have shown that a nanowire can be fabricated from DNA by separate nucleation and growth. 1-2 nm trisphosphine-labeled Au particles bind densely to DNA as catalytic seeds. Then Au electroless plating is used to grow the nanowire. The resulting nanowires are 30-40 nm wide and show ohmic behavior with a conductivity ~1/1000 of bulk Au. Quake et al. [94] have shown that DNA can be metallized in a dry environment. Evaporated Au is directly deposited on a DNA molecule bridged between electrodes. The average width of the resulting Au-clad DNA is ~10 nm.

4.2 Fabrication of Gold Nanowires

4.2.1 Methods

Lambda DNA molecules oriented by molecular combing or hydrodynamic stretching are used as templates for Au nanowire assembly. The negatively charged backbones of DNA templates bind to positively charged nanoparticles by electrostatic interaction (Chapter I). A stretched DNA molecule is a long polyanionic template with evenly distributed negative charges along its long axis. The crystallographic distance between two adjacent negative charges is about 0.34 nm. After the binding of positively charged Au particles to DNA, growth of nanoparticles can be obtained by chemical development. Continuous nanowires are fabricated this way. Figure 4.2 shows a

Reproduced with permission of the copyright owner. Further reproduction prohibited without permission.

schematic diagram of the method to prepare Au nanowires on λ DNA templates stretched and anchored between electrodes.

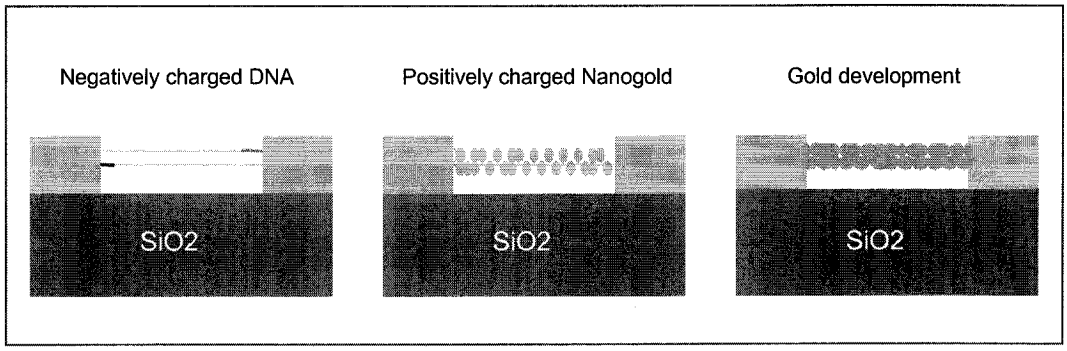

Figure 4.2. Schematic diagram of assembly of Au nanowires.

The positively charged nanogold (2022, Nanoprobes Inc., USA), about 1.4 nm in diameter, are labeled with approximately six primary amine groups. Therefore, it may assume a positive charge in neutral or acidic environment. After electrostatic interaction, the 1.4 nm nanogolds would uniformly bind to polyanionic templates. GoldEnhance (2113, Nanoprobes Inc.) was then applied to develop nanogold-DNA complexes into continuous and conductive nanowires. The GoldEnhance packaged mixture contains Au(I) cations and a reducing agent. During development, Au(I) was reduced to Au(0) that deposited on autocatalytic nanogolds. The level of nanogold growth may be controlled by different development times.

UV-vis spectrometer (Schimazu CP1650) was used to characterize surface plasmon absorption of Au nanoparticles generated by different development times. Fabricated nanowires were imaged by AFM and SEM. The Keithley probe station (SMU-236/237) was used to measure their electrical behavior.

Reproduced with permission of the copyright owner. Further reproduction prohibited without permission.

4.2.2 Nanogold Growth

Control of aggregation and growth during development of nanogolds is important to diameter and uniformity of fabricated nanowires. The novel optical property of metal nanoparticles is known as surface plasmon absorption. Unlike "free gas" electrons in bulk metals, their motion in nanoparticles is confined because size is smaller than the mean free path of an electron. As electromagnetic waves irradiate metal nanoparticles, conduction band electrons oscillate, inducing absorption and scattering. Since the maximum of surface plasmon band (SPB) and absorbance depend mainly on the size and the shape of nanoparticles [95-97], here, the level of development of the 1.4 nm nanogolds in the GoldEnhance can be characterized by UV-vis spectrometry (UVS).

In a typical experiment, nanogold was diluted to 1 μM with 20% (v.) DMSO solution. Forty μL GoldEnhance solution was mixed with 1.8 mL nanogold in a 1 cm quartz cuvette. UVS was taken for a 60 min period, once every two minutes. Figure 4.3 shows changes of SPBs of Au nanoparticles in the development of 0 min, 4 min, 10 min, 20 min, 30 min and 40 min. Due to quantum size effect, 1.4 nm nanogold is too small to absorb at ~520 nm, the maximum SPB of Au nanoparticles. There is no absorbance maximum until 4 min development (Figure 4.3). As nanogolds grew bigger, shaper SPB peaks and narrower bandwidths appeared. The bandwidths decreased with increase of the development times. On the 40 min curve, for example, the bandwidth was about 80-90 nm, by comparison with the larger bandwidths of the 4 min curve. This is consistent with the widely accepted argument [95-97]: plasmon bandwidth of Au nanoparticle is inversely proportional to the radius of particles with diameters smaller than 50 nm.

Reproduced with permission of the copyright owner. Further reproduction prohibited without permission.

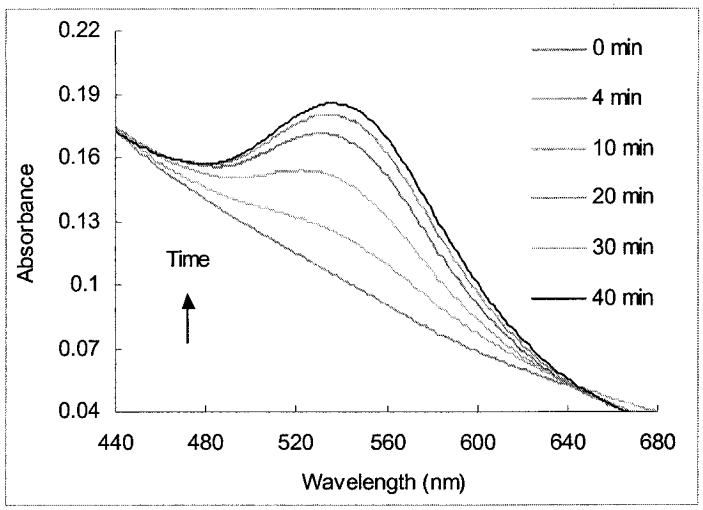

Figure 4.3. UVS spectra of nanogold development as a function of time.

The other observation was the red-shift maxima of SPBs with enlargement of Au nanoparticles. The absorption maxima of SPB shifted from 518 nm at the 4 min curve, to 534 nm at the 30 min curve, as shown at the red points in Figure 4.4. The red line is a trend of red-shift of absorbance maxima that was fitted by a three-degree polynomial approximation. The maxima at the 2 min curve, where bandwidth was broadened, was an estimate according to the trendline. Link *et al.* have explained combination of Mie's theory and TEM studies for size-dependent optical properties of Au nanoparticles with a series of diameters, from 9–99 nm [95]. The relation of absorbance maxima to size of particles, described there, was used to estimate diameters of nanogold particles grown by GoldEnhance development. The blue points were results and the trendline again was a three-degree polynomial approximation (Figure 4.4). Nanogold was enlarged from 5 nm to 50 nm in a sense of scaling development time. Au nanoparticles with diameters about 5 nm, 11.5 nm, 28 nm, 46 nm, and 50 nm were grown at the development times of 2 min, 4

Reproduced with permission of the copyright owner. Further reproduction prohibited without permission.

min, 10 min, 20 min and 30 min, respectively. No obvious changes resulted on bandwidths and maxima of absorbance after 30 min.

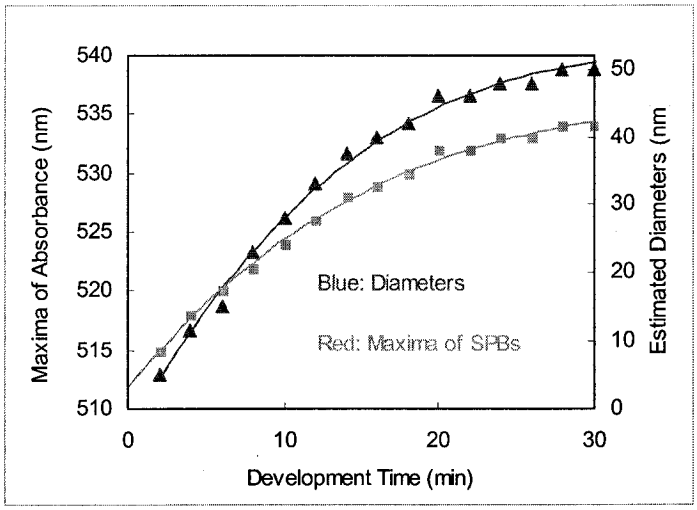

Figure 4.4. Relation of SPB maxima to particle sizes during development.

Figure 4.5(A-C) shows AFM micrographs of enlarged Au nanoparticles with diameters of 25-30 nm, 40-50 nm, and 100 nm, after development times of 10 min, 20 min and 40-60 min, respectively. 10 μL 0.1 μM nanogold (20% DMSO) was pipetted on glass coverslips. After evaporation, samples are gently rinsed with water. GoldEnhance mixture was added on samples for different autocatalytic time and followed by rinsing gently with water. The size of particles downscaled with the increase of development times. Figure 4.5D shows the color changes of solutions of Au nanoparticles with different diameters. Light brown color of 1.4 nm nanogold solution changed to purple-bluish after 30 min of development, during which the observation of red-shift colors matched with the change of absorption maxima in Figure 4.3 and Figure 4.4.

Reproduced with permission of the copyright owner. Further reproduction prohibited without permission.

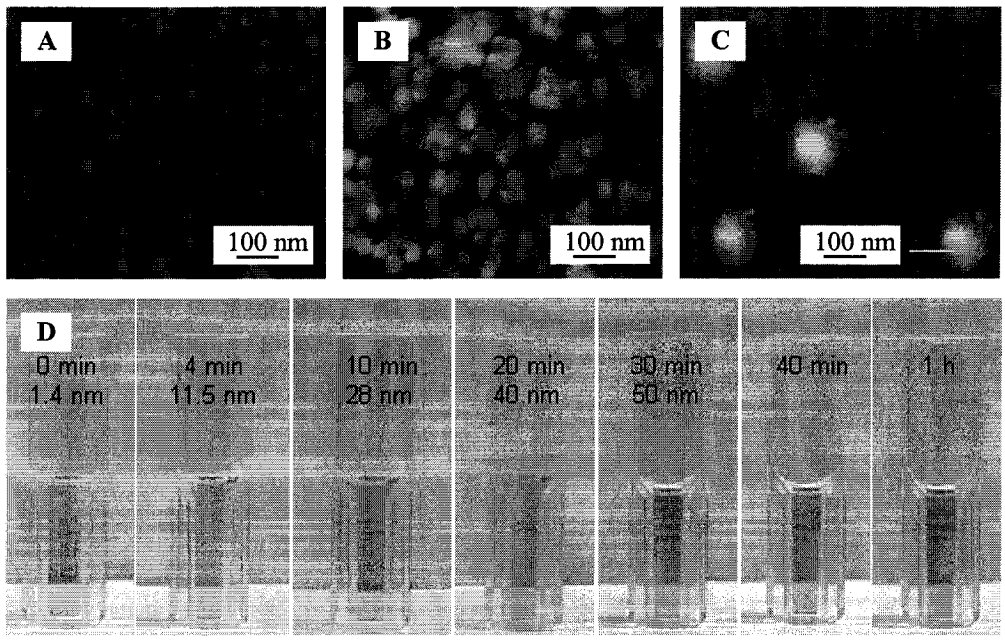

Figure 4.5. Development of Au nanoparticles. (A) 25-30 nm after 10 min. (B) 40-50 nm after 20 min. (C) 100 nm after 40-60 min. (D) Color changes of solutions of Au nanoparticles during development. Sizes of Au nanoparticles were estimated by the relation of SPR maxima to diameters in Figure 4.4. (A-D) AFM micrographs.

4.2.3 Assembly of Gold Nanowires

UVS was used to monitor spectrophotometric alterations during Au development in the presence of DNA, assuming that the interaction between Au nanoparticles and DNA may be characterized by spectrum changes at the 260 nm wavelength. As shown, Au enlargement results in spectrum alteration at the 520 nm wavelength. Twenty μL DNA solution (16 nM) was added into 1.8 mL 1 μM nanogold solution (pH 6.5), yielding to the 20:1 ratio of DNA bases to nanogold molecules. After incubation overnight, the sample was dialyzed 3 × 6 h against the buffer in DNA and nanogold. Forty μL GoldEnhance solution was added to the dialyzed solution immediately before UVS. The spectra were recorded at every two minutes for a total of 60 min. The 0 min, 10 min, 20 min, 30 min, 40 min, 50 min and 60 min spectra are shown in Figure 4.6. It is visible that

Reproduced with permission of the copyright owner. Further reproduction prohibited without permission.

the red-shift of plasmon band around the 520 nm wavelength is associated with Au development after treatment with GoldEnhance. The spectrometric alteration with time is similar to Au development in the absence of DNA (Figure 4.3). This suggests that the 1.4 nm gold particles have bound to DNA by electrostatic interactions during the overnight incubation. Dialysis would have removed unbound nanogold particles off the dialysis bag with a cut-off size of 1 μm. GoldEnhance autocatalyzed DNA-bound 1.4 nm nanogolds during the development. An absorbance peak at the 0 min curve was found at ~252 nm wavelength (Figure 4.6), ~8 nm shifts from the absorption peak of unmodified DNA. This indicates binding of Au particles to DNA may have strongly altered electronic structure of DNA bases. The spectrophotometric signals at ~252 nm wavelength, however, were not obviously altered during the entire reaction. The reason is not clear.

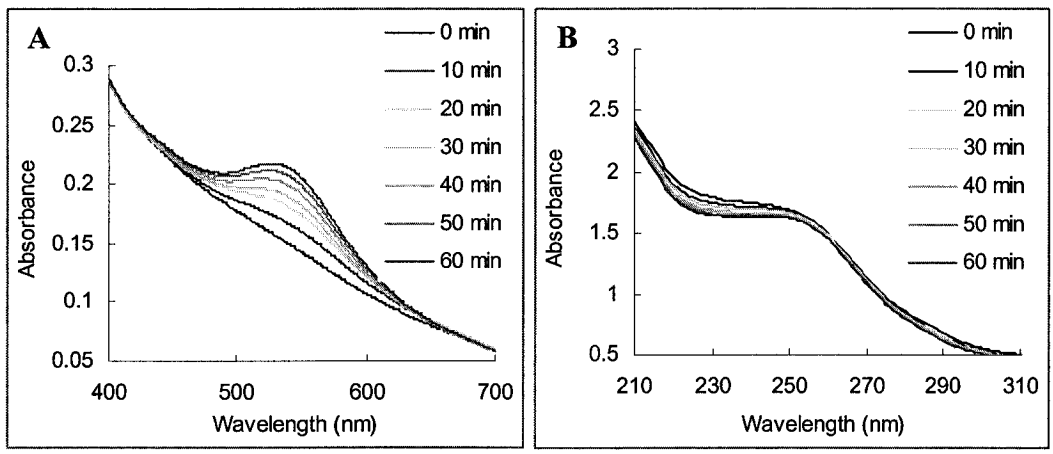

Figure 4.6. UVS spectra of nanogold development in the presence of DNA. (A) Spectra of 400-700 nm wavelength. (B) Spectra of 210-310 nm wavelength.

Preparation of nanowires in a solid support was better than in a solution. The 1.4 nm Nanogold particles serves as nucleation centers of subsequent deposition of Au(0) atoms from solution during the development, when the positively-charged primary

Reproduced with permission of the copyright owner. Further reproduction prohibited without permission.

ammine groups on Nanogold particles may have been enveloped by Au(0) deposition. Enhanced Au particles thus diffuse off DNA templates and aggregate in solution. This is shown that absorption peaks of DNA have not disappeared during the 60 min development (Figure 4.6). Most Au particles diffuse off DNA templates, and exposed aromatic bases of DNA led to the strong absorption at the ~252 nm wavelength.

Freshly cleaved mica was used as a substrate to assemble Au nanowires. In a typical experiment, 10-20 μL 1 ng/μL λ DNA (10 mM HEPES, 5 mM $MgCl_2$) was pipetted on a mica for 5 min adsorption. After rinsing with water, 10 μL nanogold (1 μM) was added for 2-3 h to allow Au particles to bind to immobilized DNA. Unbound Au(0) was removed by rinsing with water thereafter. The sample was then treated by 10 μL GoldEnhance for 10-15 min. Figure 4.7A shows an AFM micrograph of randomly deposited Au nanowires with an average height of ~25 nm. Dehydrated DNA molecules are randomly distributed on the surface. They assume many irregular conformations: loops and knots, networks, tree-like lines (Chapter III). Nanogold particles of 1.4 nm might not have evenly covered templates during incubation, resulting in irregular structures of Au(0) deposits after treatment with GoldEnhance. Stretching templates is a must for nanowire preparation. The detailed procedures in experiments of nanowire preparation after stretching are as follows:

1) Stretch modified λ DNA between two Au electrodes (Chapter III).
2) Add 20-30 μL the nanogold solution (1 μM, pH 6.5).
3) Incubate 2-3 h; rinse with water gently to remove unbound nanogold.
4) Add 10 μL GoldEnhance solution for 10-20 min.
5) Rinse with water and dry with nitrogen gas.

Reproduced with permission of the copyright owner. Further reproduction prohibited without permission.

A quasi-parallel array of Au nanowires were fabricated on stretched templates (Figure 4.7B). A total of 9 individual nanowires were anchored to an Au electrode. Nanowires were clearly separated from each other. The apparent linewidth was ~30 nm or more, and average height was 15-20 nm. The variance of nanowire linewidth and height results from the well-known convolution effect of AFM probes). Stretching of modified λ DNA molecules between two 15 μm-spaced Au electrodes was verified by fluorescence microscope (Figure 3.12). The direction of nanowires was perpendicular to the extension of the Au electrodes. The inset (Figure 4.7B) shows a specific arrangement of nanowires: three parallel wires were closely compacted to a group. The multiple positive charges of 1.4 nm nanogold may have crosslinked two adjacent polyanionic DNA strands by electrostatic interaction. Aggregation of inter-templates before binding and development of Au particles are likely responsible for the spatial arrangement of prepared nanowires. A similar structure of Au nanowires was found in Kumar's report [88], in which parallel arrays of Au nanoparticles were prepared this way.

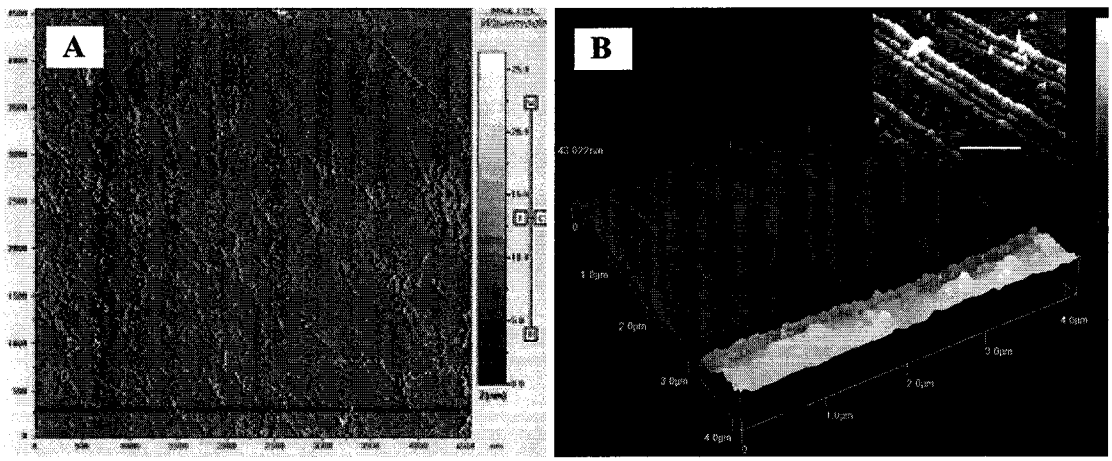

Figure 4.7. AFM micrographs of Au nanowires. (A) Assembled nanowires on mica surface; Height scale ~ 25 nm. (B) A 3D micrograph of Au nanowires anchored on a gold electrode. The apparent linewidth is ~30 nm or more, height 5-15 nm; Inset is a magnified view of Au nanowires. Scale bar 400 nm.

Reproduced with permission of the copyright owner. Further reproduction prohibited without permission.

4.2.4 Electrical Behavior

Au nanowires have been built between two electrodes, although reproducibility was not high. Figure 4.8A shows single Au nanowire with diameter of 50-100 nm that was anchored between two 3 μm-spaced Au electrodes. Electrical behavior of prepared Au nanowires was measured by the Keithley probe station (Figure 4.8B). The blue curve suggests a linear ohmic behavior of metallized DNA. By contrast, unmodified DNA shows isolation behavior (pink curve). The 3 KΩ resistance of a goldwire with ~ 10 μm length and 200 nm width corresponds to 1.57×10^{-3} Ω-cm, comparable to nanowires prepared by other groups [54]. The dramatic decrease in resistance results from metallization of DNA.

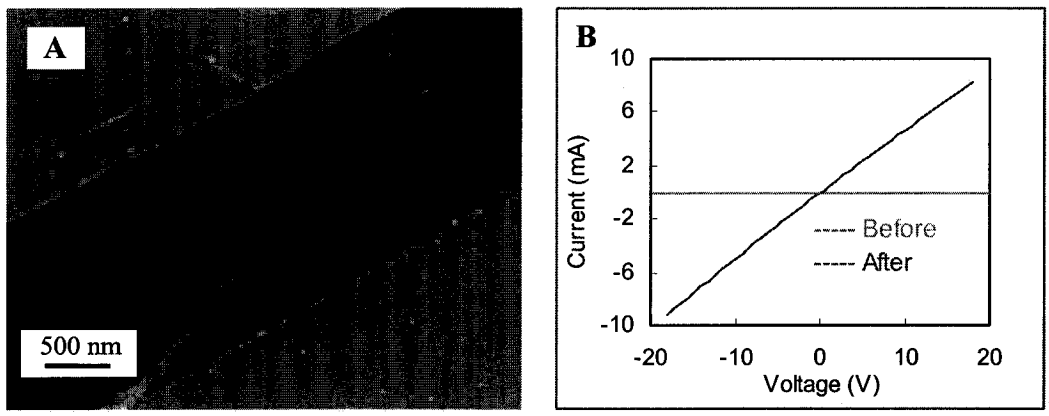

Figure 4.8. Characterization of Au nanowires. (A) AFM micrograph of Au nanowires (50-100 nm width) between two 3 μm-spaced electrodes. (B) Electrical behavior of Au nanowire (blue). The pink curve is before metallization of DNA. After Ref. [98].

4.3 Fabrication of Cobalt Nanowires

4.3.1 Introduction

Interest in one-dimensional nanoscale materials and devices, often called nanowires, nanotubes or nanorods, has risen sharply in recent years. The material

Reproduced with permission of the copyright owner. Further reproduction prohibited without permission.

properties exhibited by such structures have considerable potential for the development of functional nanoscale electronic and optoelectronic devices (Chapter I). Nanowires made of magnetic materials might be suitable for development of high-density memory storage devices or magnetic field sensors [23-25]. Fe, Co and Ni and their bimetallic nanowires exhibit the directional anisotropy of magnetic properties. For example remanence ratio and coercivity are greatly enhanced along with the long axis.

So-called bio-templated self-assembly of electrically conductive nanowires has received a good deal of attention in the scientific literature. The approach allows fabrication of 1-dimensional nanostructures from even smaller templates, often biomolecules or biomolecular complexes. Double-stranded DNA, one of many possible bio-templates, is particularly well-suited to preparation of wire-like structures by virtue of its narrow width (~2 nm), lack of branching, and ability to self-recognize and self-organize (base pairing). The first demonstration of DNA-templated metallization, by Ag, was by Braun and colleagues [54]. Evident graininess in the resulting 1-dimensional structures was apparently a consequence of differences in spatial uniformity of the metallization process. Nevertheless, the conductivity of metallized DNA was substantially greater than that of untreated material. More recently, Pd, Pt, Au, and Cu nanowires have been made by the same general approach (Chapter I). By contrast, little use has been made thus far of the bio-template approach to the preparation of magnetic nanowires.

Co and Ni nanowires have been fabricated by electroless plating on various biotemplates, for instance microtubules [99], peptides [100] and tobacco mosaic viruses [101, 102]. Here, nanoclusters of ferromagnetic Co have been self-assembled into wire-

Reproduced with permission of the copyright owner. Further reproduction prohibited without permission.

like structures on a DNA-template on a mica or silanized glass substrate. Characterization of the Co-DNA nanowires by AFM revealed a height of 10-20 nm. Control of nanowire diameter was achieved by control of Pd activation and the nanoparticle development process. Oriented Co nanowires were realized by molecular combing of the bio-template before metallization. An advantage of the approach is its lack of need of the membrane required by the electrochemical deposition process described above.

4.3.2 Methods and Experiments

4.3.2.1 Methods. A three-step process was used to deposit Co nanoclusters on DNA. The reaction scheme is as follows:

(1) $n\text{Pd(II)} + \text{DNA bases} \rightarrow n\text{Pd(II)} : \text{DNA}$

(2) $n\text{Pd(II)} : \text{DNA} + \text{DMAB} \rightarrow \text{Pd(0)}_n : \text{DNA} + \text{DMAB}^+$

(3) $\text{Pd(0)}_n : \text{DNA} + \text{DMAB} + m\text{Co(II)} \xrightarrow{heat} \text{Pd(0)}_n\text{Co(0)}_m : \text{DNA} + \text{DMAB}^+$

Pd(II) binds to DNA bases during "DNA activation" (1). In this process, Pd(II) binds the nitrogenous bases of B-DNA, mainly on the N7 sites of purines [103]. Pd(II):DNA then is reduced to Pd(0):DNA by dimethylamine borane (DMAB) (2). Co(0) deposition (3) is autocatalyzed by Pd(0) nanonuclei localized bound to DNA. Predicted advantages of Co-metallized DNA prepared in this way are good wire uniformity and limited unwanted reaction products; Co(0) will only grow on Pd(0):DNA.

4.3.2.2 Material Preparation. Bacteriophage λ DNA from New England Biolabs (USA) was used in all experiments. All other chemicals were from Sigma-Aldrich (USA). Pd(II):DNA was prepared by dissolving DNA in 20 mM HEPES (4-(2-hydroxyethyl)-1-piperazineethanesulfonic acid) buffer, pH 6.0, and dialyzing extensively.

Reproduced with permission of the copyright owner. Further reproduction prohibited without permission.

Solution of 0.2 mL 1 mM Na_2PdCl_4 in HEPES buffer was added to 1 mL dialyzed DNA at a nitrogenous base concentration of 80 μM, determined by UVS at 260 nm (Shimadzu 1650PC, Japan). Such mixtures were incubated at 37 °C for 24 h to allow equilibration of binding of Pd(II) to DNA. The Co electroless plating bath was 10 mM $CoCl_2$, 2.5 g/L DMAB, 29.4 g/L sodium citrate and 15.5 g/L boric acid, pH 6-7 [104]. The bath was saturated with nitrogen gas immediately before use to drive off dissolved oxygen.

4.3.2.3 Sample Preparation. Ten μL 0.5 ng/μL untreated DNA in Mg-HEPES buffer (5 mM $MgCl_2$, 20 mM HEPES, pH 6.0) was pipetted onto freshly-cleaved muscovite mica (grade V-1, Structure Probe, Inc., USA). After 5 min adsorption, samples were rinsed with 18.2 MΩ-cm water (Millipore, USA), dried with N_2 gas, and characterized by AFM (see below). In a typical Co electroless plating experiment, as-prepared Pd(II):DNA was diluted with Mg-HEPES to 5 ng/μL DNA. 30 μL of this material was pipetted onto mica. 100 μL Co plating bath was added to samples for 10-15 min. Co deposition was accelerated by incubation of the mixture at 50° C. Reactions were terminated by extensive rinsing with water. Samples were characterized by AFM after drying with N_2 gas. As a control, Pd(II):DNA was treated with 80 mM DMAB instead of Co plating bath. Samples of non-activated DNA were prepared by simultaneous mixing of DNA, Pd(II) ions, and Co plating bath on mica. After 10 min samples were rinsed with water and dried. Another type of sample was prepared by immersing immobilized DNA on mica in 1 mM Pd(II) for 1 h. Unbound Pd(II) was removed by water. Co plating bath was added to samples for 15 min and incubated at the temperature of 50° C. Products were rinsed and dried afterwards.

Reproduced with permission of the copyright owner. Further reproduction prohibited without permission.

Molecular combing was used to align DNA prior to metallization. 100 μL 5 ng/μL DNA was oriented on a silanized glass slide by the method described in ref. [57-59]. Samples were immersed in 1 mM Pd(II) solution for 4 h. Activated samples were rinsed with water to remove unbound Pd(II) and treated for 10-15 min in Co plating bath at 50 °C. Reactions were terminated by rinsing with a large volume of water.

4.3.2.4 Instrumentation. Dialyzed Pd(II):DNA was added to Co plating bath at 50 °C, yielding a 2.2 mL mixture of 80 μM DNA bases and 5 mM Co(II). UVS spectra were recorded immediately after mixing. A HEPES buffer was used to blank the instrument, and the path length of the quartz cuvette was 1 cm. Large-amplitude noise below 230 nm, attributable to components of the mixture, was recorded but is not shown for clarity. Progressive increase in apparent absorbance below 300 nm may have been due to scattering by Pd(0) or Co(0) nanoparticles [105,106]. Spectra were taken at 0 min, 10 min, 20 min, and 40 min.

Structural information on Co-metallized DNA was obtained using a Q-scope 350 AFM (Quesant Instrument Corp., USA). All samples were characterized by the tapping-mode in air. The silicon nitride cantilever tip had a resonant frequency of about 175 KHz. Data were acquired at 1-1.5 Hz scanning rate.

Elemental analysis by EDX was done using an Amray 1830 scanning electron microscope (USA) coupled to an X-ray detector for EDX analysis. The sampling region corresponded to metallized DNA and thus was brighter than the background. It was not possible to collect data on a single nanoparticle as it is not possible to image a single nanoparticle with this instrument. In view of this, the EDX experiment tells us about the material composition of a nanowire, not a single nanoparticle.

Reproduced with permission of the copyright owner. Further reproduction prohibited without permission.

A Nikon TS100F inverted fluorescence microscope (Japan) coupled to a 100× oil immersion objective lens was used to image and record molecular combing of DNA. Images were obtained using a Nikon Coolpix 4700 digital camera (Japan). Scale bars were calibrated using a Richardson test slide (Gen III, Electron Microscopy Sciences, USA). The fluorescent dye YOYO-1 was from Molecular Probes (USA).

4.3.3 Results and Discussion

4.3.3.1 Formation of Pd(0) Nuclei on DNA. Figure 4.9 shows an AFM image of untreated DNA molecules on freshly-cleaved mica. Mg^{2+} formed an "electrostatic bridge" between the negatively-charged mica surface and phosphate groups in the DNA backbone. The molecular surface appears continuous and smooth. The average height is ~0.5 nm in both figures, in good agreement with reported AFM heights of DNA on mica [107-109]. The observed heights were smaller than the crystallographic diameter of a double-stranded DNA because of the tip broadening effect of AFM.

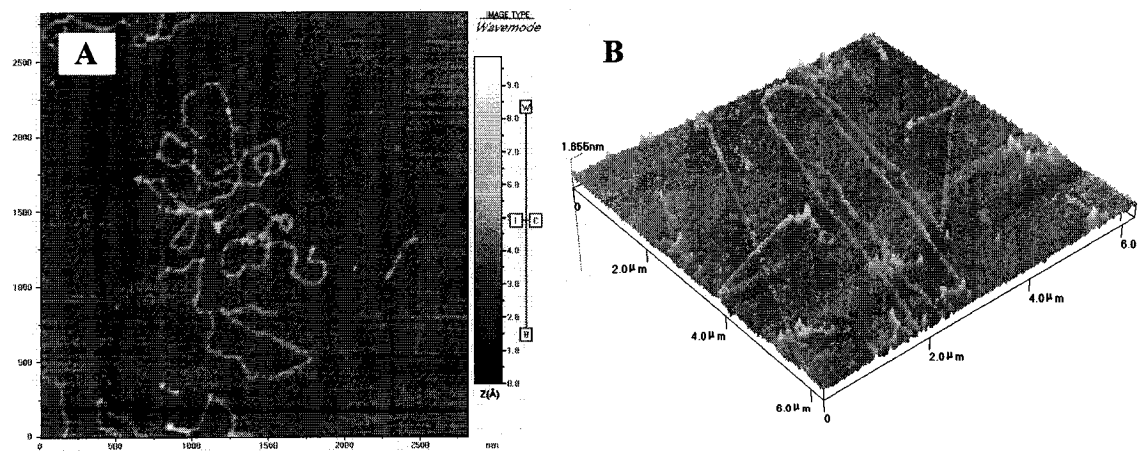

Figure 4.9. AFM micrographs of untreated λ DNA molecules. (A) Scan area 2.5 × 2.5 μm, the height scale 1 nm. (B) The 3D view of a 6× 6 μm area, the height scale 1.5 nm.

Reproduced with permission of the copyright owner. Further reproduction prohibited without permission.

Activation of DNA with Pd(II) (reaction scheme 1) was required for subsequent electroless plating with Co. Binding of Pd(II) ions to DNA was demonstrated by UVS by heat denaturation of Pd(II):DNA complexes (not shown). A decrease in melting temperature relative to untreated DNA was assumed to indicate the coordination of divalent cations by DNA bases during the activation process, distorting base stacking and inducing hyperchromicity.

DMAB can reduce Pd(II) to Pd(0) [110], even when the Pd(II) ions are bound to DNA [80-82]. Figure 4.10A shows that Pd(0):DNA complex, formed by oxidation of DMAB, has a different appearance from untreated DNA by AFM (Figure 4.9). The surface of Pd(0)-bound DNA seems rough, and the height is about 2 nm greater than for untreated DNA (Figure 4.10B). The change appears to have resulted from self-assembly and aggregation of reduced Pd(0) atoms on the DNA template. Individual Pd(0) particles were not detected by AFM in the present work, apparently due to limited lateral resolution of the instrument. Possible mechanisms of Pd(0) aggregate formation are as follows. Pd(0) atoms will diffuse on the DNA surface to minimize free energy. Kind *et al.* found 1-4 nm "islands" of Pd(0) after DMAB treatment of a monoatomic layer of Pd(II) bound to surface amines [111]. The islands may result from diffusion and aggregation of reduced Pd(0) atoms, the binding energy of Pd(0)-amine being lower than that of Pd(II)-amine. Pd(0):DNA may have a lower binding energy than Pd(II):DNA, and reduced atoms may diffuse on DNA and aggregate into small particles. Another possibility is that Pd(0) aggregation results from the observed shortening of the length of DNA on binding (Figure 4.10A), bringing the bound atoms closer together and making it easier for them to interact. Onoa *et al.* have reported that the average length of a

Reproduced with permission of the copyright owner. Further reproduction prohibited without permission.

Pd(II):DNA complex is only 30% that of untreated DNA [109]. Pd(II) ions may "stack" onto DNA before reduction, with aggregates of Pd(II) ions becoming Pd(0) on treatment with a reducing agent.

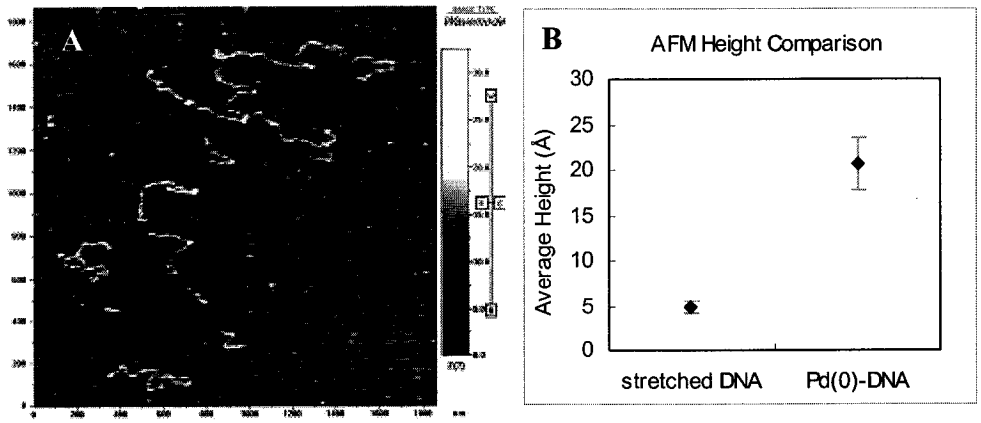

Figure 4.10. Pd(0):DNA hybrid and unmodified DNA. (A) Pd(0):DNA hybrid reduced by the DMAB solution. Height scale 3.5 nm; (B) Comparison of average heights of unmodified DNA and prepared Pd(0):DNA. The error bar was from the standard deviation (1σ). Data were from the histogram analysis of the AFM software.

4.3.3.2 Assembly of Co(0) Nanowires. Pd and Pt nanoparticles are suitable for heterogeneous catalysis [83,101]. It was found that Pt(0) nanoparticles of 1 nm diameter could not be detected by AFM but did catalyze deposition of Au(0) [83] and that subnanometer Pd(0) nuclei catalyzed Co deposition [101], the size of the clusters being estimated from known dimensions of the tobacco mosaic virus. Pd-activated electroless deposition of Co is widely used in industry to prepare thin metallic coatings. Experiments described here indicate that this technology can be adapted to plating Co onto DNA, a 1-dimensional biotemplate.

Figures 4.11(A-D) show that treatment of Pd(II):DNA with Co plating bath resulted in the deposition of 10-20 nm-high Co nanoclusters on DNA. EDX confirmed that the majority of metallized DNA samples is Co metal (Figure 4.11E). The

Reproduced with permission of the copyright owner. Further reproduction prohibited without permission.

morphology of the nanostructures implies that Pd(0) nuclei had distributed more or less uniformly on DNA prior to Co(0) deposition. A few islands were formed off the templates; presumably these originated from the diffusion of Pd nuclei or Co nanoparticles. Nanowires grew to an average height of 25 nm after a second treatment of the DNA sample in the Co reducing bath (Figure 4.11D).

Results presented here imply that Pd(0) nucleation centers are formed on DNA by Co deposition. DMAB does not react directly with Co(II) [104]. Instead, Pd(0) nanoclusters act as autocatalytic agents, enabling oxidation of DMAB and reduction of Co(II). Co(0) deposits on Pd(0) nuclei only. As shown in Figures 4.11, regions of height 10-20 nm were found on Pd-activated DNA after treatment in Co plating bath. This implies that Pd(0) nanoclusters served as nucleation centers for Co(0) deposition.

Reproduced with permission of the copyright owner. Further reproduction prohibited without permission.

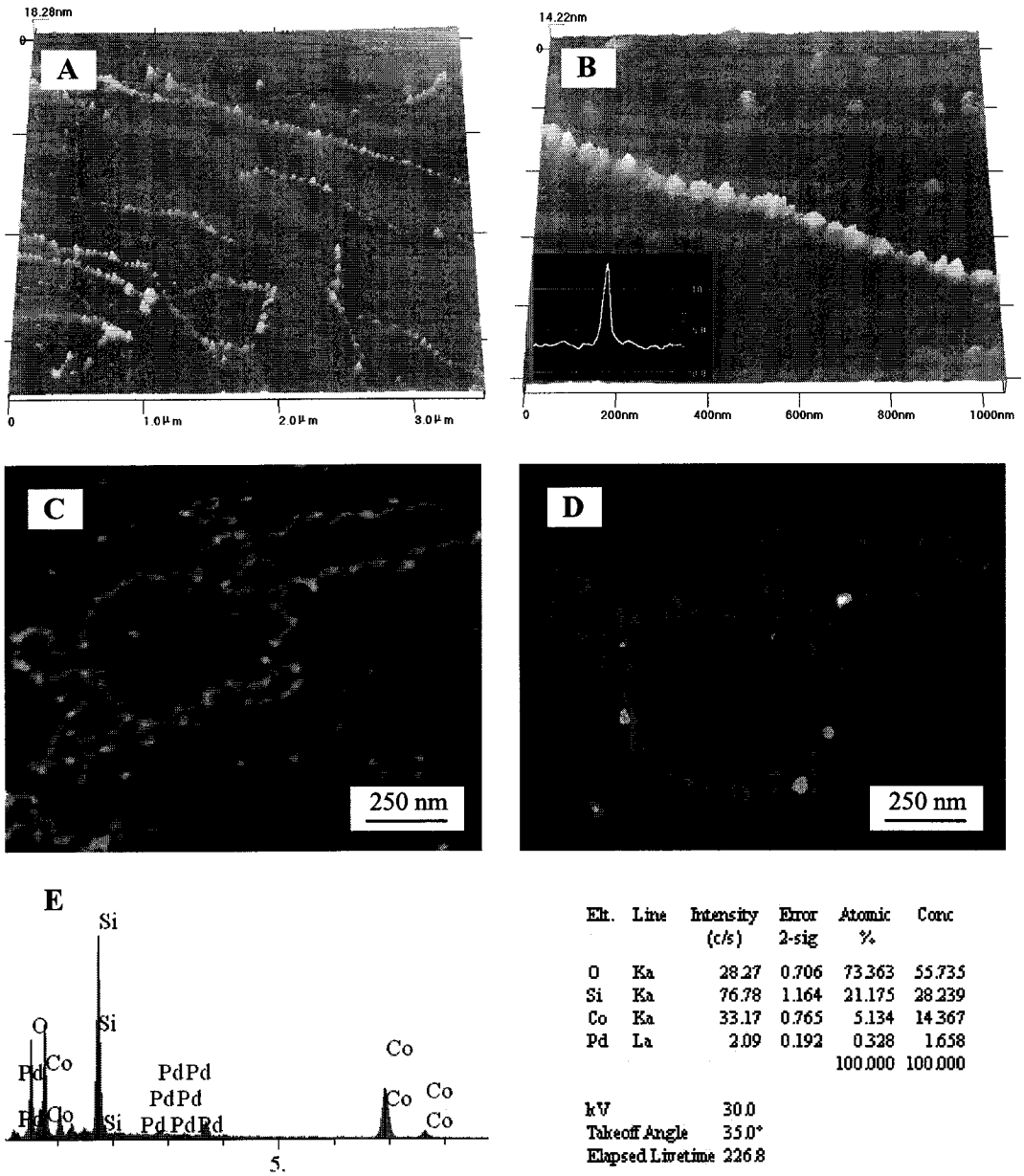

Figure 4.11. Characterization of Co nanowires. (A-C) Pd(II):DNA complex solution treated with the Co electroless plating bath. (A) The area is 3.5 × 3.5 μm^2, the height scale ~18 nm. (B) The area is 1.0 × 1.0 μm^2, the height scale ~14 nm. Inset, height profile of the same structure in nm. (C) The area is 1.5 × 1.5 μm^2, the height scale is ~10 nm. (D) Second treatment of Pd(II):DNA complex with Co plating bath. The height scale is ~30 nm. (E) EDX spectrum of aggregated Pd(II):DNA complex treated with Co plating bath. The tics on the horizontal scale represent 1 keV. Right table is the element analysis of components in samples. Si and O are from the substrate. Minor contributions of other elements are not labeled for clarity.

Reproduced with permission of the copyright owner. Further reproduction prohibited without permission.

Reaction of Pd(II):DNA and of non-activated DNA with Co reducing bath was monitored by UVS (Figure 4.12). A shoulder is evident at 260 nm in the spectra of activated DNA taken at 0 min and 10 min (Figure 4.12A). This indicates that reduced Pd and Co nanoclusters had not fully coated DNA by this time; DNA bases absorb strongly at this wavelength. The shoulder is barely visible, however, in the 20 and 40 min curves. Adsorption of Pd(0) and Co(0) onto DNA alters spectral properties of the macromolecule. The spectra give a sense of the time scale of deposition. By contrast, no change in absorption at 260 nm was detected with non-activated DNA: the 260 nm shoulder peaks are evident in the 20 and 40 min curves (Figure 4.12B). It would appear that randomly-adsorbed Pd and Co did not fully coat DNA in the absence of activation.

The inset in Figure 4.12A shows absorbance at 515 nm as a function of reaction time. An aqueous solution of Co(II) is pink and absorbs photons with a peak intensity at 515 nm. With 10 min post-mixing, the Co(II) signature peak was noticeably decreased, implying that cations had been deposited from solution onto DNA. Forty min later, the Co(II) ions were almost completely reduced to Co(0) (catalyzed by Pd(0)), as the peak at 515 nm had nearly vanished. During this process, a thin black film was deposited on the inner surface of the quartz cuvette used for UVS. The solution turned blue immediately on addition of HCl, indicating the presence of Co(III). This reaction is further proof of deposition of metallic Co(0). Both DNA-bound Pd(0) and free Pd(0) were able to initiate Co(II) reduction, as shown in Figure 4.12A and 4.12B. The deposition rate induced by free Pd(0) is faster than DNA-bound Pd(0), but slower reduction of Co(II) allows better control of the size and shape of the resulting Co(0) nanostructures.

Reproduced with permission of the copyright owner. Further reproduction prohibited without permission.

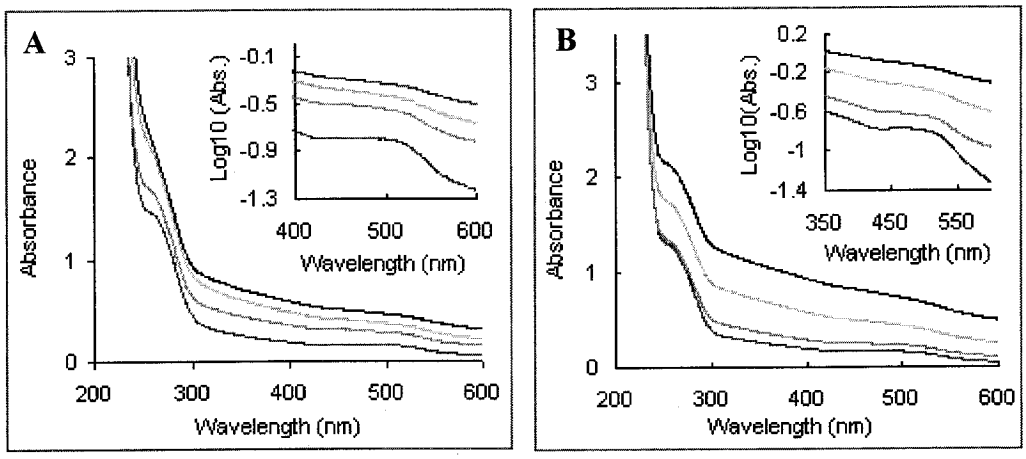

Figure 4.12. UVS spectrum of DNA in Co plating bath as a function of time. (A) Pd(II)-activated DNA. (B) Non-activated DNA. Spectra were taken at 0 min, 10 min, 20 min, and 40 min. Arrows indicate the direction of increasing time. The spectra at 0 min were recorded immediately after mixing DNA and plating bath. The inset shows a magnified view of the spectra in the 400-600 nm range.

Deposition of Co onto DNA cannot be initiated in a DMAB-based reducing bath without activating the DNA. Attempted deposition of Co onto non-activated DNA yielded AFM images which suggest that most of the DNA did not become metallized (Figure 4.13A). This is consistent with UVS data (Figure 4.13B). "Islands," however, formed on and off the DNA, apparently from random deposition of Pd(0) and Co(0) on the substrate. It also was found that uniformity of Co metallization was scaled with Pd(II) activation time. Deposition of Co onto DNA activated for 1 h resulted in Co nanoparticles 7-11 nm high on DNA (Figure 4.13B). Metal coverage is only 70-80% at best. That is, a continuous solid was not formed. Non-metallized DNA was not suitable for deposition of Co. This resembles the work of Mertig et al., who have reported that the extent of metallization correlates with duration of activation of DNA by Pt(II) [84].

Reproduced with permission of the copyright owner. Further reproduction prohibited without permission.

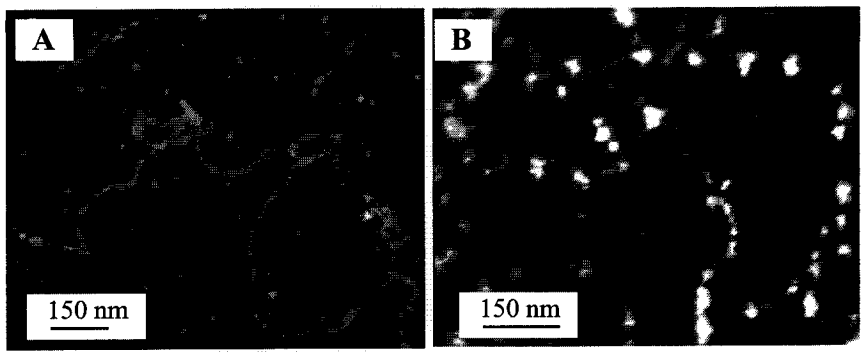

Figure 4.13. AFM images of DNA following treatment with Co plating bath. (A) Non-activated DNA. The height scale is 5 nm. (B) DNA with 1 h activation with Pd(II). The height scale is 11 nm.

Realization of the potential of the technology for practical applications will require control over the spatial arrangement of nanowires [112]. Molecules of DNA can be orientated into a parallel array by "molecular combing." In this process, one end of a DNA molecule is anchored on silanized glass, and migration of the meniscus during evaporation stretches the molecule. Figure 4.14 shows a parallel array of Co nanowires after metallization of pre-combed DNA. The average width of the structures is 35 nm wide, and the average height is 10 nm. An arrow indicates the direction of motion of the meniscus during combing. The inset shows a micrograph of oriented DNA molecules stained with YOYO-1, a fluorescent dye. Pd(II)-activated DNA proved less amenable to combing than unmodified DNA. Presumably this is because sticky ends of DNA must bind vinyl groups on silanized glass prior to combing and stretching. Bases on the sticky ends of activated DNA may have become coordinated to Pd(II) during activation, preventing binding to surface vinyl groups.

Reproduced with permission of the copyright owner. Further reproduction prohibited without permission.

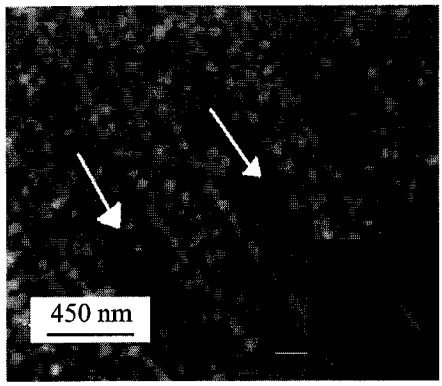

Figure 4.14. Parallel arrays of Co nanowires. The height scale is ~11 nm. Arrows indicate the direction of motion of the meniscus. The image was obtained by AFM. The inset is a photomicrograph obtained by fluorescence microscopy, showing orientated DNA molecules stained with a dye. The scale bar is 10 μm.

DNA can be activated for electroless plating by adsorption of Pd(II) in aqueous solution or on a solid support. The two approaches resulted in similar Co nanostructures. The process involving surface-activated Pd(II):DNA is slightly less time consuming than solution-activated materials. A small quantity of Pd(II) remained on the surface after rinsing with water and was readily reduced to Pd(0). The increased concentration of nucleation centers led to a higher rate of Co deposition rate. To test whether nanoclusters deposited on DNA were composed of Co, Pd(II):DNA was treated with DMAB instead of Co plating bath (Figure 4.10A). No particle of a diameter larger than 3.5 nm was found by AFM. This implies that the visible particles in the AFM micrographs were not pure Pd(0). Only after treatment of activated DNA in Co plating bath were nanoparticles evident. For instance, the clusters evident in Figure 4.14 were obtained only after treatment with Co reducing bath.

Reproduced with permission of the copyright owner. Further reproduction prohibited without permission.

4.3.4 Magnetic Property

The vibrating sample magnetometer (VSM, DMS-880A, Digital measurement systems, USA) at Grambling state university was used to characterize magnetic property of DNA-templated magnetic nanowires. Because the VSM is not able to characterize the samples prepared on a mica or silanized glass (Section 4.3.2), Co nanowires were prepared by a different approach. The prepared Pd(II):DNA complex solution was mixed with Co plating bath on a Si substrate or in a test tube. Here DNA templates are "free" in solution without the immobilization step that has been used in the previous section. The structures of Co deposits on free DNA templates are characterized by a SEM (DSM 942, Carl Zeiss, Grambling state university) before measurement of magnetic property. In a typical experiment, 50 μL Pd(II):DNA complex solution (20 μM DNA bases) and 100 μL Co electroless plating bath were added on a Si substrate on a 50° C hotplate. The mixture turns black in a few minutes, indicating Co(0) metal deposition (section 4.3.2). After 8 min, the reaction was terminated by rinsing with a large amount of water.

Figure 4.15A and B show structures of prepared Co nanowires adsorbed on a Si substrate. EDX (LPX1 S, Kevex) confirmed that the majority material of the samples is Co(0) metal (not shown). Co wires with the average diameter of 70-80 nm appear random coils, similar to the macroscopic structures of DNA molecules in solution. This is different from immobilized and stretched DNA on a solid support. The microscopic structure, however, suggests the same mechanism of Pd nucleation and Co growth governing the process as in the preparation of Co nanowires on immobilized or stretched templates. Few non-structured deposit is found. High resolution micrograph reveals

Reproduced with permission of the copyright owner. Further reproduction prohibited without permission.

necklace-like structures between adjacent Co particles on a single nanowire (Figure 4.15B), similar to most reports on metallization of DNA.

Hysteresis loop describes the magnetization changes of material with an applied alternating magnetic fields. A ferromagnetic material is magnetized to saturation when the applied field is strong enough to align internal domains of the material. The lack of retraceability means that part of magnetization remains when the applied field drops to zero. The history-dependent nature of a ferromagnetic material represented by a hysteresis loop is widely used in the magnetic recording and memory storage industry. VSM samples of DNA-templated Co nanowires were prepared in test tubes. Co black deposits were collected and rinsed with ethanol three times, as well as a large amount of water. After drying in a vacuum chamber, 2-5 mg powder was characterized by VSM. Figure 4.15C and D show the measured hysteresis loop at room temperature in an applied magnetic field of 10 k Oersteds. Magnetization of ferromagnetic Co nanowires were not totally saturated at this field and temperature. Nevertheless, the loop shows the ferromagnetism of prepared Co nanowires that has a coercivity of 214.2 Oe and squareness of 0.17. The similar result has been shown for samples prepared by using different ratios of Pd(II) ion to DNA bases. Further study is required to reveal magnetic properties of Co nanowires synthesized in the presence of DNA: for example, supermagnetism in the zero field cooled (ZFC) experiment, anisotropy along the long axis of wires, and the effect of DNA templates on magnetic properties.

Reproduced with permission of the copyright owner. Further reproduction prohibited without permission.

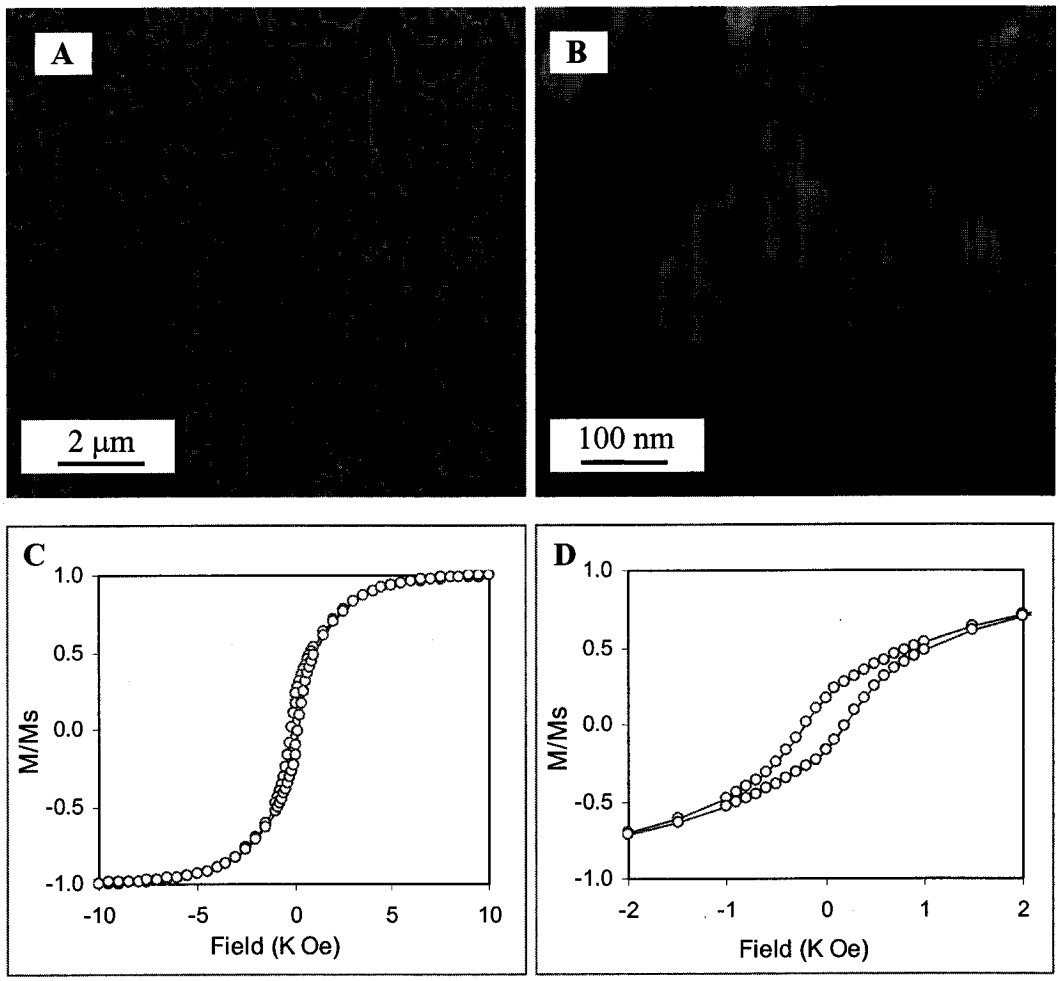

Figure 4.15. Characterization of magnetic Co nanowires. (A-B) SEM micrograph of Co nanowires deposited on a Si substrate. (C-D) The measured hysteresis loop by VSM of Co nanowires prepared in solution.

4.4 Fabrication of Nickel Nanowires

4.4.1 Introduction

Magnetic Ni nanowire is as important as Co nanowires in the development of high-density memory storage devices or magnetic field sensors. We have demonstrated that a Co nanocluster chain can be synthesized by DNA templates in section 4.3. Here, Ni(0) nanocluster chains ~22 nm in diameter have been assembled on DNA templates in a three-step electroless deposition process. Parallel arrays of Ni nanocluster chains were

Reproduced with permission of the copyright owner. Further reproduction prohibited without permission.

fabricated on DNA templates oriented prior to metallization. Ideally, DNA-templated nanowires would be assembled by so-called heterogeneous growth, meaning that target metals will grow on templates only. In practice, however, background deposits tend to be large. Here, growth of Ni(0) clusters was limited to the surface of Pd(0) nuclei bound to DNA. The reductant, DMAB does not react with Ni(II) ions in bulk solution. So less secondary nucleation in solution during Ni(0) growth will lower non-structured background deposits. A brief comparison of Ni(0) growth on immobilized DNA and on free DNA in bulk solution is provided.

4.4.2 Materials and Methods

Ni(0) nanocluster chains were prepared by Ni(0) electroless deposition on DNA substrates in a dimethylamine borane (DMAB)-based reducing bath. The reaction scheme was as follows:

(1) $n\text{Pd(II)} + \text{DNA bases} \rightarrow n\text{Pd(II)} : \text{DNA}$

(2) $n\text{Pd(II)} : \text{DNA} + \text{DMAB} \rightarrow \text{Pd(0)}_n : \text{DNA} + \text{DMAB}^+$

(3) $\text{Pd(0)}_n : \text{DNA} + \text{DMAB} + m\text{Ni(II)} \xrightarrow{heat} \text{Pd(0)}_n\text{Ni(0)}_m : \text{DNA} + \text{DMAB}^+$

The step known as "DNA activation" (reaction scheme 1) involves the binding of Pd(II) ions to DNA bases by coordination coupling. Pd(0) nanoparticles nucleate and grow on immobilized DNA in step 2. Pd(0):DNA hybrids selectively catalyze Ni(0) deposition from solution in a subsequent process (reaction scheme 3).

4.4.2.1 Material Preparation. Bacteriophage λ DNA (48.5 kb) from New England Biolabs (USA) was used in all experiments. All other chemicals were from Sigma-Aldrich (USA). DNA was dialyzed against a 10 mM HEPES (4-(2-hydroxyethyl)-1-

Reproduced with permission of the copyright owner. Further reproduction prohibited without permission.

piperazineethanesulfonic acid) buffer, pH 6.5 to remove EDTA. The Pd(II) solution was 1 mM $PdCl_2$ in 10 mM HEPES and 1 M NH_4Cl, pH 6.5. Cl^- ions prevent Pd(II) complexes from hydrolysis [111]. Pd(II):DNA complexes were reduced with 0.25 g/L DMAB solution. The Ni electroless plating bath consisted of 20 mM nickel(II) acetate tetrahydrate, 2.5 g/L DMAB, 29.4 g/L sodium citrate, and 15.5 g/L boric acid, pH 6-7 [104]. Immediately before use, the bath was saturated with nitrogen gas to remove dissolved oxygen. The Pd(II):DNA complex solution was prepared by adding 50 μL Pd(II) solution to 1 mL dialyzed DNA solution (10 μM bases) and incubating the mixture in a dark room for at least 3 h. The solution was used for UVS samples to monitor DNA activation and SEM samples for Ni(0) deposition.

4.4.2.2 Sample Preparation. Unmodified DNA was imaged by AFM as a reference to study alteration of structure after formation of the Pd(0):DNA complexes. 1-2 ng/μL DNA in 5 mM $MgCl_2$ and 10 mM HEPES buffer (pH 6.5) were deposited on freshly-cleaved muscovite mica (grade V-1, Structure Probe, Inc., USA). Mg^{2+} functions as an "electrostatic bridge" between the negatively-charged mica surface and negatively-charged DNA backbones. After 10 min, samples were rinsed with 18.2 MΩ-cm water (Millipore, USA), dried with nitrogen gas, and imaged by AFM. Parallel arrays of DNA were prepared by combing unmodified DNA on a silanized coverslip [57-59]. Orienting of DNA molecules was confirmed by AFM.

For the samples of Ni(0) deposition on immobilized DNA, 20 μL Pd(II) solution was pipetted onto mica or silanized glass after deposition of DNA. After 3 h incubation in a humidity chamber, the liquid was removed by filter paper. Then 10 μL DMAB solution was deposited. After 10-20 sec, the samples were rinsed with a large amount of water,

Reproduced with permission of the copyright owner. Further reproduction prohibited without permission.

dried with nitrogen gas, and imaged by AFM to study structures of the Pd(0):DNA complexes. The substrate with Pd(0):DNA complexes was transferred to a 50° C hotplate and treated with 50 μL Ni plating bath. The reaction was terminated after 5-6 min by rinsing with a large amount of water. Samples were dried with nitrogen and characterized by AFM. Ni(0) was deposited on non-activated DNA by adding Pd(II) solution and DNA on a substrate and treating with Ni reducing bath immediately thereafter. DNA activation was verified by recording UVS spectra of unmodified DNA, Pd(II) ions, and the prepared Pd(II):DNA complex solution at different temperatures. Pd(II) solution absorbs at 260 nm, so the absorbance of DNA in the complex was obtained by subtracting the Pd(II) spectrum from the Pd(II):DNA spectrum [85]. The fraction melted was calculated by relative absorbance, assuming that both unmodified DNA and Pd(II):DNA complexes were 100% melted at 95° C; absorbance does not change this temperature.

DNA templates are in bulk solution prior to metallization. A 50 μL Pd(II):DNA complex solution was treated with 50 μL Ni plating bath on a Si substrate at 50° C. The reaction was terminated after 3-5 min by rinsing with a large amount of water. Samples were dried with nitrogen gas and imaged by SEM.

4.4.2.3 Instrumentation. Unmodified DNA, Pd(0):DNA and Ni(0) nanocluster chains were characterized in air with a Q-scope 350 AFM (Quesant Instrument Corp., USA) in tapping mode. Si_3N_4 cantilever tips had a resonant frequency of 175 KHz. Images were acquired at a scanning rate of 1-1.5 Hz. Height analysis was done with ScanAtomic® SPM software. Ni deposition on free DNA was characterized by SEM (Amray 1830, USA). Elemental analysis was done by EDX spectroscopy. A Shimadzu 1650PC UV-vis spectrometer (Japan) was outfitted with a temperature controller

Reproduced with permission of the copyright owner. Further reproduction prohibited without permission.

(Isotemp 3006, Fisher Scientific, USA) for absorbance analysis. Corresponding buffers were used as blanks, and the path length was 1 cm.

4.4.3 Results and Discussion

Ni(0) nanocluster chains were synthesized by formation of Pd(0) clusters on immobilized DNA. The Pd(0) clusters served as nucleation centers to catalyze deposition of Ni(0) from aqueous solution. DMAB does not react with Ni(II) ions in solution, so Ni(0) metal grows on the surface of pre-formed Pd(0) nanoparticles only. "Non-structured" deposition of Ni(0) thus was limited. DNA activation is the key to formation of the Pd(0):DNA hybrid structures on a substrate. This determines Ni(0) coverage on templates, background deposits, and target Ni(0) nanostructures. It has been shown that DNA cannot be fully metallized without appropriate activation, and that the extent of metallization on templates relates to duration of DNA activation [84]. The purpose of this step is to coat the templates with metal ions.

4.4.3.1 Formation of Pd(0) Nuclei on DNA. The binding of divalent transition metal ions to DNA bases results in deformation of B-DNA structures [103]: for example, the reduction of base stacking or pairing. Unstacking of DNA bases during thermal denaturation induces hyperchromicity; denatured single-stranded DNA absorbs more at 260 nm than double-stranded DNA. UVS was used to measure the difference in the melting behavior of modified DNA and Pd(II)-DNA complex (Figure 4.16A). The melting of Pd(II):DNA shows a ~15 °C negative temperature shift relative to unmodified DNA, indicating that a greater fraction of Pd(II):DNA complex than unmodified DNA was melted at a given temperature. This is indirect evidence of the binding of Pd(II) ions

Reproduced with permission of the copyright owner. Further reproduction prohibited without permission.

to DNA bases during the 3 h activation step. The coordination coupling of Pd(II) ions to DNA bases results in progressive base unstacking with temperature increase. Pd(II):DNA complexes do not melt below 50° C (Figure 4.16A). At this temperature the unstacking of DNA bases by complexation is not strong enough to break the double helices of DNA. The structure therefore was maintained in the subsequent steps of the nanowire fabrication processes.

DMAB is shown to reduce Pd(II):DNA to Pd(0):DNA [80-82]. AFM has been used to investigate unmodified DNA (Figure 4.16B) and the result of treating the Pd(II)-DNA complex with DMAB (Figure 4.16C). Pd(0) nanoparticles on DNA had an average height of 2-3 nm, slightly greater than non-metallized DNA. The known convolution effect of AFM tips prevents direct comparison of height with apparent width. Larger particles were not deposited on the substrate. None of the Pd(0) clusters were higher than 4 nm under the described conditions. The macroscopic structure of Pd(0):DNA complexes was clearly different from that of untreated DNA molecules. As shown in Figure 4.16B, DNA molecules on a mica appear smooth and continuous. The average height is ~0.5 nm, consistent with other reports in the scientific literature [107-109]. The Pd(0):DNA complexes, by contrast, appear relatively rough and distorted. The contour length is ~2.5 μm, ~16% of the crystallographic length of an unmodified λ DNA molecule (~16 μm). Onoa *et al.* [109] studied the morphology of Pd-famotidine-DNA adducts, and found a ~1 nm height increase and 70% length decrease in λ DNA molecules on binding Pd(II) ions. Similarly, *Seidel et al.* [85] found that the length of Pt(II)-λ DNA was 1.5-2.9 μm. The length of DNA may have shortened during activation.

Reproduced with permission of the copyright owner. Further reproduction prohibited without permission.

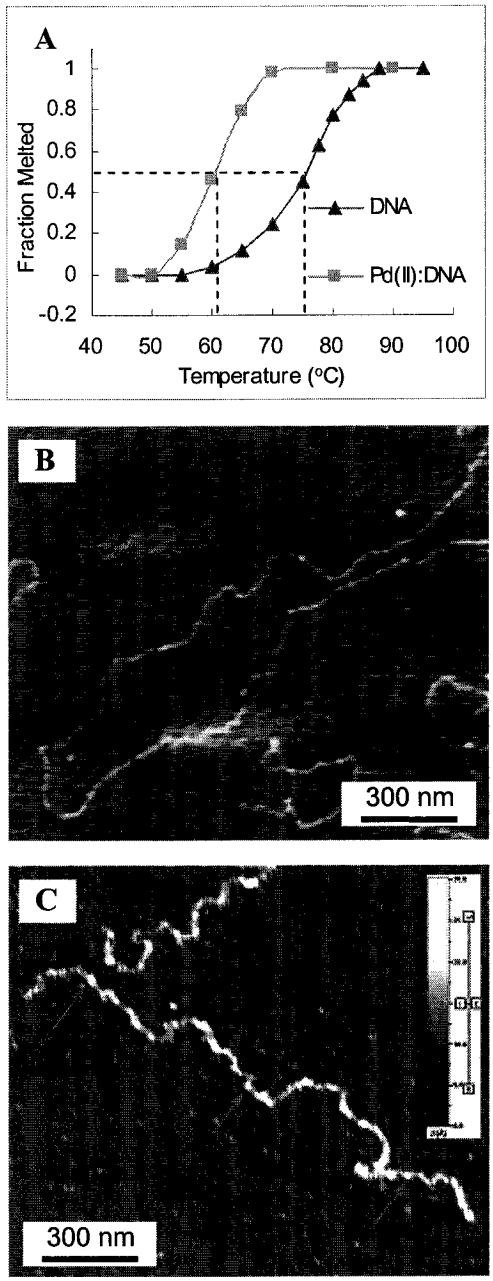

Figure 4.16. DNA activation and formation of Pd(0):DNA complexes. (A) Melting behavior of unmodified DNA and Pd(II):DNA complex in the range of 45-95 °C. (B) AFM image of unmodified DNA on mica. The height scale is ~0.9 nm. (C) AFM image of Pd(0):DNA complex on mica. The height scale is ~3 nm. Arrows indicate Pd(0) nanoparticles.

Various nanoclusters have successfully been coated on DNA templates [80-93]. In most cases, however, metal is deposited both on and off the templates. The mechanism

Reproduced with permission of the copyright owner. Further reproduction prohibited without permission.

of forming nucleation centers on DNA is not yet fully understood. In the present work, the shortening effect of metal-DNA complexes may contribute to nucleation. Concomitant with chain shortening, metal ions may become "stacked" on DNA binding sites during the activation process. After being reduced, the "stacked" metal ions on DNA will become small metal aggregates. The mechanism of autocatalysis is nucleation-limited, so neighboring metal atoms will rapidly migrate to the small aggregates on DNA, forming nucleation centers for further growth. The size of the nuclei might be 1-7 nm. The reactive heterocyclic bases of DNA, where the metal ions bind, also might play a role. Pt(0) nucleation on DNA in the presence of DMAB has been discussed [83-85]. DNA bases enhance the electron affinity of Pt(II):DNA complexes. The reduction kinetics favor the Pt(II) ions bound to DNA over free ions. Here, by analogy, Pd(II) ions on templates are first reduced to small Pd(0) aggregates as a result of the electron affinity enhancement by reactive DNA bases. Then, reduced Pd(0) atoms in neighboring areas diffuse to the small Pd(0) aggregates on DNA, forming metastable Pd(0) nanoclusters. The suggested role of DNA bases might apply to finely-tuned systems only, in a narrow range of concentration ratio of all reactants [85]. The reaction scheme used here and in other reports, however, differ from that in ref. [85]. Further study is needed to understand formation of nucleation centers on DNA.

Various biotemplates have been used to assemble metal nanocluster chains or nanowires by the catalysis of small foreign nuclei. Ford *et al.* used 1 nm Pt(0) nanoparticles bound to DNA to catalyze Au(0) growth [83]. Knez *et al.* synthesized 3 nm wide Ni(0) and Co(0) nanowires on a tobacco mosaic virus template by the catalysis of Pd(0), Pt(0) or Au(0) nuclei [101-102]. We have fabricated Co(0) nanocluster chains

Reproduced with permission of the copyright owner. Further reproduction prohibited without permission.

about 20 nm height on DNA templates using catalytic Pd(0) (Section 4.3). Here, we show that preformed 2-3 nm Pd(0) nanoclusters on DNA can catalyze Ni(0) deposition with limited non-structured background.

4.4.3.2 Ni(0) Deposition on Immobilized DNA. Reaction of non-activated DNA solution with Ni plating bath results in random Ni(0) deposits over the entire substrate (Figure 4.17A). By contrast, deposition of Ni(0) nanoclusters occurred predominantly on DNA templates after treatment with Ni plating bath (Figure 4.17B and 4.17C). Nanoclusters 15-21 nm high were more or less uniformly distributed on DNA templates. EDX confirmed that the majority component of the resulting structures was Ni(0) (Figure 4.17D). Most DNA templates were coated with Ni(0) deposits. Only a few non-structured particles were deposited off the templates, presumably resulting from diffusion of reduced Pd(0) or Ni(0) nanoclusters. Since the reductant, DMAB, does not react directly with Ni(II) ions, less Ni metal is reduced in bulk solution. Instead, Ni(0) nanoclusters deposit predominantly on immobilized DNA templates. This can be attributed to localization of preformed Pd(0) nucleation centers on the templates after activation and treatment with DMAB, as shown in Figure 4.16C. In the case of non-activated DNA, by contrast, free Pd(II) ions not bound to DNA were reduced to Pd(0) particles in bulk solution, and these spread over the entire surface. The Ni(0) nanoparticles grown thereafter, therefore, did not fully coat the DNA templates and formed a random pattern.

A specific distribution on a 2D substrate will be required to make nanowires useful in nanoelectronics. This will perhaps be particularly true for magnetic nanowires. Magnetic properties of ferromagnetic Co/Ni/Fe nanowires are determined by orientational anisotropy [113]: remanence ratio and coercivity are greatly enhanced along

Reproduced with permission of the copyright owner. Further reproduction prohibited without permission.

the long axis of high aspect-ratio wires due to interaction of adjacent nanoscale magnetos in the longer direction. Here, quasi-parallel arrays of Ni nanocluster chains were fabricated on oriented DNA templates by using "molecular combing, in which one end of a DNA molecule is anchored on silanized glass by hydrophobic interaction between chain termini of DNA and surface vinyl groups. Meniscus movement then stretches the molecules [57-59].

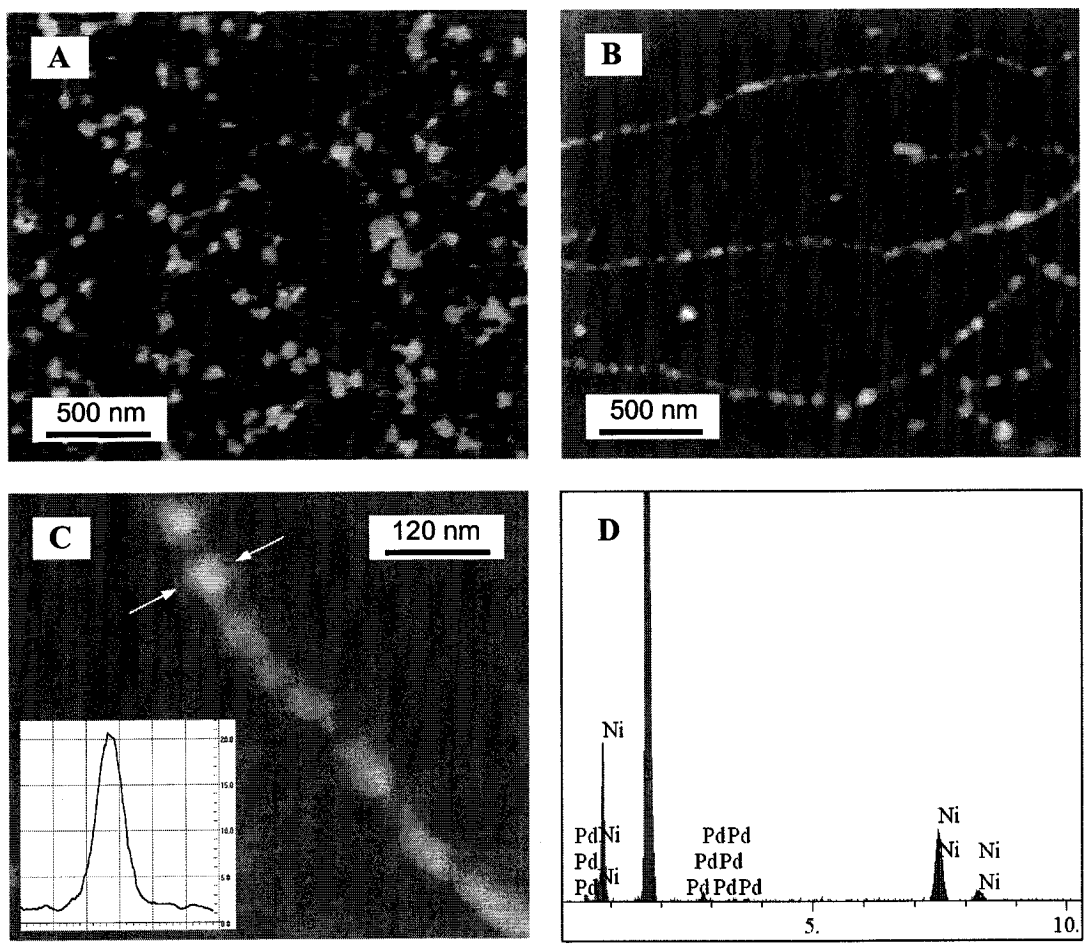

Figure 4.17. AFM characterization of Ni deposition on Pd(0):DNA. (A) Non-activated DNA treated with Ni plating bath. The height scale is ~30 nm. (B) Pd(0):DNA on a surface treated with Ni plating bath. The height scale is ~21 nm. (C) A magnified view (600 × 600 nm^2) of Ni(0) deposition. Inset, height profile of a 20 nm particle (arrow). (D) EDX spectrum of Ni plating bath-treated Pd(0):DNA. The unit tic on the horizontal scale is 1 keV. The largest peak is due to the substrate. Minor contributions of other elements are not labeled for clarity.

Reproduced with permission of the copyright owner. Further reproduction prohibited without permission.

Figure 4.18A shows combed DNA molecules parallel with the direction of meniscus motion. An advantage of this method is that DNA molecules can become well oriented and strongly immobilized on a surface. No apparent lift-off of DNA templates occurred during further processing. Figure 4.18B shows a parallel array of Ni nanostructures up to 22 nm in height after the metallization described above. The distance between two adjacent Ni chains, which ranges from 200 nm to 1 μm, may be tuned by adjustment of DNA concentration. Magnetic properties of such structures will be enhanced along the longer axis. An advantage of the DNA-templated nanowire assembly developed here is that parallel array of nanowires on a substrates can be achieved by orienting DNA templates. Distribution of templates on a substrate is not altered by the metallization process.

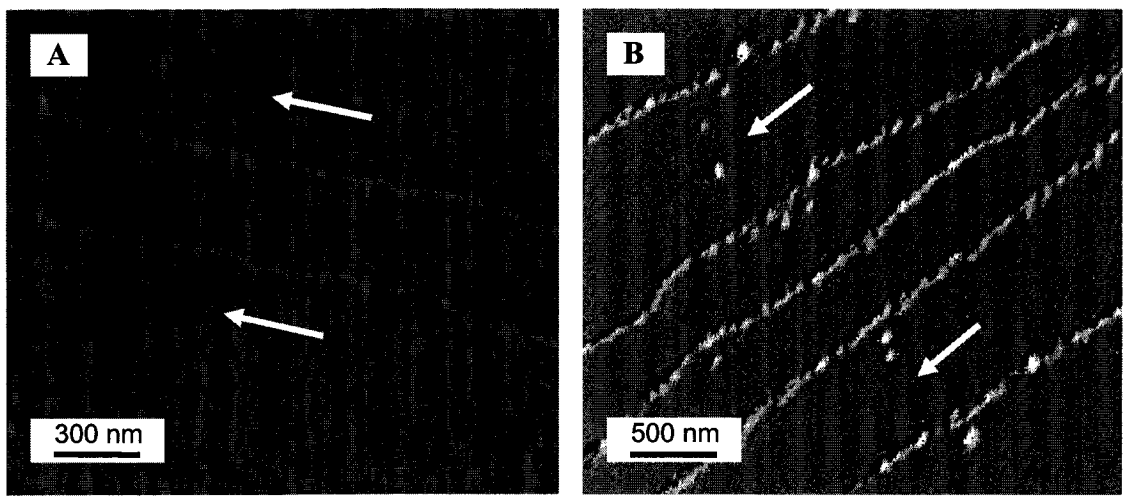

Figure 4.18. Arrays of DNA templates and Ni nanocluster chains. Arrows indicate the direction of meniscus movement during combing. (A) Combed DNA molecules. Height scale is ~1 nm. (B) Combed DNA templates after metallization by Ni. Height scale is ~22 nm.

Ni(0) clusters deposit on DNA templates by selective catalysis. The governing mechanism, nucleation and growth, is similar to other reports [80-93]. It may be

Reproduced with permission of the copyright owner. Further reproduction prohibited without permission.

surprising that particles as small as a few nanometers in diameter can condense onto DNA in the absence of protective ligands, which are widely used in preparation of metal nanoparticles by chemical reduction. For example, 3-5 nm Pd [80], 4-6 nm Au [83], 3 nm Pt [84], 3 nm Cu [92] and here 2-3 nm Pd and 15-21 nm Ni have been chemically reduced and deposited on surface-immobilized DNA templates without apparent agglomeration. Richter *et al.* [114] have described this as DNA functioning as a protective ligand, preventing reduced primary nanoparticles from coalescing. The view is supported by our experiments and others, although the underlying reasons are unclear. We find that small nanoparticles do not form a continuum on DNA. Instead, nanoscale gaps are typical between adjacent nanoparticles in most reports on metallization of DNA. This implies that particle growth on DNA is limited in the direction of template extension. We also find that the reaction of non-activated DNA with Ni plating bath is faster than that of Pd-activated DNA under similar conditions. Larger particles form in the non-activated DNA-based reaction in a shorter period of time (Figure 4.17A). Similarly, Mertig *et al.* have found larger Pt nanoparticles after treatment of non-activated DNA with a reducing agent [84]. In both cases, "free" primary nanoparticles not associated with DNA may have coalesced and grown rapidly in bulk aqueous solutions. As a result, particle growth is less limited in bulk solution than on DNA. The experiments involving non-activated DNA further indicate that DNA functions as a protective agent during metallization.

4.4.3.3 Ni(0) Deposition on Free DNA. The reaction of Pd(II)-DNA complex with Ni electroless plating bath was monitored by UVS (Figure 4.19A). A shoulder of 260 nm, at which nucleic acids absorb strongly, is evident at the 0 min spectrum, indicating the

Reproduced with permission of the copyright owner. Further reproduction prohibited without permission.

presence of "bare" DNA. The shoulder, however, becomes less visible with the progress of the reaction, when Ni(0) deposits from solution by the catalysis of earlier-reduced Pd(0):DNA. The shoulder is hardly visible after 6 min, suggesting that Ni(0) deposition on DNA templates alters the spectral properties of the molecule. By contrast, no such alteration is detected in the reaction based on non-activated DNA (not shown). Ni(II) aqueous solution appears light green and has the absorption maximum at the 390 nm wavelength. The Ni(II) signature was noticeably decreased during the reaction (Figure 4.19A), implying that Ni(II) ions had been reduced. Black deposits were visible during the process and turned green immediately upon addition of HCl solution, suggesting that the black deposits are metal Ni(0).

The spreading and immobilization of DNA strands and nucleation centers may also be also responsible for the formation of metastable particles on DNA without apparent large agglomeration. Ni cluster chains in Figure 4.17B and Figure 4.18B were developed by Ni electroless plating on well-dispersed and immobilized DNA substrates. Growth or aggregation of pre-formed particles is diffusion-limited because nucleation centers were immobilized on separate strands of DNA. Coalescence or aggregation, however, is less limited by diffusion on free DNA substrates. Figure 4.19B shows an example of Ni nanocluster chains prepared by reaction of Pd(II):DNA complex solution with Ni plating bath. In this case, DNA molecules are mobile as a result of thermal fluctuation. Reduced metal-DNA complexes readily coalesce into larger structures when free DNA templates collide and stick. The arrow indicates an intersection of perhaps two or three chains (Figure 4.19B). The resulting Ni(0) cluster chains, therefore, have large diameters of 80-150 nm. The evidence described here suggests that the nucleation and

Reproduced with permission of the copyright owner. Further reproduction prohibited without permission.

growth depends more or less on the mobility of DNA templates in the electroless deposition process. On well-dispersed and immobilized DNA substrates, small metastable metal particles can nucleate and grow without apparent large agglomeration.

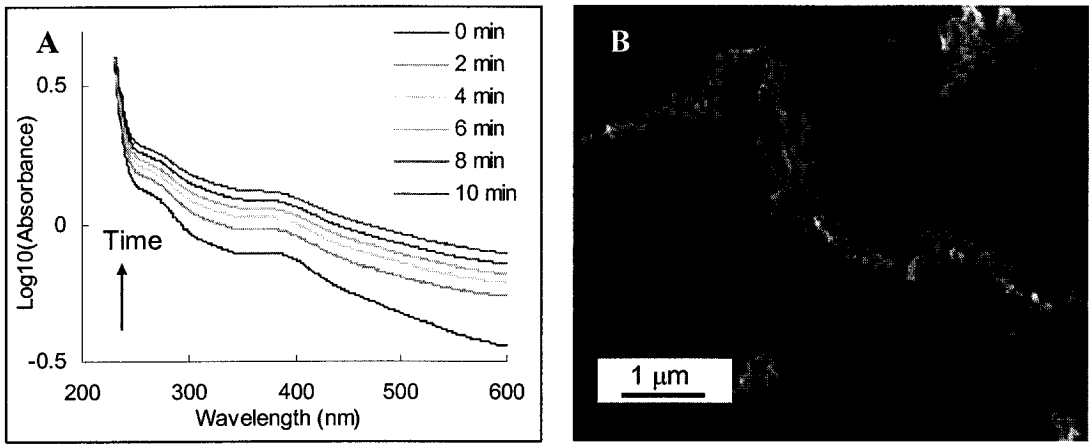

Figure 4.19. Ni deposition on free DNA in solution. (A) UVS spectrum of Pd(II):DNA in Ni plating bath as a function of time. Spectra were taken at 0,2,4,6,8,10 min. The spectrum at 0 min was recorded immediately after adding Pd(II):DNA complex solution to the plating bath. The y-axis is shown in logarithm for clarity. (B) SEM micrograph of Ni nanoclusters chains (80-150 nm diameter) on Si surface.

4.5 Summary

My present work has shown that one-dimensional Au, Co and Ni metal nanowires have been assembled *in-situ* on single DNA molecule templates. UVS was used to monitor the kinetics of reactions in solution. AFM, SEM, EDX, probe station and VSM have been used to characterize structures, electrical and magnetic properties of prepared metal nanowires. Au nanowires of 20-50 nm are synthesized by the development of 1.4 nm gold nuclei that have bound to DNA templates by electrostatic coupling. The I-V curve of Au nanowires anchored between two 15 μm-spaced electrodes has shown a linear ohmic behavior. Ferromagnetic Co and Ni nanocluster chains or nanowires with diameters of 10-150 nm have been fabricated on immobilized DNA or free DNA by

Reproduced with permission of the copyright owner. Further reproduction prohibited without permission.

electroless plating. Parallel arrays of Co and Ni nanocluster chains were obtained by metallization of oriented templates. Pd(0) nuclei of 2-3 nm on DNA serves as nucleation centers to catalyze growth of target Co or Ni metals in a successive reduction. The step of DNA activation by Pd(II) is crucial to the coverage of metal on templates, non-structured deposits and heterogeneity of the resulting structures. An advantage of the described three-step reactions over most reports on metallization of DNA is that fabrication process is controlled by nucleation of seeding metal particles and growth of target metals. The reductant, DMAB, does not react with target metal ions in bulk solution. So less secondary nucleation in solution during growth will lower non-structured background deposits.

Reproduced with permission of the copyright owner. Further reproduction prohibited without permission.

CHAPTER V

SYNTHESIS OF SS-DNA TEMPLATES

5.1 Introduction

Metallized DNA nanowires that were projected to be interconnecting wires in future nanocircuits have been prepared [54, 80-93] by using λ DNA molecules as a template. Significant challenges remain, however, with regard to understanding the fabrication process and improving wire conductivity. The resistivities of Au nanowires, for example, varies from 3.4×10^{-3} Ω-m [54] to 3.0×10^{-5} Ω-m [91], corresponding to 1.5×10^{5} and 1.5×10^{3} times higher than bulk polycrystalline Au, respectively. A large variance in resistance was observed, ranging from 1 kΩ to 35 kΩ for Pd nanowires [80-82]. Uncontrollable nucleation and growth of nanoparticles along λ DNA templates are believed to be key factors for determining wire uniformity and conductivity.

Low conductivity or a high variability in conductivity results from their non-uniform nanostructures: inter-granular gaps, ill-aggregated branches and necklaces, and large grain size distribution [115-117]. Therefore, the electrons may not transport directly along the 1D metalwires but by scattering though the grain boundaries or by throttling at those gaps and branches. Investigation on nanoparticle growth suggests that randomly ordered metallic nuclei lead to a low uniformity of grown aggregates and thus a low electrical conductivity [118-120]. However, it is hard to achieve highly ordered nuclei in

Reproduced with permission of the copyright owner. Further reproduction prohibited without permission.

a continuously happening nucleation and growth process which were observed in almost all literatures about DNA-templated nanowires. Metal nuclei continuously deposit and grow through the whole period of the reactions, so the freshly grown metal aggregates are much smaller than those grown at early stages. Large size distribution is responsible for those inter-granular gaps, branches and necklaces of as-prepared nanowires.

5.2 Design and Synthesis

The novel approach – pre-nucleated growth using single strand DNA (ssDNA) – is to improve nanowire structure and conductivity. This is the first proposal for growth of nanowires on a ssDNA. The unique property of molecular recognition of ssDNA can be used for specific placement and assembly of nano-scale electrical elements (Section 5.3). This approach requires design and synthesis of ssDNA templates. The techniques of conventional molecular biology, for example ligation, restriction digestion, and polymerase chain reaction (PCR), are utilized in synthesis.

5.2.1 Methods

Figure 5.1 shows a schematic diagram of the 4-step procedures to obtain ssDNA templates. The design and synthesis were based on the 190 bp duplex [121]. The DNA was modified by inserting *Ban I* recognition sites on its two ends to ensure that ligated DNA multimers have the same repeated sequence as the monomer. The duplexes of 240 bp, 420 bp, and 600 bp were synthesized by ligating two 30-mer adaptors to the two ends of the monomer (180 bp), dimmer (360 bp) and trimmer (540 bp), respectively. After

Reproduced with permission of the copyright owner. Further reproduction prohibited without permission.

PCR amplification, the ssDNA templates with the lengths of 82, 143, and 204 nm can be achieved by using λ exonuclease digestion.

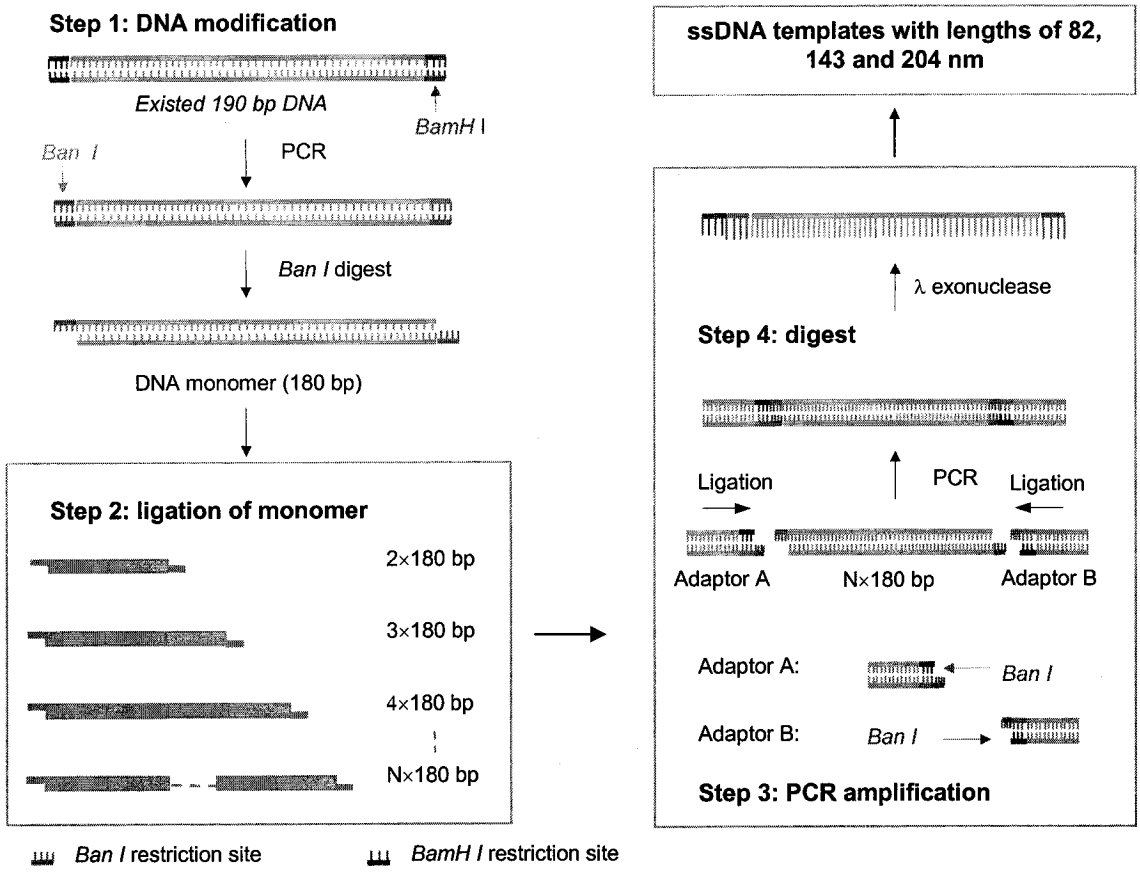

Figure 5.1. Schematic diagram of synthesis of ssDNA templates.

Agarose gel electrophoresis used in all experiments to verify ligation and PCR process was carried out at Dr. Haynie's lab by using the analysis setup for nucleic acids: UV transilluminator (Spectroline, TV-312 S), Olympus digital camera, Labnet gel tank and power station. The gradient thermocycler (TC-512, Techne) was used in PCR experiments. T4 DNA ligase and *Ban I* restriction enzyme were from New England Biolabs. Pfu DNA polymerase for PCR was from Stratagene. All oligos (L1-L4) for PCR amplification were from Synthegen. Gel filtration of the thiol-modified oligos was

Reproduced with permission of the copyright owner. Further reproduction prohibited without permission.

performed to remove excessive DTT. The protocols for spin column purification and gel extraction were from Qaigen. Two-time elution at 50° C was used in all experiments to improve DNA recovery (not shown).

5.2.2 Results and Discussion

The detailed procedures of synthesis are described in my practicum report for an M.S. degree [122]. Here, I outline the results of synthesis of designed ss-DNA templates.

5.2.2.1 DNA Modification. The starting 190 bp DNA has two *BamH I* restriction sequences on the ends [121]. The palindromic sequence of the enzyme is not suitable here, because self-ligation of *BamH I* digests results in DNA lock of uniquely repeated sequence. *Ban I* with a non-palindromic recognition sequence was used to replace the *BamH I* restriction sequence by PCR using two 37-mer primers that contain the *Ban I* sequences. The resulting 198 bp DNA (Lane 4 and 5, Figure 5.2A) were slightly slower than the 190 bp DNA (Lane 2 and 3, Figure 5.2A) in a gel electrophoresis. The 190 bp and amplified 198 bp DNA were digested by *Ban I*, and digests were then subjected to a self-ligation reaction (Figure 5.2B). The lane 3 shows the self-ligated 360 bp, 540 bp and 720 bp from digests of the 198 bp DNA. By contrast, no such self-ligation was observed for the starting 190 bp DNA (Lane 2, Figure 5.2B).

5.2.2.2 Synthesis of SS-DNA Templates. The monomer DNA was obtained by *Ban I* digestion of 198 bp DNA. Self-ligation results in the dimer (360 bp) and trimer (540 bp). To synthesize the three PCR templates, two 30-mer adaptors (L12, L34) must be ligated to two ends of the monomer, dimer and trimer duplex to serve as binding sites in subsequent PCR (Figure 5.1). Adaptor L12 and L34 were obtained by annealing the

Reproduced with permission of the copyright owner. Further reproduction prohibited without permission.

corresponding oligonucleotides at gradually decreased temperatures (Chapter III). Ligation was the major work in preparation of the three PCR templates because ligation efficiency exponentially decreases with the increase of ligation steps.

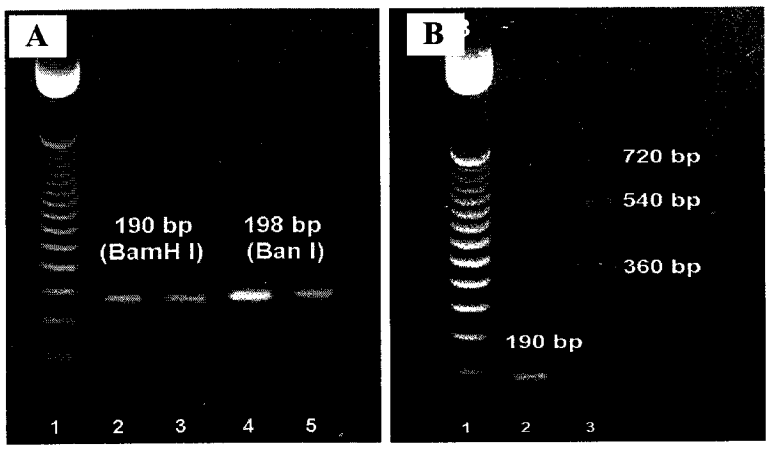

Figure 5.2. Gel electrophoresis for the modified 198 bp DNA duplex. (A) Lane 1 is a 50 bp ladder; Lane 2 and 3 are the starting 190 bp duplex; Lane 4 and 5 are the 198 bp DNA with *Ban I* recognition sites. (B) Approval of incorporation of *Ban I* restriction sites in the 198 bp DNA. Lane 2 is the 190 bp DNA after *Ban I* digestion and self-ligation. Lane 3 is the 198 bp DNA after *Ban I* digestion and self-ligation. (2.5% agarose, 60 V)

The 240 bp and 420 bp PCR templates were synthesized by the ligation sequences of "L12-180-L34" and "L12-360-L34" respectively, where 180 means the monomer duplex and 360 means the dimer duplex. PCR products of amplified 240 bp and 420 bp DNA are shown in Figure 5.3A and B. Different ligation sequences for preparation of 600 bp PCR templates were tested because of low efficiency in the four-step ligation. In each step, the longer DNA to be ligated, the lower the ligation efficiency. Materials were inevitably lost in gel extraction after ligation. Three different ligation approaches were performed in a total of 152 times of gel analysis. The first two approaches are "L12-540-L34" and "210(L12)-180-210(L34)", where 540 means the trimer duplex, and 210(L12) means ligation products of 180 monomer and adaptor L12. These two ways of ligation,

Reproduced with permission of the copyright owner. Further reproduction prohibited without permission.

however, did not result in the 600 bp PCR templates because of low ligation efficiency and circularization of the 540 bp duplex [122]. Many efforts were made to improve ligation, including an increase of starting concentration of 180 bp monomer and two adaptors, longer time ligation with increased amount of ligase, use of PEG, second elution during gel extraction, etc.. None of these methods, however, could significantly increase the yield of the 600 bp PCR templates.

Conversion of the target 600 DNA duplex was not improved until the new approach of synthesis. The 210(L12) DNA, which is extracted from *Ban I* digests of PCR-amplified 420 bp DNA, was used as starting material. According to the sequence of the 420 bp DNA, *Ban I* digestion lead to three fragments, 210(L12), 180 bp monomer, and L34. There is no *Ban I* digestion sequence in the 210(L12) fragment because of one base mismatch. The advantage of this approach is that the 210(L12) duplex does not have nicks. Large amount of the fragment can be obtained by PCR and digestion, instead of by low efficient ligation. Figure 5.3C shows PCR products by the 600 bp DNA templates synthesized by the new approach.

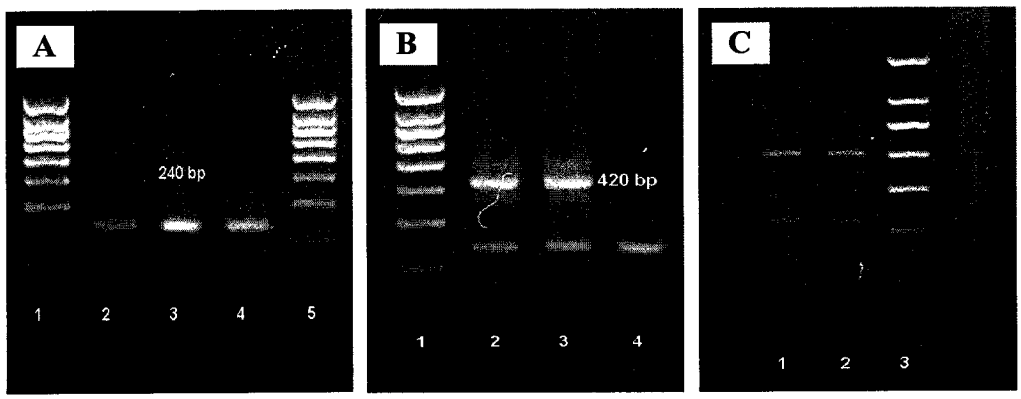

Figure 5.3. Gel electrophoresis for PCR-amplified target DNA duplex. (A) 240 bp DNA duplex in Lane 2 and 4. Lane 1 and 5 are a 100 bp ladder. (B) 420 bp DNA duplex in Lane 2 and 3. Lane 1 is a 100 bp ladder. Lane 4 is 240 bp DNA. (C) 600 bp DNA duplex in lane 1-2. Lane 3 is a 100 bp ladder. (2.5% agarose, 60 V)

Reproduced with permission of the copyright owner. Further reproduction prohibited without permission.

The sequencing results show that about 85% sequenced bases in the fragments of 240 bp and 420 bp match with the designed sequences. For the 600 bp fragment, however, there was no strong signal. This might result from the low concentration of the amplified 600 bp fragment. Lambda exonuclease digestion is simple and effective to generate ssDNA from dsDNA. The enzyme removes mono-nucleotides from duplex DNA, preferentially starting with 5′-phosphorylated ends. Of three PCR-amplified dsDNA, all 5' ends of upper strands are modified by thiol groups, which prevent the exonuclease from binding. After a kination reaction, 5'-end-phosphorylated lower strands will be degraded during λ exonuclease digestion. All 3 PCR-amplified DNA duplexes were tested by digestion reaction, after which they were smear in gel electrophoresis. This suggests that ssDNA templates be generated by degradation of the corresponding dsDNA using λ exonuclease.

5.3 Future Work

A key advantage of the pre-nucleated growth using ssDNA for nanowire fabrication is that metal nanoparticles can be placed onto specific sites of a DNA template as precisely as lengths of a few nucleotide bases. The distance between two adjacent nanoparticles is programmable by changing length of the oligonucleotide. It is possible to improve nucleation and growth of metal nanoparticles by controlling distribution of preformed metal nuclei along a template. In addition, lengths of nanowires are flexible because they are determined by steps of ligation.

Figure 5.4 shows the design of ssDNA templates and arrangement of 1.4 nm Au nuclei used in preparation of Au nanowires (Chapter IV). The 240 bp, 420 bp, and 600 bp

Reproduced with permission of the copyright owner. Further reproduction prohibited without permission.

duplexes were synthesized by ligation and PCR. After lambda exonuclease digestion, the corresponding ssDNA molecules with lengths of 82 nm, 143 nm, and 204 nm, serves as templates for nanowire fabrication. Longer templates may be achieved by more steps of ligation of monomers. Each of 35-mer thiol-modified oligonucleotide (Oligo) A, B, C, and D is bound by Au-thiol coupling to one 1.4 nm Nanogold that was used to fabrication of Au nanowires (Chapter IV). Au-capped oligos are annealed to ssDNA templates by their complementary sequences. "Proof-reading" during base pairing rules out possible nonspecific binding. As a result, Au nuclei are site-specifically placed on stretched templates with 15 nm distance between two adjacent particles. The well-ordered Au particles serve as nucleation centers to catalyze growth of continuous nanowires during development of nanogolds. Fabricated nanowires will have uniform grain sizes and be free of branches and gaps, favorable to the transport of electrons.

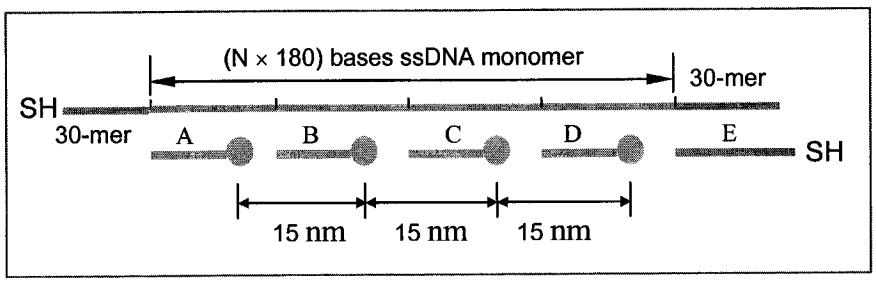

Figure 5.4. Design of the ss-DNA templates. The lengths are 82 nm (N=1), 143 nm (N=2), and 204 nm (N=3). Each of 35-mer thiol-capped Oligo A, B, C and D is bound to one 1.4 nm Nanogold by Au-thiol coupling. After annealing, Au nanoparticles will be placed on stretched templates with an inter-particle distance of 15 nm. The 15 nm inter-particle space is "programmable" by selection of bases of oligonucleotides.

Table 5.1 lists expected advantages of the novel approach by comparison with the conventional approach by using λ DNA as templates. The key advantage of the novel approach is high uniformity of nanoparticles and high electrical conductivity.

Reproduced with permission of the copyright owner. Further reproduction prohibited without permission.

Table 5.1. Comparison of two approaches for nanowire fabrication.

Disadvantages of λ-DNA as template	**Advantages of the novel approach**
Fixed length of λ-DNA : 16 μm	Flexible lengths of wires (from 82 nm to longer)
Low uniformity of metallization: large size distribution, branches, and gaps	High uniformity, narrow grain size distribution, and free of gaps and branches
Uncontrollable nuclei size	Equally spaced metal nuclei with unique size
Low electrical conductivity	High electrical conductivity

Reproduced with permission of the copyright owner. Further reproduction prohibited without permission.

CHAPTER VI

SUMMARY

This dissertation is concerned about assembly of one-dimensional nanowires using single DNA molecules as a template. The contents involved are interdisplinary, such as molecular biology, biochemistry, lithographic microfabrication and molecule-based nanoassembly. A novel strategy to build nanoscale materials and devices is so-called "bottom up" directed nanoassembly, in which novel and functional structures are made of and organized by atoms, molecules, nanoparticles, and organic polymers. The purpose of this work is to study the mechanism and process in preparation of metal nanowires using DNA templates.

Nanowires are a special family in a variety of non-conventional structures created by nanotechnology. They are widely recognized as important elements in the development of certain futuristic nanoscale devices in nanoelectronics, optoelectronics and NEMS. An individual DNA molecule is a natural template for nanowire fabrication. The linear polynucleotide chain has a width of 2 nm and a length of 0.34 nm per nucleoside subunit. Small building blocks, for example metal ions, nanoparticles and organic molecules can be stuck to polyanionic backbones or chelating bases of DNA by electrostatic interaction or coordination coupling. These interactions have been utilized in literature to assemble metal nanocluster chains and nanowires.

Reproduced with permission of the copyright owner. Further reproduction prohibited without permission.

My colleague and I have shown that magnetic nanoparticles can be assembled on DNA by electroless plating [123, 124, 127, 129]. This is first time that literature has shown the assembly of magnetic nanowires by DNA templates. The three-step process in nanowire fabrication is DNA activation by Pd(II), formation of Pd(0) nuclei on DNA, and growth of target metal. The advantage over the methods in literature on metallization of DNA is the separation of nucleation and growth. The reducing agent does not react with target metal ions during growth, so there is less secondary nucleation in solution during growth. As a result, 10-30 nm Co(0) and Ni(0) only deposit on pre-formed Pd(0) nanoparticles with the average diameters of 2-3 nm. VSM has confirmed that prepared nanowires are ferromagnetic. Parallel arrays of Co and Ni nanocluster chains were achieved by orienting DNA templates prior to metallization. The step of DNA activation by Pd(II) is key to the coverage of metal on templates, non-structured deposits and heterogeneity of the resulting structures. We have shown that the target metal deposits randomly on the surface without appropriate activation.

This method is a novel approach for nanowire fabrication, pre-nucleated nanowire growth using designed and synthesized ssDNA templates [125, 130]. This provides one possibility for improving the uniformity of DNA nanowires. Single-stranded DNA is uniquely suited to molecular recognition. Individual Au nanonuclei can be made to adhere to designated sites on a linear template with a precision of a few nanometers. According to the described design and synthesis, 1.4 nm Au nanoparticles can be placed on the 82 nm, 143 and 204 nm long ssDNA templates with 15 nm inter-distance between two adjacent Au particles. Uniformly distributed Au seeds should result in nanowires of higher uniformity and conductivity than DNA molecules randomly coated with

Reproduced with permission of the copyright owner. Further reproduction prohibited without permission.

nanoparticles. Also, in place of λ DNA, which is microns long and used in almost all the reports discussed above, one could exploit methods of molecular biology to create DNA nanowires of any desired length.

Individual DNA molecules must be separated and stretched to serve as nanowire templates. Various methods have been used to orient DNA molecules that would otherwise be randomly coiled in aqueous solution or on a surface. Parallel arrays of DNA have been achieved by using molecular combing, in which surface tension generated by movement of meniscus extended DNA on a silanized glass. Spin stretching has also been used to stretch DNA. Rotation shear force stretches DNA molecules that distribute radially on a substrate. Two sticky ends of λ DNA molecules have been engineered by hybridization and ligation. DNA capped with a thiol group covalently bind to Au electrode surface. Hydrodynamic flow has been applied to stretch modified DNA between two Au electrodes. They have been fabricated by standard lithography. An enzymatic assay has been used to approve the modification of DNA.

Many experiments in this work are trial-and-error. In DNA stretching, for example, tiny environmental factors might have a huge affect on the process. The ideal force acting on a single DNA molecule is about 10 pN, which stretches λ DNA to about its crystallographic length. Another unexpected factor, for example flow convection or vibration force, however, may have broken DNA during stretching. AFM is used to characterize DNA, Pd(0):DNA complex, and metal nanowires by height. Variation from 1.5 nm to 0.4 nm was found on mica-adsorbed DNA molecules. This might not be explained by the known tip broadening effect.

Reproduced with permission of the copyright owner. Further reproduction prohibited without permission.

Functional nanowires in electronics must meet the following three demands. One, the dimensions of the structures must be smaller than what can be achieved by conventional lithography. Molecule-templated nanoassembly can be used to realize the required length scale. Two, the distinctive properties of assembled 1D structures must be at least comparable to the properties of the corresponding bulk material. And three, it must be possible to place assembled wires at specific positions on the substrate. Although many fundamental issues need to be better understood, nanowires assembled by DNA have great potential to meet these three requirements. Preliminary applications of DNA-templated nanowires in electronics have already been demonstrated in literature. DNA will increasingly be recognized as an important building block, not only in life science, but also in futuristic nanostructures and manufacturing processes.

Reproduced with permission of the copyright owner. Further reproduction prohibited without permission.

REFERENCES

1. P.J. Silverman, "The Intel lithography roadmaps," *Intel Tech. J.*, **6**, 55, 2002

2. The 2004 International Technology Roadmap for Semiconductors (ITRS), 2004

3. K.H. Brown, "Economic challenges on the path to 22 nm," *Fut. Fab. Intl.*, **17**, 18, 2004

4. M.C. Roco, "The future of the national nanotechnology initiative," www.nano.gov/html/res/slides.pdf, Nov. 2003

5. Y. Huang, X. Duan, Y. Cui, L. Lauhon, K. Kim, C.M. Lieber, "Logic gates and computation from assembled nanowire building blocks," *Science*, **294**, 1313, 2001

6. Y. Cui and C.M. Lieber, "Functional nanoscale electronic devices assembled using silicon nanowire building block," *Science*, **291**, 851, 2001

7. X. Duan, Y. Huang, Y. Cui, J. Wang, C.M. Lieber, "Indium phosphate nanowires as building blocks for nanoscale electronic and optoelectronic devices," *Nature*, **409**, 66, 2001

8. C. Niu, V. Sahi, J. Chen, J. W. Parce, S. Empedocles, J.L. Goldman, "High-performance thin-film transistors using semiconductor nanowires and nanoribbons," *Nature*, **425**, 274, 2003

9. Y. Cui, Z. Zhong, D. Wang, W.U. Wang, C.M. Lieber, "High performance silicon nanowire field effect transistors," *Nano Lett.*, **3**, 149, 2003

10. M.H. Huang, S. Mao, H. Feick, H. Yan, Y. Wu, H. Kind, E. Weber, R. Russo, P. Yang, "Room-temperature ultraviolet nanowire nanolasers," *Science*, **292**, 1897, 2001

11. J.C. Johnson, H.J. Choi, K.P. Knutsen, R.D. Schaller, P. Yang, R.J. Saykally, "Single gallium nitride nanowire lasers," *Nature Mater.*, **1**, 101, 2002

12. X. Duan, Y. Huang, R. Agarwal, C.M. Lieber, "Single-nanowire electrically driven lasers," *Nature*, **421**, 241, 2003

13. H. Yan, R. He, J. Johnson, M. Law, R.J. Saykally, P. Yang, "Dendrite nanowire UV laser array," *J. Am. Chem. Soc.*, **125**, 4728, 2003

Reproduced with permission of the copyright owner. Further reproduction prohibited without permission.

14. J.C. Johnson, H. Yan, R.D. Schaller, L.H. Haber, P. Yang, R.J. Saykally, "Single nanowire lasers," *J. Phys. Chem. B*, **105**, 11387, 2000

15. M. Law, D. Sirbuly, J. Johnson, J. Goldberger, R. Saykally, P. Yang, "Ultralong nanoribbon waveguides for sub-wavelength photonics integration," *Science*, **305**, 1269, 2004

16. M.C. McAlpine, R.S. Friedmann, S. Jin, K.H. Lin, W.U. Wang, C.M. Lieber, "High-performance nanowire electronics and photonics on glass and plastic substrates," *Nano Lett.*, **3**, 1531, 2003

17. H. Kind, H. Yan, M. Law, B. Messer, P. Yang, "Nanowire UV photodetector and optical switches," *Adv. Mater.*, **14**, 158, 2002

18. F. Favier, E. Walter, M. Zach, T. Benter, R.M. Penner, "Hydrogen sensors and switches from electrodeposited palladium mesowire arrays," *Science*, **293**, 2227, 2001

19. J. Wang, M.S. Gudiksen, X. Duan, Y. Cui, C.M. Lieber, "Highly polarized photoluminescence and photodetection from single indium phosphide nanowires," *Science*, **293**, 1455, 2001

20. Y. Cui, Q. Wei, H. Park, C.M. Lieber, "Nanowire nanosensors for highly sensitive and selective detection of biological and chemical species," *Science*, **293**, 1289, 2001

21. A. Maiti, J.A. Rodriguez, M. Law, P. Kung, J.R. McKinney, P. Yang, "SnO_2 nanoribbons as NO_2 sensors: insights from first-principles calculations," *Nano. Lett.*, **3**, 1025, 2003

22. J. Hahm and C.M. Lieber, "Direct ultrasensitive electrical detection of DNA and DNA sequence variations using nanowire nanosensors," *Nano Lett.*, **4**, 51, 2004

23. L. Piraux, J. George, J. Despres, C. Leroy, E. Ferain, R. Legres, K. Ounadjela, A. Fert, "Giant magnetoresistance in magnetic multilayered nanowires," *Appl. Phys. Lett.*, **65**, 2484, 1994

24. T. Thurn-Albrecht, J. Schotter, C.A. Kastle, N. Emley, T. Shibauchi, L. Krusin-Elbaum, K. Guarini, C.T. Black, M.T. Tuominen, T.P. Russell, "Ultrahigh density nanowire arrays grown in self-assembled diblock copolymer templates," *Science*, **290**, 2126, 2000

25. K. Nielsch, R.B. Wehrspohn, J. Barthel, J. Kirschner, U. Gosele, "Hexagonally ordered 100 nm period nickel nanowire arrays," *Appl. Phys. Lett.*, **79**, 1360, 2001

Reproduced with permission of the copyright owner. Further reproduction prohibited without permission.

26. R.S. Wagner and W.C. Ellis, "Vapor-liquid-solid mechanism of single crystal growth," *Appl. Phys. Lett.*, **4**, 89, 1964

27. E.I. Givargizov, "Fundamental aspects of VLS growth," *J. Cryst. Growth*, **31**, 20, 1975

28. Y. Wu and P. Yang, "Direct observation of vapor-liquid-solid nanowire growth," *J. Am. Chem. Soc.*, **123**, 3165, 2001

29. A.M. Morales and C.M. Lieber, "A laser ablation method for the synthesis of crystalline semiconductor nanowires," *Science*, **279**, 208, 1998

30. X. Duan and C.M. Lieber, "Laser-assisted catalytic growth of single crystal GaN nanowires," *J. Am. Chem. Soc.*, **122**, 188, 2000

31. X. Duan and C.M. Lieber, "General synthesis of compound semiconductor nanowires," Adv. *Mat.*, **12**, 298, 2000

32. G.E. Possin, "A method for forming very small diameter wires," *Rev. of Sci. Instru.*, **41**, 772, 1970

33. C.R. Martin, "Nanomaterials: a membrane-based synthetic approach," *Science*, **266**,1961, 1994

34. C.J. Brumlik and C.R. Martin, "Template synthesis of metal microtubules," *J. Am. Chem. Soc.*, **113**, 3174, 1991

35. C.J. Brumlik, V.P. Menon, C.R. Martin, "Template synthesis of metal microtubule ensembles utilizing chemical, electrochemical and vacuum deposition techniques," *J. Mater. Res.*, **9**, 1174, 1994

36. S.A. Sapp, B.B. Lakshmi, C.R. Martin, "Template synthesis of bismuth telluride nanowires," *Adv. Mater.*, **11**, 402, 1999

37. M. Wirtz and C.R. Martin, "Template fabricated gold nanowires and nanotubes," *Adv. Mat.*, **15**, 455, 2003

38. T.M. Whitney, J.S. Jiang, P.C. Searson, C.L. Chien, "Fabrication and magnetic properties of arrays of metallic nanowires," *Science*, **261**, 1316, 1993

39. A. Blomdel, J.P. Meier, B. Doudin, J.-Ph. Ansermet, "Giant magnetoresistance of nanowires of multilayers," *Appl. Phys. Lett.*, **65**, 3019, 1994

40. L. Piraux, J. George, J. Despres, C. Leroy, E. Ferain, R. Legres, K. Ounadjela, A. Fert, "Giant magnetoresistance in magnetic multilayered nanowires," *Appl. Phys. Lett.*, **65**, 2484, 1994

Reproduced with permission of the copyright owner. Further reproduction prohibited without permission.

41. K. Liu, K. Nagodawithana, P.C. Searson, C.L. Chien, "Perpendicular giant magnetoresistance of multilayered Co/Cu nanowires," *Phys. Rev. B*, 51, 7381, 1995

42. A. Fert and L. Pirauxet, "Magnetic nanowires," *J. Magn. Magn. Mater.*, **200**, 338, 1999

43. M. Tanase, L.A. Bauer, A. Hultgren, D.M. Silevitch, L. Sun, D.H. Reich, P.C. Searson, G.J. Meyer, "Alignment of fluorescent nanowires," *Nano Lett.*, **1**, 155, 2001

44. B. Lakshmi, P.K. Dorhout, C.R. Martin, "Sol-gel template synthesis of semiconductor nanostructures," *Chem. Mater.*, **9**, 857, 1997

45. B. Lakshmi, C.J. Patrissi, C.R. Martin, "Sol-gel template synthesis of semiconductor oxide micro- and nanostructures," *Chem. Mater.*, **9**, 2544, 1997

46. C.R. Martin, "Template polymerization of conductive polymer nanostructures," in Handbook of Conducting Polymers, 2nd Ed., J.R. Reynolds, T. Skotheim, R. Elsenbaumer, Eds., Marcel Dekker, Inc., , Chap. 16, pp. 409-421, 1997

47. C.R. Martin, "Template synthesis of electronically conductive polymer nanostructures," *Acc. Chem. Res.*, **28**, 61, 1995

48. C.R. Martin, Z. Cai, L.S. Van Dyke, W. Liang, "Template synthesis of conducting polymers - enhanced conductivity, enhanced supermolecular order, interesting microstructures," *Polym. Mater. Sci. Eng.*, **64**, 204, 1991

49. C.R. Martin, Z. Cai, L.S. Van Dyke, W. Liang, "Template synthesis of electronically conductive polymers," *Polym. Prepr.*, **32**, 89, 1991

50. Y. Huang, X. Duan, Q. Wei, C.M. Lieber, "Directed assembly of one-dimensional nanostructures into functional networks," *Science*, **291**, 630, 2001

51. M.S. Dresselhaus, "Overview of bismuth nanowires for thermoelectric applications," in *Chemistry, Physics and Materials Science of Thermoelectric Materials: Beyond Bismuth Telluride.*, edited by M.G. Kanatzidis, S.D. Mahanti, T.P. Hogan and M.F. Thorpe, Kluwer Academic/Plenum Publishers, New York, Boston, Dordrecht, London, Moscow, pages 1-17, 2003

52. P.A. Alivisatos, K.P. Johnsson, X. Peng, T.E. Wilson, C.J. Loweth, M.P. Bruchez, P.G. Schultz, "Organisation of 'nanocrystal molecules' using DNA," *Nature*, **382**, 609, 1996

53. C.A. Mirkin, R.L. Letsinger, R.C. Mucic, J.J. Storhoff, "A DNA-based method for rationally assembling nanoparticles into macroscopic materials," *Nature*, **382**, 607, 1996

Reproduced with permission of the copyright owner. Further reproduction prohibited without permission.

54. E. Braun, Y. Eichen, U. Sivan, G. Ben-Yoseph, "DNA templated assembly and electrode attachment of a conducting silver wire," *Nature*, **391**, 775, 1998

55. C.J. Loweth, W.B. Caldwell, X. Peng, A.P. Alisisatos, P.G. Schultz, "DNA-based assembly of gold nanocrystals," *Ange. Chem. Intl. Ed.*, **38**, 1808, 1999

56. B. Giese, J. Amaudrut, A. Kohler, M. Spormann, S. Wessley, "Direct observation of hole transfer through DNA by hopping between adenine bases and by tunneling," *Nature*, **412**, 318, 2001

57. A. Bensimon, A. Simon, A. Chiffaudel, V. Croquette, F. Heslot, D. Bensimon, "Alignment and sensitive detection of DNA by a moving interface," *Science*, **265**, 2096, 1994

58. D. Bensimon, A.J. Simon, V. Croquette, A. Bensimon, "Stretching DNA with a receding meniscus: experiments and models," *Phys. Rev. Lett.*, **74**, 4754, 1995

59. J.-F. Allemand, D. Bensimon, L. Jullien, A. Bensimon, V. Croquette, "pH-dependent specific binding and combing of DNA," *Biophys. J.*, **73**, 2064, 1997

60. X. Michalet, R. Ekong, F. Fougerousse, S. Rousseaux, C. Schurra, N. Hornigold, M. Slegtenhorst, J. Wolfe, S. Povey, J.S. Beckmann, A. Bensimon, "Dynamic molecular combing: stretching the whole human genome for high-resolution studies," *Science*, **277**, 1518, 1997

61. H. Yokota, F. Johnson, H. Lu, R.M. Robinson, A.M. Belu, M.D. Garrison, B.D. Ratner, B.J. Trask, D.L. Miller, "A new method for straightening DNA molecules for optical restriction mapping," *Nucl. Acids Res.*, **25**, 1064, 1997

62. K. Otobe and T. Ohtani, "Behavior of DNA fibers stretched by precise meniscus motion control," *Nucl. Acids Res.*, **29**, e109, 2001

63. J.M. Schurr and S.B. Smith, "Theory for the extension of a linear polyelectrolyte attached at one end in an electric field," *Biopoly.*, **29**, 1161, 1999

64. S.B. Smith and A.J. Bendich, "Electrophoretic charge density and persistence length of DNA as measured by fluorescence microscopy," *Biopoly.*, **29**, 1167, 1999

65. R.M. Zimmermann and E.C. Cox, "DNA stretching on functionalized gold surfaces," *Nucl. Acid Res.*, **22**, 492, 1994

66. M. Washizu and O. Kurosawa, "Electrostatic manipulation of DNA in microfabricated structures," *IEEE Trans. Indus. Appl.*, **26**, 1165, 1990

Reproduced with permission of the copyright owner. Further reproduction prohibited without permission.

67. M. Washizu, O. Kurusawa, I. Arai, S. Suzuki, N. Shimamoto, "Applications of electrostatic stretch and positioning of DNA," *IEEE Trans. Indus. Appli.*, **31**, 447, 1995

68. T. Yamamoto, O. Kurosawa, H. Kabata, N. Shimamoto, M. Washizu, "Molecular surgery of DNA based on electrostatic micromanipulation," *IEEE Trans. Indus. Appl.*, **36**, 1010, 2000

69. T.T. Perkins, S.R. Quake, D.E. Smith, S. Chu, "Relaxation of a single DNA molecule observed by optical microscopy," *Science*, **264**, 822, 1994

70. T.T. Perkins, D.E. Smith, R.G. Larson, S. Chu, "Stretching of a single tethered polymer in a uniform flow," *Science*, **268**, 83, 1995

71. S. B. Smith, Y. Cui, C. Bustamante, "Overstretching B-DNA: the elastic response of individual double-stranded and single-stranded DNA molecules," *Science*, **271**, 795, 1996

72. H. Yokota, J. Sunwoo, M. Sarikaya, G. van den Engh, R. Aebersold, "Spin-stretching of DNA and protein molecules for detection by fluorescence and atomic force microscopy," *Anal. Chem.*, **71**, 4418, 1999

73. J.Y. Ye, K. Umemura, M. Ishikawa, R. Kuroda, "Atomic force microscopy of DNA molecules stretched by spin-coating technique," *Anal. Biochem.*, **281**, 21, 2000

74. J. Sagiv, "Organized monolayers by adsorption: formation and structure of oleophobic mixed monolayers on solid surfaces," *J. Am. Chem. Soc.*, **102**, 92, 1980

75. M.E. Hogan and R. Austin, "Importance of DNA stiffness in protein–DNA binding specificity," *Nature*, **329**, 263, 1987

76. C.D. Bain, J. Evall, G.M. Whitesides, "Formation of monolayer films by the spontaneous assembly of organic thiols from solution onto gold," *J. Am. Chem. Soc.*, **111**, 321, 1989

77. D.Y. Petrovykh, M.J. Tarlov, L.J. Whitman, "Quantitative analysis and characterization of DNA immobilized on gold," *J. Am. Chem. Soc.*, **125**, 5219, 2003

78. J.F. Marko and E. Siggia, "Stretching DNA," *Macromole.*, **28**, 8759, 1995

79. D.E. Smith, H.P. Babcock, S. Chu, "Single polymer dynamics in steady shear flow," *Science*, **276**, 2016, 1997

80. J. Richter, M. Mertig, W. Pompe, I. Mönch, H.K. Schackert, "Construction of highly conductive nanowires on a DNA template," *Appl. Phys. Lett.*, **78**, 536, 2001

Reproduced with permission of the copyright owner. Further reproduction prohibited without permission.

81. J. Richter, R. Seidel, R. Kirsch, M. Mertig, W. Pompe, J. Plaschke, H.K. Schackert, "Nanoscale palladium metallization of DNA," *Adv. Mater.*, **12**, 507, 2000

82. J. Richter, M. Mertig, W. Pompe, H. Vinzelberg, "Low-temperature resistance of DNA-templated nanowires," *Appl. Phys. A*, **74**, 725, 2002

83. W.E. Ford, O. Harnack, A. Yasuda, J.M. Wessels, "Platinated DNA as precursors to templated chains of metal nanoparticles," *Adv. Mater.*, **13**, 1793, 2001

84. M. Mertig, L.C. Ciacchi, R. Seidel, W. Pompe, "DNA as a selective metallization template," *Nano Lett.*, **2**, 841, 2002

85. R. Seidel, L.C. Ciacchi, M. Weigel, W. Pompe, M. Mertig, "Synthesis of platinum cluster chains on DNA templates: conditions for template-controlled cluster growth," *J. Phys. Chem. B*, **108**, 10801, 2004

86. K. Keren, M. Krueger, R. Gilad, G. Ben-Yoseph, U. Sivan, E. Braun, "Sequence-specific molecular lithography on single DNA molecules," *Science*, **297**, 72, 2002

87. K. Keren, R.S. Berman, E. Braun, "Patterned DNA metallization by sequence-specific localization of a reducing agent," *Nano Lett.*, **4**, 323, 2004

88. A. Kumar, M. Pattarkine, M. Bhadbhade, A.B. Mandale, K.N. Ganesh, S.S. Datar, C.V. Dharmadhikari, M. Sastry, "Linear superclusters of colloidal gold particles by electrostatic assembly on DNA templates," *Adv. Mater.*, **13**, 341, 2001

89. M. Sastry, A. Kumar, S. Datar, C.V. Dharmadhikari, K.N. Ganesh, "DNA-mediated electrostatic assembly of gold nanoparticles into linear arrays by a simple drop-coating procedure," *Appl. Phys. Lett.*, **78**, 2943, 2001

90. F. Patolsky, Y. Weizmann, O. Lioubashevski, I. Willner, "Au-particle nanowires based on DNA and polylysine templates," *Ange. Chem. Intl. Ed.*, **41**, 2323, 2002

91. O. Harnack, W.E. Ford, A. Yasuda, J.M. Wessels, "Tris(hydroxymethyl)phosphine-capped gold particles templated by DNA as nanowire precursors," *Nano Lett.*, **2**, 91, 2002

92. C.F. Monson and A.T. Woolley, "DNA-templated construction of copper nanowires," *Nano Lett.*, **3**, 359, 2003

93. H.A. Becerril, R.M. Stoltenberg, C.F. Monson, A.T. Woolley, "Ionic surface masking for low background in single- and double-stranded DNA-templated silver and copper nanorods," *J. Mater. Chem.*, **14**, 611, 2004

94. S.R. Quake and A. Scherer, "From micro to nano fabrication with soft materials," *Science*, **290**, 1536, 2000

Reproduced with permission of the copyright owner. Further reproduction prohibited without permission.

95. S. Link and M.A. El-Sayed, "Spectral properties and relaxation dynamics of surface plasmon electronic oscillations in gold and silver nanodots and nanorods," *J. Phys. Chem. B*, **103**, 8410, 1999

96. G. Mie, "Beitrage zur optik truber medien, speziell kolloidaler metallosungen," *Ann. Phys.*, **25**, 377, 1908

97. U. Kreibig and M. Vollmer, "Optical properties of metal clusters," Springer, Berlin, ISBN: 0387578366, 1995.

98. K. Dai, "DNA-templated metallic nanowire fabrication," M.S. Thesis, Louisiana Tech University, May 2003

99. M. Mertig, R. Kirsch, W. Pompe, "Biomolecular approach to nanotube fabrication," *Appl. Phys. A*, **66**, S723, 1998

100. R.R. Naik, S.E. Jones, C.J. Murray, J.C. McAuliffe, R.A. Vaia, O. Stone, "Peptide templates for nanoparticle synthesis derived from polymerase chain reaction-driven phage display," *Adv. Funct. Mater.*, **14**, 25, 2004

101. M. Knez, A.M. Bittner, F. Boes, C. Wege, H. Jeske, E. Maiβ, "Biotemplate synthesis of 3-nm nickel and cobalt nanowires," *Nano Lett.*, **3**, 1079, 2003

102. M. Knez, M. Sumser, A.M. Bittner, C. Wege, H. Jeske, T.P. Martin, K. Kern, "Spatially selective nucleation of metal clusters on the tobacco mosaic virus," *Adv. Funct. Mater.*, **14**, 116, 2004

103. J. Duguid, V.A. Bloomfield, J. Benevides, G.J. Thomas, "Raman spectroscopy of DNA-metal complexes. I. Interactions and conformational effects of the divalent cations: Mg, Ca, Sr, Ba, Mn, Co, Ni, Cu, Pd, and Cd," *Biophys. J.*, **65**, 1916, 1993

104. G.O. Mallory and J.B. Hajdu, Electroless plating – fundamentals and applications, William Andrew Publishing, 0-936569-07-7, 1990

105. A. Henglein, "Colloidal palladium nanoparticles: reduction of Pd(II) by H_2; Pd(core)Au(shell)Ag(shell) particles," *J. Phys. Chem. B*, **104**, 6683, 2000

106. B.G. Ershov, N.L. Sukhov, E. Janata, "Formation, absorption spectrum, and chemical reactions of nanosized colloidal cobalt in aqueous solution," *J. Phys. Chem. B*, **104**, 613, 2000

107. M. Bezanilla, S. Manne, D. E. Laney, Y.L. Lyubchenko, H.G. Hansm, "Adsorption of DNA to mica, silylated mica and minerals: characterization by atomic force microscopy," *Langmuir*, **11**, 655, 1995

Reproduced with permission of the copyright owner. Further reproduction prohibited without permission.

108. R. Seidel, M. Mertig, W. Pompe, "Scanning force microscopy of DNA metallization," *Surf. Inter. Ana.*, **33**, 151, 2002

109. G.B. Onoa, G. Cervantes, V. Moreno, M.J. Prieto, "Study of the interaction of DNA with cisplatin and other Pd(II) and Pt(II) complexes by atomic force microscopy," *Nucl. Acid Res.*, **26**, 1473, 1998

110. W.J. Dressick, C.S. Dulcey, J.H. Georger, G.S. Calabrese, J.M. Calvert, "Covalent binding of Pd catalysts to ligating self-assembled monolayer films for selective electroless metal deposition," *J. Electrochem. Soc.*, **141**, 210, 1994

111. H. Kind, A.M. Bittner, O. Cavalleri, K. Kern, "Electroless deposition of metal nanoislands on aminothiolate-functionalized Au(111) electrodes," *J. Phys. Chem. B*, **102**, 7582, 1998

112. Y. Huang, X. Duan, Q. Wei, C.M. Lieber, "Directed assembly of one-dimensional nanostructures into functional networks," *Science*, **291**, 630, 2001

113. H. He and N. J. Tao, "Encyclopedia of nanoscience and nanotechnology," V 5, pp 1-18, ISBN 1-58883-001-2, American Scientific Publishers, 2003

114. J. Richter, "Metallization of DNA," *Physica E*, **16**, 157, 2003

115. C.N.R Rao, "Metal nanoparticles, nanowires and carbon nanotubes," *Pure and Appl. Chem.*, **72**, 21, 2000

116. P.P. Edwards, R.L. Johnston, C.N.R. Rao, "Metal clusters in chemiestry," Wiley-VCH, Weinheim, 1999

117. H.S. Nalwa (ed.) "Nanostructured materials and nanotechnology," Academic Press, ISBN 0125139209, 2002

118. K.R. Brown, D.G. Walter, M.J. Natan, "Seeding of colloidal Au nanoparticle solutions. 2. Improved control of particle size and shape," *Chem. Mater.*, **12**, 306, 2000

119. N.R. Jana, L. Gearheart, C.J. Murphy, "Evidence for seed-mediated nucleation in the chemical reduction of gold salts to gold nanoparticles," *Chem. Mater.*, **13**, 2313, 2001

120. A. Henglein, "Formation and absorption spectrum of copper nanoparticles from the radiolytic reduction of $Cu(CN)_2^-$," *J. Phys. Chem. B*, **104**, 1206, 2000

121. S. Anabathula, "Design and synthesis of DNA for the fabrication of DNA-templated gold nanowire," M.S. thesis, Louisiana Tech University, May 2004

Reproduced with permission of the copyright owner. Further reproduction prohibited without permission.

122. Q. Gu, "Design and synthesis of single-stranded DNA templates for nanowire precursors," M.S. Practicum report, Louisiana Tech University, August, 2005

123. Q. Gu, C. Cheng, D.T. Haynie, "Cobalt metallization of DNA: toward magnetic nanowires," *Nanotechnology*, **16**, 1358, 2005

124. Q. Gu, C. Cheng, S. Suryanarayanan, D. T. Haynie, "DNA-templated fabrication of Ni nanocluster chains," submitted, 2005

125. Q. Gu, C. Cheng, R. Gonela, S. Suryanarayanan, K. Dai, D.T. Haynie, "DNA nanowire fabrication," submitted to *Nanotechnology*, 2005

126. C. Cheng, Q. Gu, D.T. Haynie, "Self-Assembly of metallic nanowires from aqueous solution," *Nano Letters*, **5**, 175, 2005

127. Q. Gu, N. Seetala, D.T. Haynie, "DNA-templated assembly of ferromagnetic nanowires," in preparation.

128. Q. Gu, K. Dai, S. Anabathula, C. Cheng, R. Gonela, D.T. Haynie, "Metallic nanowire fabrication by DNA templated self- assembly," *The 3rd LA Confer. on Commer. of Microsys., Mater., and Nanotech.*, Ruston, LA, 2002

129. Q. Gu, C. Cheng, D.T. Haynie, "Cobalt metallization of DNA," Report of invention to Louisiana Tech University, May 2005

130. D.T. Haynie, Q. Gu, K. Dai, S. Anabathula, "Design and synthesis of single stranded DNA templates for nanowire precursors," Report of invention to Louisiana Tech University, July 2005

Reproduced with permission of the copyright owner. Further reproduction prohibited without permission.